USAAVLABS TECHNICAL REPORT 67-18

ROTOR AIR LOADS, BLADE MOTION, AND STRESS CAUSED BY TRANSIENT INPUTS OF SHAFT TORQUE AS RELATED TO STOPPABLE ROTOR OPERATION

By

L. Segel

May 1967

U. S. ARMY AVIATION MATERIEL LABORATORIES
FORT EUSTIS, VIRGINIA

CONTRACT DA 44-177-AMC-77(T)

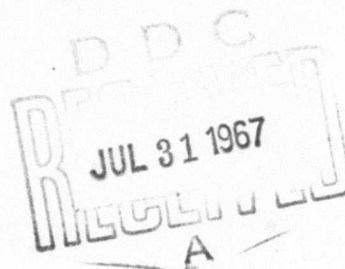CORNELL AERONAUTICAL LABORATORY, INC.
BUFFALO, NEW YORK

This report has been reviewed by the U. S. Army
Aviation Materiel Laboratories and is considered
to be technically sound.   The report is published
for the exchange of information and the stimulation
of ideas.

ROTOR AIR LOADS, BLADE MOTION, AND STRESS CAUSED BY TRANSIENT INPUTS OF SHAFT TORQUE AS RELATED TO STOPPABLE ROTOR OPERATION

CAL Report BB-1840-S-2

by
L. Segel

Prepared by

Cornell Aeronautical Laboratory, Inc.
Buffalo, New York

for

U. S. ARMY AVIATION MATERIEL LABORATORIES
FORT EUSTIS, VIRGINIA

SUMMARY

The transient-response calculation method reported in USAAVLABS Technical Report 65-65 is extended to yield aerodynamic loadings and elastic-blade motions in response to inputs of shaft torque. Whereas transient blade-load calculations were previously restricted to low-advance-ratio flight conditions in which the flow relative to the blade is primarily two-dimensional, aerodynamic loadings are also calculated in this study for flight conditions in which the flow relative to the blade may occur predominantly in the radial direction. As was done previously, the rotor is assumed to continue to translate in level, constant-speed flight during the short time interval for which transient responses are computed. Since the method requires that the wake geometry be specified, the assumption is made that the vertical displacement of the wake results from the induced velocity yielded by momentum theory, as determined by the instantaneous thrust of the rotor. The aerodynamic forces and moments are based on quasi-static considerations and, therefore, the omission of shed vorticity in the wake is believed to be consistent with the adopted quasi-static approach.

Loadings, bending moments, and modal responses are obtained for a teetering rotor experiencing both a 100- and a 50-percent power loss. Similarly, responses are computed for a "rigid" rotor experiencing a 100-percent power loss and for a "rigid" rotor being braked from an initial operational condition corresponding to 100-percent rpm and a nominal value of zero lift. This "rigid" rotor is also started up from a stopped position. Examination of the results obtained in these computations indicates (1) that reasonable aerodynamic loadings can be predicted for all values of the radial to tangential velocity ratio and (2) that there exist no loading or structural response phenomena for the examined flight condition which would indicate that power loss, braking, and rotor stopping have serious consequences with respect to the creation of unusual blade-wake interaction phenomena.

FOREWORD

The study reported herein was conducted at the Cornell Aeronautical Laboratory, Inc., by Mr. L. Segel during the period May 1965 to December 1966. This program was sponsored by the U. S. Army Aviation Materiel Laboratories, Fort Eustis, Virginia, and was monitored by Mr. J. E. Yeates.

Acknowledgement is made of the invaluable assistance provided by Mr. E. F. Chmielewski (Computer Service Department, CAL) who wrote the digital-computing program.

The guidance and suggestions provided by Mr. F. A. DuWaldt merit recognition.

The author also wishes to thank Messrs. T. T. Chang and F. Fung for their contributions in the development of the equations of motion needed for this study.

TABLE OF CONTENTS

LIST OF ILLUSTRATIONS

LIST OF SYMBOLS

b	semichord, ft
C_D	drag coefficient
C_L	lift coefficient
c	blade chord, ft
$c.p.$	location of center of pressure, measured from leading edge of blade, ft
D	aerodynamic drag, lb
$\overline{D}$	aerodynamic force component parallel to the shaft plane, lb
$\overline{\overline{D}}$	aerodynamic force component along the negative η axis, lb
$\hat{D}$	aerodynamic force component parallel to the root chord, lb
$\dfrac{dC_L}{d\alpha}$	lift-curve slope yielded by two-dimensional wind-tunnel tests, nondimensional
e	chordwise distance of c. g. from the elastic axis
$e_D, \tilde{e}_D$	drag hinge offsets (see Figure 8), ft
e_F	flap hinge offset (see Figure 8), ft
e_H	$e_F + e_D + e_P$, ft
$e_P, \tilde{e}_P, \tilde{\tilde{e}}_P$	feathering hinge offsets (see Figure 8), ft
e_o	distance from feathering axis, x_ψ , to the elastic axis (positive for elastic axis ahead of the feathering axis), ft
e_I	$e_D + e_P$, ft
$f_v^{(p)}(\zeta)$	chordwise displacement as a function of ζ for the pth bending mode, ft/ft
$f_w^{(p)}(\zeta)$	flapwise displacement as a function of ζ for the pth bending mode, ft/ft

$f_\phi^{(q)}(\zeta)$ torsional displacement as a function of ζ for the qth torsion mode, rad/rad

GF generalized force or moment, lb or ft-lb

i an index designating a blade of the rotor

ib an index designating the wake trailed by blade i

j an index designating a spanwise segment of the rotor blade

$k_v^{(p)}$ ratio of the chordwise displacement of the blade tip to the flapwise displacement of the tip in the pth bending mode

L aerodynamic lift, lb

$\bar{L}$ aerodynamic force component along axis perpendicular to the shaft plane, lb

$\underline{L}$ aerodynamic force component along the positive ζ axis, lb

$\hat{L}$ aerodynamic force component perpendicular to the root chord, lb

LCN number of spanwise blade segments

l an index designating a spanwise position in the wake or a segment endpoint on the blade

M Mach number

$M_{1/4}$ aerodynamic pitching moment about the one-quarter chord, ft/sec

m an index designating an instant of time

$\bar{m}$ an index designating an azimuthal position in the wake

NB number of blades

$\bar{Q}$ drive or brake torque applied to rotor shaft, ft-lb

Q_A aerodynamic drag torque of one blade, ft-lb

q generalized displacement, ft or rad

R rotor radius, ft

U total velocity of air relative to blade, ft/sec

U_ζ air velocity relative to the blade along the positive ζ axis, ft/sec

U_η air velocity relative to the blade along the negative η axis, ft/sec

U_ξ air velocity relative to the blade along the positive ξ axis, ft/sec

$\tilde{u}$ x -component of velocity induced by the wake, ft/sec

V forward flight speed, ft/sec

v chordwise displacement of the elastic axis in the positive η direction (see Figure 9), ft

$\tilde{v}$ y -component of velocity induced by the wake, ft/sec

w flatwise displacement of the elastic axis in the positive ζ direction (see Figure 9), ft

$\tilde{w}$ $\tilde{w}_T + \tilde{w}_A$, ft/sec

$\tilde{w}_A$ z -component of velocity induced by wake elements adjacent to the blade, ft/sec

$\tilde{w}_T$ z -component of velocity induced by all free-wake elements other than elements adjacent to blade, ft/sec

$\tilde{w}_b$ z -component of velocity induced by the bound circulation on the blade, ft/sec

x, y, z coordinates of a right-handed orthogonal axis system whose origin and orientation are given by appropriate subscripts

α^{20} $\tan^{-1} \dfrac{U_\zeta}{U_\eta}$, rad

α_s angle of attack of rotor shaft (positive for forward tilt of the rotor shaft), rad

β flap angle of blade relative to the shaft plane (see Figure 8), rad

Γ circulation (either bound or free), ft^2/sec

Γ^* circulation determined by geometric factors and the $\tilde{w}_T$ component of downwash, ft^2/sec

ζ lead-lag angle of blade (see Figure 8), rad

$\bar{\eta}$ η distance from the elastic axis to the three-quarter chord at center of blade segment, ft

θ pitch angle of root chord relative to shaft plane, rad

$\bar{\theta}$ tilt angle of swashplate relative to shaft plane, rad

$\tilde{\theta}$ $\theta + \theta_\zeta + \phi$, rad

$\hat{\theta}$ $\theta + \theta_\zeta$, rad

$\overset{\star}{\theta}$ $\theta_\zeta + \phi$, rad

$\bar{\theta}_{IC}$ cosine cyclic pitch component of swashplate tilt angle, rad

$\bar{\theta}_{IS}$ sine cyclic pitch component of swashplate tilt angle, rad

θ_ζ twist of blade relative to root chord, rad

μ mass moment of inertia about the elastic axis per unit span, lb-sec^2

ξ, η, ζ coordinates of a right-handed orthogonal axis system used to define a point on a blade; an axis system located with its origin at a control point, with ξ and η lying in a plane tangent to the blade; coordinates of wake end points in the x-y-z space defined in Figure 7

ρ density of air, slugs/ft^3

σ generalized symbol for the influence coefficient yielding induced velocity at a specified point per unit strength of vorticity in a given vortex element, 1/ft

$\bar{\sigma}$ induced-velocity coefficient of a spanwise-oriented element of bound vorticity, 1/ft

$\bar{\bar{\sigma}}$ induced-velocity coefficient of a chordwise-oriented element of bound vorticity, 1/ft

ϕ torsional deformation of blade about elastic axis (see Figure 9) rad

ψ azimuth angle of rotor ($\psi = 0$, when reference blade is oriented along positive x axis), rad

Ω angular velocity of rotor, rpm

Note: A single dot over a variable denotes the first time derivative; a double dot denotes the second time derivative.

INTRODUCTION

Accurate prediction of blade loadings, motion, and stress experienced by helicopter rotors in forward flight requires that a multitude of aerodynamic and structural dynamic phenomena be modeled in a comprehensive manner. This analysis objective has led to the performance of many studies [References 1 through 8] which have demonstrated that mathematical models can provide considerable assistance in isolating the factors responsible for the vibratory behavior exhibited by rotary wings. In particular, the development of means for calculating the temporal and spacial distribution of inflow induced by the rotor wake [References 9 through 11] must be cited as a major forward step. This development has made it possible to eliminate the classical simplifying assumption of uniform inflow from rotor-loading calculations, which is a desirable procedure when there is need to predict the higher harmonic components of the excitation and response of the dynamic system represented by the rotary wing.

Wake models enabling the calculation of nonuniform inflow were applied initially in predicting the cyclic or periodic behavior of rotary wings in steady, forward flight. More recently, under the sponsorship of USAAVLABS, a study [Reference 12] was conducted for the purpose of developing a computer methodology suitable for obtaining the non-periodic response of a rotary wing caused by a transient input of blade pitch. In this latter study, it was assumed that the forward flight trajectory of the rotor hub does not vary during the time interval of interest. Further, blade flexibility was neglected since the primary objective was to develop a practical definition of the transient vorticity and geometry of a rotor wake to demonstrate the feasibility of computing the air loads produced during the transient interval. Accordingly, a mathematical model was generated to describe a rotor rotating at a fixed angular

velocity and possessing only a flapping degree of freedom. As was
done in studies of steady-state blade loads, the transport velocities
of elements of wake vorticity were estimated and specified, a priori.
A subsequent comparison of calculations and experimental data dem-
onstrated that the prediction of nonperiodic air loadings on rotary
wings is a feasible task.

The successful completion of this preliminary study led to a
recommendation for introducing additional degrees of freedom into
the model such that blade loadings and elastic motions in the flapwise,
edgewise,and pitchwise directions, as well as the angular-velocity
of the rotor shaft, could be predicted as functions of transient inputs
of blade pitch and/or shaft torque. The recommended research
objective was to obtain an understanding of the dynamics of rotor
blades following a power failure, for example, and to investigate
further rotor behavior during starting and stopping conditions such
as would occur in stopped-rotor designs. Specifically, it was recom-
mended that a study be made to determine the transient response
characteristics of rotary wings as a function of (1) the blade-wake
relationships and (2) the inertial, elastic, and aerodynamic coupling
forces and moments that prevail during the transient interval.

In making this recommendation, it was recognized that the
high advance ratios, associated with stopped-rotor designs, cause
flow conditions in which the existing aerodynamic analysis procedures
for rotors are not valid. The development and validation of theories
suitable for predicting aerodynamic loads on rotor blades at high
advance ratios are held to be a major research task, whose execution
has recently been initiated. Nevertheless, it was essential that some
effort be made, as part of the study documented in this report, to
come to grips with this problem. This was done. From the research
point of view, it is believed that the aerodynamic model developed in

2

this study constitutes a significant first step toward the resolution of the analysis difficulties posed by the operation of rotors at very high advance ratios.

Accordingly, the first part of this report is devoted to presenting the reasoning behind the procedure adopted to compute loadings in the presence of large components of radial flow. Information of interest to the general reader is given in the body of the report, and a more detailed accounting of certain facets of the aerodynamic model are given in Appendix II. Subsequent to the discussion of the development of an aerodynamic theory having increased validity at high advance ratios, a brief description is given of the overall simulation model, again with the details being placed in appropriate appendixes. The computational methodology employed to obtain numerical results is also described briefly. This section is followed by a discussion of the results of calculations that were made using the developed model. Conclusions drawn from these results and recommendations for further research conclude the report.

Throughout the report, TBL-I refers to the computational model developed and reported in Reference [12] for Transient Blade Loads, with TBL-II used to designate the computational model developed in the current study.

3

STATEMENT OF THE PROBLEM

The examination of blade loadings, motions, and stresses occurring during a power loss or during a gradual starting or stopping process is facilitated by expanding the analysis developed in Reference [12] to determine

(1)   the inplane loads

(2)   the pitching moments about the feathering axis (i. e. , the control loads)

(3)   the rigid-blade motions (flap, lead-lag, pitch)

(4)   the flexible blade motions (flapwise and chordwise bending, blade twist) and

(5)   the angular-velocity response of the rotor shaft

as caused by time-varying changes in swashplate displacement and shaft torque.

If a rotor is subjected to a negative angular acceleration as a result of a power loss or a braking torque, advance ratios of increasing magnitude are encountered, which, in the limit, reach infinity when the rotor stops. Thus, the rotor blades will be exposed to a variety of flow geometries that cannot be described adequately by existing aerodynamic analyses. It follows that the requirement to calculate aerodynamic loadings at high advance ratios constitutes the major problem to be resolved in this investigation. In prior studies of rotor air loads, the radial components of flow (i. e. , flow along the blade) have been neglected, thereby permitting the use of two-dimensional section data for lift, drag, and pitching moment. Discrepancies between calculated and measured performance at advance ratios in excess of 0. 3 (e. g.,

4

References [13] and [14]) have indicated the inadequacy of two-dimensional theory at high advance ratios. The question arises as to the upper bound of advance ratio for which a two-dimensional treatment is satisfactory.

In addition to the computational complexities introduced by the use of a more elaborate aerodynamic analysis, the inclusion of the lead-lag, feathering, and blade flexibility degrees of freedom constitutes a significant expansion of the computing program used in TBL-I. A further complication encountered in TBL-II is the loss of the linear relationship between blade azimuth and time as a result of shaft torque being treated as one of the independent variables of the study.

In retrospect, it may be stated that the extension of the analysis procedure described in Reference [12] has consisted of three major tasks. The first task was the development of equations of motion applicable to a variable-rpm rotor (i. e., the rotor has shaft displacement as a degree of freedom) in which each blade can be assumed to have as many as 11 degrees of freedom (three rigid-blade displacements, six coupled flapwise and chordwise bending modes, and two uncoupled torsion modes). The second task was the generation of an aerodynamic model (namely, a system of horseshoe vortices and control points) that yields a distribution of bound vorticity which can be converted to representative loadings for any ratio of radial to tangential flow velocities. The third task consisted of generating a machine-computing program corresponding to the developed mathematical model.

5

THE DEVELOPMENT OF AN AERODYNAMIC MODEL SUITABLE
FOR CALCULATING LOADINGS AT HIGH ADVANCE RATIOS

The aerodynamic model used in TBL-I contained the following assumptions:

1.   The wake is trailed from the trailing edge of the blade and is represented by discrete vortex lines trailed as a consequence of a stepwise rate of change of the total circulation along the span.

2.   Each segment of the blade is treated in accordance with the Prandtl assumption that the bound vorticity on a given section extends continuously in the spanwise direction, resulting in a chordwise distribution of bound vorticity that is characteristic of the two-dimensional airfoil. The consequence of this simplification is that replacement of the chordwise distribution of bound vorticity by a lifting line at the quarter chord results in the requirement for flow tangency at the three-quarter chord being equivalent to finding the lift on a two-dimensional section, operating at an effective angle of attack equal to the free-stream angle of attack minus the angle of attack induced by the free wake.

By restating the above assumptions in mathematical form, the effective "strip" nature of the analysis used in TBL-I becomes clear. With the chordwise distribution of vorticity corresponding to a two-dimensional flow replaced by a "lumped" bound vortex at the quarter chord (extending to plus and minus infinity), the velocity induced by

this bound vortex at the three-quarter chord is

$$\tilde{w}_b = - \frac{\Gamma_j}{2 \pi b_j} \qquad (1)$$

where

$\tilde{w}_b$ is the velocity induced by the bound vortex of infinite length

Γ_j is the strength of the bound vortex at the jth span location with this strength assumed to extend to plus and minus infinity

b_j is the half chord at the jth span location.

For the assumed two-dimensional flow, the requirement for flow tangency at the three-quarter chord may be stated as

$$\tilde{w}_b + \tilde{w}_w(j) + \left(\alpha_j' U_j \right)_{3/4} = 0 \qquad (2)$$

where

$\tilde{w}_w(j)$ is the velocity induced by the free vorticity in the wake at the three-quarter chord of the jth span segment

and

$\left(\alpha_j' U_j \right)_{3/4}$ is the component of the free-stream velocity perpendicular to the blade at the three-quarter chord where α' and U are defined only in terms of velocities lying in a plane perpendicular to the span of the blade.

Equations (1) and (2) yield that

$$\Gamma_j = 2 \pi b_j U_j \left[\alpha_j' + \frac{\tilde{w}_w(j)}{U_j} \right]. \qquad (3)$$

7

On identifying the constant, 2π, as the theoretical lift-curve slope for a two-dimensional flat plate, it is seen that the following holds for a real airfoil:

$$\Gamma_j = b_j \, U_j \, C_\ell(j)$$

where

$C_\ell(j)$ is an experimentally determined lift coefficient for a two-dimensional section at an effective angle of attack equal to $\alpha_j' + \dfrac{\overline{w}_w(j)}{U_j}$.

It is seen that the above model contains the full influence of the three-dimensional wake and, furthermore, retains the advantage of using two-dimensional section characteristics for the airfoil. Although it is possible to compute an asymmetrical loading increment that results from a radial component of the free-stream velocity reacting with chord-wise components of the bound vorticity, this computation is approximate, at best, since the boundary condition as applied does not include this radial component of the free stream.

In order to obtain a calculation procedure that is applicable to the flow regime wherein a high-aspect-ratio wing becomes a very low-aspect-ratio lifting surface, the foregoing "strip" analysis must be modified. One obvious alternative is to utilize a lifting-surface approach. Such an approach would involve a large number of control points and would necessitate computing the velocity induced both by the bound vorticity on the blade and the free vorticity in the wake at each and every control point. For very practical reasons, namely, computer capacity, it was necessary that the number of control points be restricted to a minimum. In addition, it was necessary to adopt a system of vortices for representing a wing in the presence of oblique flow such that the new system reduces to a vortex model that is appropriate for computing loadings at low advance ratios and is, in practice, equivalent to that used previously

8

for the "strip" analysis. A means for checking the reasonableness of the loadings yielded at low advance ratios by the modified aerodynamic calculation procedure is thereby assured.

During the process of developing an aerodynamic model suitable for TBL-II, an examination of the literature indicated that moderately low-aspect-ratio lifting surfaces are characterized by a relatively constant distribution of loading over the span (References [15] through [17]). Moreover, this relatively constant spanwise loading tends to prevail at all positions along the chord. Further, a sheet of vorticity emanates from the side edges of the low-aspect-ratio surface and this sheet proceeds to roll up into two pronounced wing-tip vortices lying above the plane of the wing. For a very low-aspect-ratio surface, it appears appropriate to approximate the observed constant loadings across the span and the existence of the side-edge vortex sheet by the system of horseshoe vortices diagrammed in Figure 1.
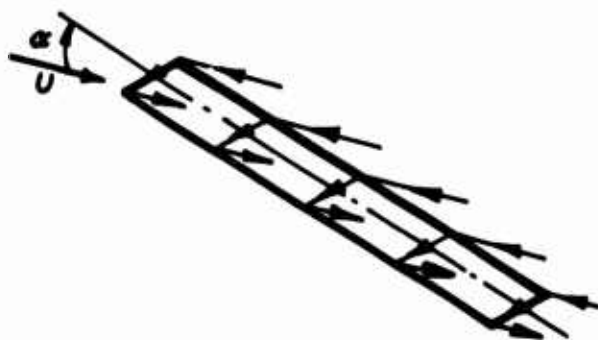
Figure 1. HORSESHOE-VORTEX REPRESENTATION OF A LOW-ASPECT-RATIO SURFACE WITH SHARP EDGES AT THE WING TIPS AT ANGLE OF ATTACK, α.

9

Figure 1, as drawn, is representative of a rotor blade exposed to a completely radial flow. The sharply defined side-edge separation would exist for a lifting surface having very sharp edges at the wing tips. On a helicopter rotor blade, these side edges consist, however, of a rounded leading edge and a sharp trailing edge where "leading" and "trailing" are defined in terms of a flow that is primarily tangential to the blade. With these edge properties present, questions arise as to the manner in which side-edge separation would develop on a rotor blade exposed to an exclusively radial flow. This problem of defining the geometry and location of the vortex sheets emanating from a lifting surface becomes even more difficult when a typical rotor blade is exposed to a flow which is other than completely radial or is exposed to a flow of varying obliquity as caused by a slow rotation rate.

In view of the large gap in our understanding of the manner in which a rounded edge delays the creation of the vortex sheet associated with the long side-edge dimension, the assumption is made, in the TBL-II analysis, that vorticity is never released into the free stream simultaneously from the two radial edges of the blade. Instead, it is assumed that vorticity is released at the sharp trailing edge of the blade whenever the local component of tangential flow is positive and from the rounded leading edge whenever the local component of tangential flow is negative. In this manner, the wake geometry existing at low advance ratios is preserved, such that the single vortex sheet associated with the radial distribution of loading in predominantly tangential flow becomes a single vortex sheet emanating from a long side edge when the flow is exclusively radial. Thus, the wing-tip separation, which is produced by two sharp side edges of a low-aspect-ratio surface exposed to a radial flow (see Figure 1), will take the form diagrammed in Figure 2(a) as a result of the "single-sheet assumption". Further, for an oblique flow condition (e.g., for the case of the blade located in the retreating half of the rotor), it is assumed that the bound and adjacent free vorticity would have the geometry diagrammed in Figure 2(b).

10

(a) A ROTOR BLADE EXPOSED TO A RADIAL FLOW; $\mu = \infty$.

(b) A RETREATING ROTOR BLADE WITH THE INBOARD SECTION LOCATED IN A REVERSED-FLOW REGION.
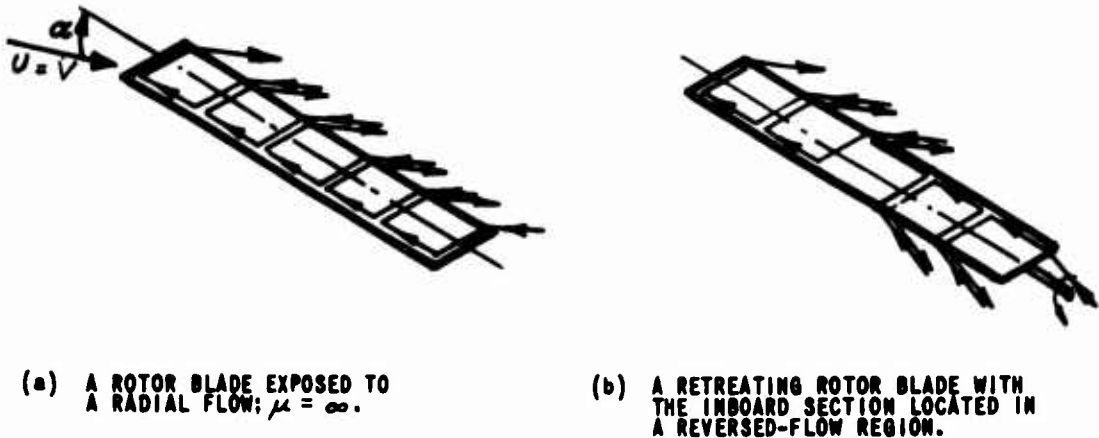
Figure 2. ASSUMED HORSESHOE-VORTEX REPRESENTATION

In this manner, it is possible to extend the "strip" analysis to include the regime of highly oblique flow in which a high-aspect-ratio wing becomes a very low-aspect-ratio lifting surface. First, it is assumed that the high-aspect-ratio loadings, as yielded by the model diagrammed in Figure 3, can be obtained with little loss in accuracy by shifting the spanwise bound vortices from the quarter chord to the leading edge and placing the control point at the midchord (see Figure 4).
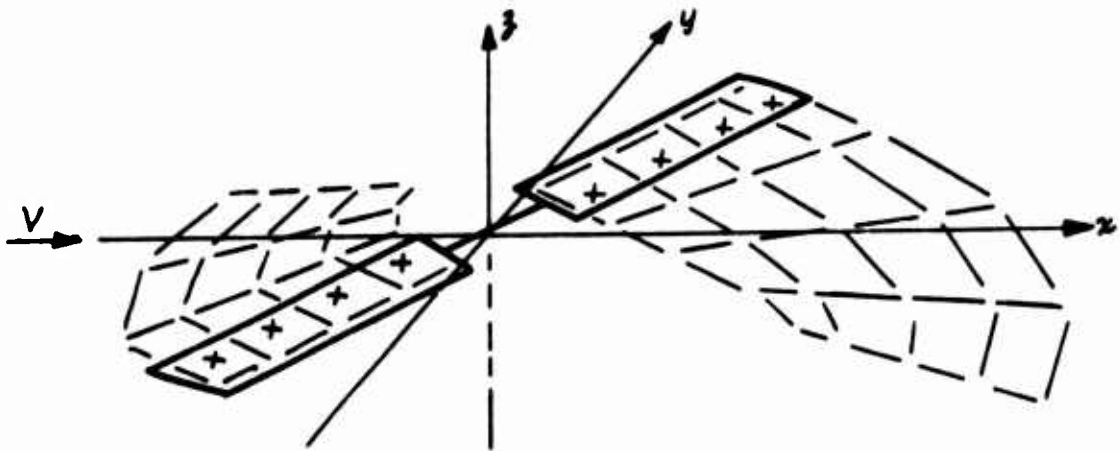
Figure 3. HORSESHOE-VORTEX REPRESENTATION OF A ROTARY WING AT LOW ADVANCE RATIOS.

11

The geometry diagrammed in Figure 4 (specifically,with the bound element of spanwise vorticity located at the leading edge) prevails whenever a given blade section is in a normal flow region. The geometry diagrammed in Figure 4 is reversed (i. e., the bound element of spanwise-oriented vorticity is located at the trailing edge) whenever a given blade section is located in the reversed flow region (i. e., the local tangential component of flow is negative).
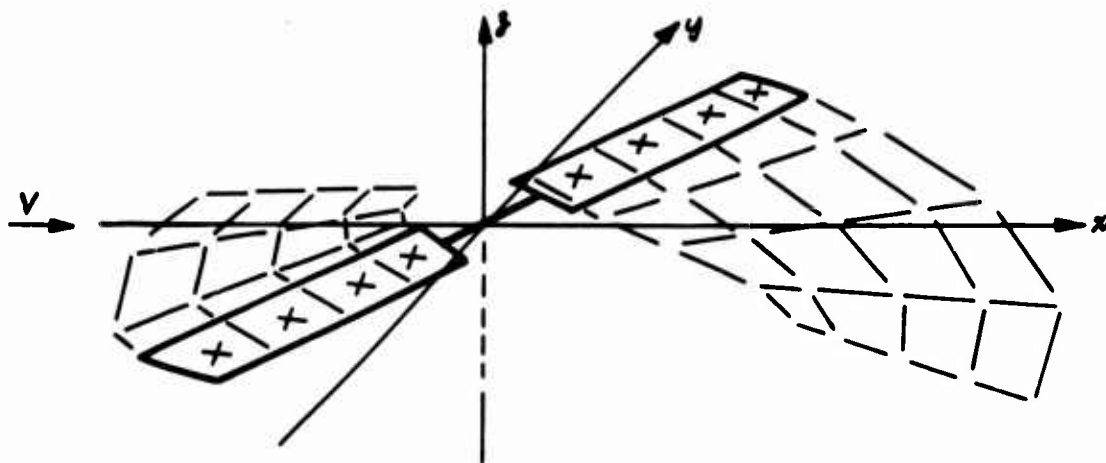
Figure 4.   MODIFIED HORSESHOE-VORTEX REPRESENTATION OF A ROTARY WING: BOUND VORTEX AT LEADING EDGE; CONTROL POINT AT MIDCHORD.

In addition to the assumed shift in (1) the location of the radially oriented bound vortex and (2) the point at which the condition of flow tangency is to be satisfied, it is apparent that the so-called Prandtl simplification cannot be used to satisfy the boundary condition on the low-aspect-ratio blade. Elimination of the Prandtl simplification means that it is necessary to compute, at each control point, the velocities induced by each radial- and chordwise-oriented element of vorticity assumed to represent the lifting surface as well as the velocities

12

induced by the free wake. Further, the boundary condition must be generalized to include all components of the total flow vector relative to the blade segment under consideration. The equations that yield the unknown circulation strengths on the blade accordingly derive from a "three-dimensional" boundary condition; viz.,

$$\widetilde{w}_b(j) + \widetilde{w}_w(j) + U_\zeta(j) = 0 \tag{4}$$

where

$U_\zeta(j)$ is the component of the total free-stream velocity perpendicular to the blade at the control point of the radial segment

and

$\widetilde{w}_b(j)$ and $\widetilde{w}_w(j)$ can be expressed symbolically as

$$\widetilde{w}_b(j) = \sum_{j} \bar{\sigma}_j^{\,i} \, \Gamma_{j-i}$$

$$\widetilde{w}_w(j) = \sum_{ib} \sum_{m} \sum_{i} \sigma'_{ib,m,i} \, \Gamma_{ib,m,i} \tag{5}$$

where

$\bar{\sigma}_i^{\,i}$ and $\sigma'_{ib,m,i}$ are the induced velocity coefficients of the bound and free vorticity, respectively.

Prior to accepting the above-outlined aerodynamic model as a means for determining loadings at high advance ratios and at azimuth angles in the vicinity of 0 and 180 degrees, computations were performed to ascertain whether Equations (4) and (5) yield loadings in agreement with low-aspect-ratio wing theory; namely, the linear theory applicable to vanishingly small angles of attack. If the angle of attack of the blade diagrammed in Figure 2(a) is

13

assumed to approach zero, the f. e vortices trailing radially in the free airstream will lie in the plane of the wing and the resulting system of vortices reduces to the system diagrammed in Figure 5.
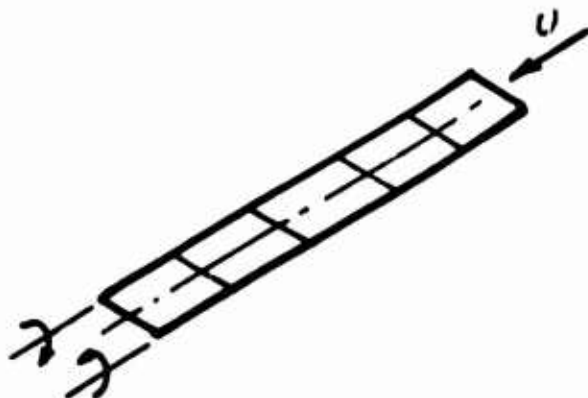
Figure 5.   HORSESHOE-VORTEX REPRESENTATION OF LOW-ASPECT-RATIO WING
AT AN INFINITESIMAL ANGLE OF ATTACK.

A loading calculation, equivalent to linear airfoil theory, consists of evaluating the induced velocity coefficient matrix corresponding to the system of vortices diagrammed in Figure 5. An aspect ratio of 0.1 was selected. Calculations were performed for both 10 and 20 radial segments involving 10 and 20 control points, respectively.

14

For the assumed radial flow with no sideslip component present, the boundary condition expressed for all control points has the form

$$\left[\sigma\right]\left\{\Gamma_j\right\} + \left\{\begin{matrix}\alpha\,U\\\vdots\\\vdots\end{matrix}\right\} = 0 \,.$$

The solution of the above set of equations for the unknown circulations, Γ_j, can be written symbolically as

$$\left\{\frac{\Gamma_j}{U\alpha}\right\} = \left[\sigma\right]^{-1}\left\{\begin{matrix}-1\\\vdots\\\vdots\end{matrix}\right\} \,.$$

The quantities, $\Gamma_j/U\alpha$, are "lumped" values of the chordwise distribution of loading and can be converted to a continuous loading distribution by obtaining the nondimensional variable, $\dfrac{\partial \gamma/\alpha U}{\partial x}$, where x is the distance along the chord and γ is the local strength of the spanwise vorticity as distributed along the chord. The results of the calculation are presented in Figure 6, and it is observed that the chordwise distribution of circulation is characteristic of that exhibited by very low-aspect-ratio surfaces.
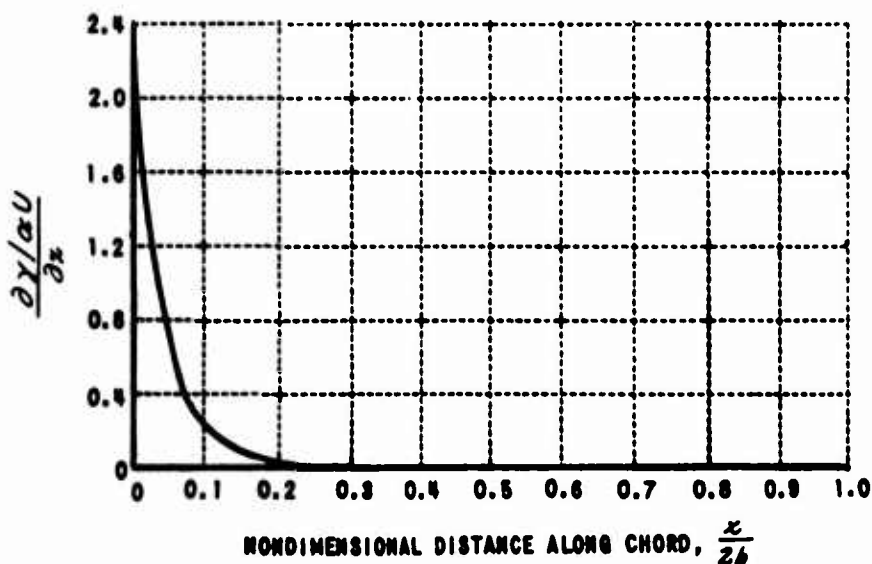
Figure 6. CHORDWISE DISTRIBUTION OF CIRCULATION ON A RECTANGULAR WING OF 0.10 ASPECT RATIO.

On noting that the total lift is given by the following identity:

$$\int_0^c \frac{\partial(\rho U \gamma s)}{\partial x} dx = \rho U^2 C_L b s$$

where

> b is the half chord
>
> s is the span

and

> γ is the local circulation with constant strength across the span,

we find that C_L/α is

$$\frac{C_L}{\alpha} = \frac{1}{b} \int_0^{2b} \frac{\partial \gamma/\alpha U}{\partial x} dx .$$

On performing the integration, we obtain $\frac{C_L}{\alpha} = 0.209$. If the spanwise distribution of circulation had been assumed to be elliptical instead of rectangular, the lift-curve slope would be $0.209 \times \frac{\pi}{4} = .164$, which compares very favorably with the value of 0.157 yielded by the low-aspect-ratio wing theory of Jones (Reference [18]).

The above-described system of horseshoe vortices and locations for satisfying the condition of flow tangency is thus found to yield acceptable chordwise loadings for the low-aspect-ratio case and is known to be a satisfactory approximation of the spanwise distribution of loading for high-aspect-ratio surfaces. As a result of the assumptions made with respect to the convection of the vorticity trailed into the air stream, this aerodynamic model contains the mechanism wherein the loading of the low-aspect-ratio surface becomes a nonlinear function of the angle of attack. Demonstration of the adequacy of the model at the two extremes of aspect ratio forms the basis of the heuristic argument that the model will yield adequate results throughout the spectrum of effective aspect ratios and advance ratios encountered by the blades of a rotary wing.

16

Equation (5) shows that the simple relationship between $\widetilde{w}_{b}(j)$
and Γ_j given by Equation (1) does not hold for the three-dimensional
definition of the boundary condition. Accordingly, it is not possible
to apply the three-dimensional boundary condition and obtain a result
similar to Equation (3) which can be interpreted in terms of empirical
data obtained from two-dimensional tests of various airfoil sections.
Note also that the horseshoe-vortex model in the proposed form will
yield loadings that derive only from circulatory forces. However, it
is most desirable that the model include means for approximating
the influence of viscosity on the slope of the lift curve and means
for introducing forces resulting from viscous effects. Further, the
influence of Mach number on the two-dimensional lift-curve slope
should be accounted for in this analysis in order that the model produce
the same results at low advance ratios as would be obtained from
TBL-I. Finally, it was desirable that means be devised for predicting
the center of pressure location along the tangential direction, irre-
spective of whether the flow past the blade was primarily tangential
or radial, in order to compute pitching moments about the feathering
and elastic axes. These objectives were achieved by appropriate
extensions and modifications of the vortex model, the details of which
are described in Appendix I. The logic for these modifications was
dictated by the requirement that the application of the proper boundary
conditions,when the flow is primarily two-dimensional, should reduce
the model to the one appropriate for the high-aspect-ratio analysis
as used in TBL-I. Appendix I also describes the manner in which
the system of horseshoe vortices placed at the blade are altered
whenever a portion of the blade is in the reversed flow region.

In developing the load-calculation procedure outlined above,
the question arose as to the manner in which to introduce the influence
of a local stalled flow into the three-dimensional boundary condition.
Examination of Equation (4) shows that this formulation of the boundary

17

condition has no built-in "mechanism" for limiting the circulation on the blade as might be caused by flow separation. Since it appeared desirable that some form of stall limit be included, at least for the case where the flow is primarily two-dimensional, means are provided for limiting the bound circulation computed at low advance ratios to the value given by the maximum lift coefficient obtained in two-dimensional wind-tunnel tests.

This limiting procedure is readily implemented by defining the maximum circulation in the jth horseshoe vortex to be given by

$$\Gamma_j)_{max} = b_j \left[U_{\eta_j}^2 + U_{\xi_j}^2 + U_{\zeta_j}^2 \right]^{1/2} C_{\ell}(j)_{max} \tag{6}$$

where

U_{η_j}, U_{ξ_j}, and U_{ζ_j} are the tangential, normal, and radial components of the free-stream velocity at the jth radial segment

and

$C_{\ell}(j)_{max}$ is the local maximum lift coefficient produced in two-dimensional flow.

Note that at low values of advance ratio, Equation (6) yields

$$\Gamma_j)_{max} \cong b_j U_{\eta_j} C_{\ell}(j)_{max} \tag{7}$$

and for the flow condition with predominantly radial flow, yields

$$\Gamma_j)_{max} \cong b_j U_{\zeta_j} C_{\ell}(j)_{max} . \tag{8}$$

It is necessary to show that, whereas Equation (7) does impose a limit on Γ_j for a two-dimensional flow, the same two-dimensional value of $C_{\ell}(j)$ does not impose a similar limit when the flow is predominantly radial. For the radial flow case, the peak value of circulation

18

occurs at the leading edge (i. e., at the tip of the blade) and for the
0.10 aspect-ratio surface treated earlier is given by

$$\Gamma_j)_{peak} \cong 1.6 \, U_\zeta \, \alpha \; .$$

On defining

$$\Gamma_j)_{max} \cong 1.6 \, U_\zeta \, \alpha)_{stall}$$

and on using Equation (8), the stall angle of attack, under conditions
of radial flow, is

$$\alpha)_{stall} \cong \frac{b_j}{1.6} \, C_\ell(j)_{max} \; .$$

On assuming $C_\ell(j)_{max} = 1.3$ (a reasonable assumption for low Mach
numbers), the stall angle of attack for the radial-flow case is approxi-
mately 37 degrees. This angle is sufficiently large to make it apparent
that a limitation, based on the maximum lift-coefficients produced by
the airfoil sections in two-dimensional flow, does not impose a sig-
nificant restriction on the values of lumped circulation that define
the loading when the blade is exposed to a predominantly radial flow.

THE DYNAMICS OF A ROTOR-WAKE SYSTEM

A discussion of the simulation developed to represent the time-varying response of a flexible, rotary wing is facilitated by considering the various simulation submodels that combine to represent the total dynamic system. These submodels are arbitrarily designated here as: (1) the "wake model", (2) the "aerodynamic model", and (3) the "structural model". Their general character and interaction with each other are discussed in this section together with the assumptions and simplifications that were made for purposes of achieving a tractable computer program. A more complete description of the submodels will be found in appendixes to this report.

It proved convenient to develop the TBL-II simulation with two separate aerodynamic submodels. One of the aerodynamic models is a slight extension of that employed in TBL-I in that two-dimensional airfoil data are used to obtain both lift and drag loadings on the blade. The second model is that devised to calculate the loadings on blades exposed to flow of high obliquity. The motivation for incorporating an aerodynamic "strip" theory into TBL-II stemmed from the need to obtain a convenient checking procedure for the digital program itself and from the need to ascertain whether the aerodynamic model suitable for high-advance-ratio calculations produces correct results at low advance ratios.

In developing the TBL-II simulation, a continual compromise had to be made between the objective of achieving broad generality and the requirement for remaining within the capacity of the available computing equipment. In practice, it is very difficult to make this choice since it is not always clear whether a particular feature of the model is a significant determinant of the behavior to be exhibited by the overall system. Experience and judgment are called upon in the selection of the model features outlined in the following sections.

20

AXES, ROTOR GEOMETRY, KINEMATICS

Figure 7 shows the x-y-$\jmath$ axis system selected to define the geometry of the wake. Note that the origin is placed at the hub of the rotor, with the x-axis directed rearward, parallel to the horizontal direction of flight. Figure 7 shows that the rotor shaft is assumed to tilt only in the x-$\jmath$ plane. Thus, we ignore any lateral tilt of the rotor shaft, since the tilt angle is usually small in trimmed, level flight. Both a nonrotating and a rotating set of axes (with the $\jmath_1$ axis aligned along the rotor shaft) are used to define the azimuthal displacement of the rotor. (See Figure 7.) Additional axes are used, as shown in Figures 8 and 9
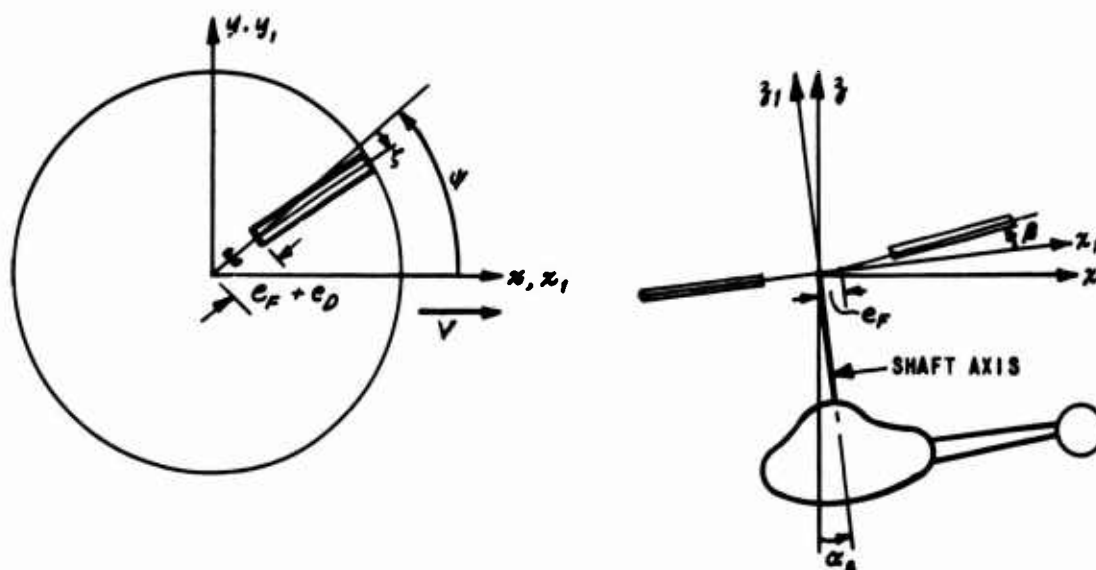
Figure 7. AXES USED TO DEFINE WAKE GEOMETRY AND THE ROTATION OF THE ROTOR SHAFT.

to define the rigid-blade displacements about the flapping, lead-lag, and feathering hinges, respectively. Note that offsets are permitted for these three hinges, with the assumption being made that a blade flaps, lags, and feathers in that order. By means of proper specification of the offset dimensions and by further restriction of the number of rigid-blade degrees of freedom, the fully articulated rotor reduces to a teetering rotor or the so-called "rigid" rotor.
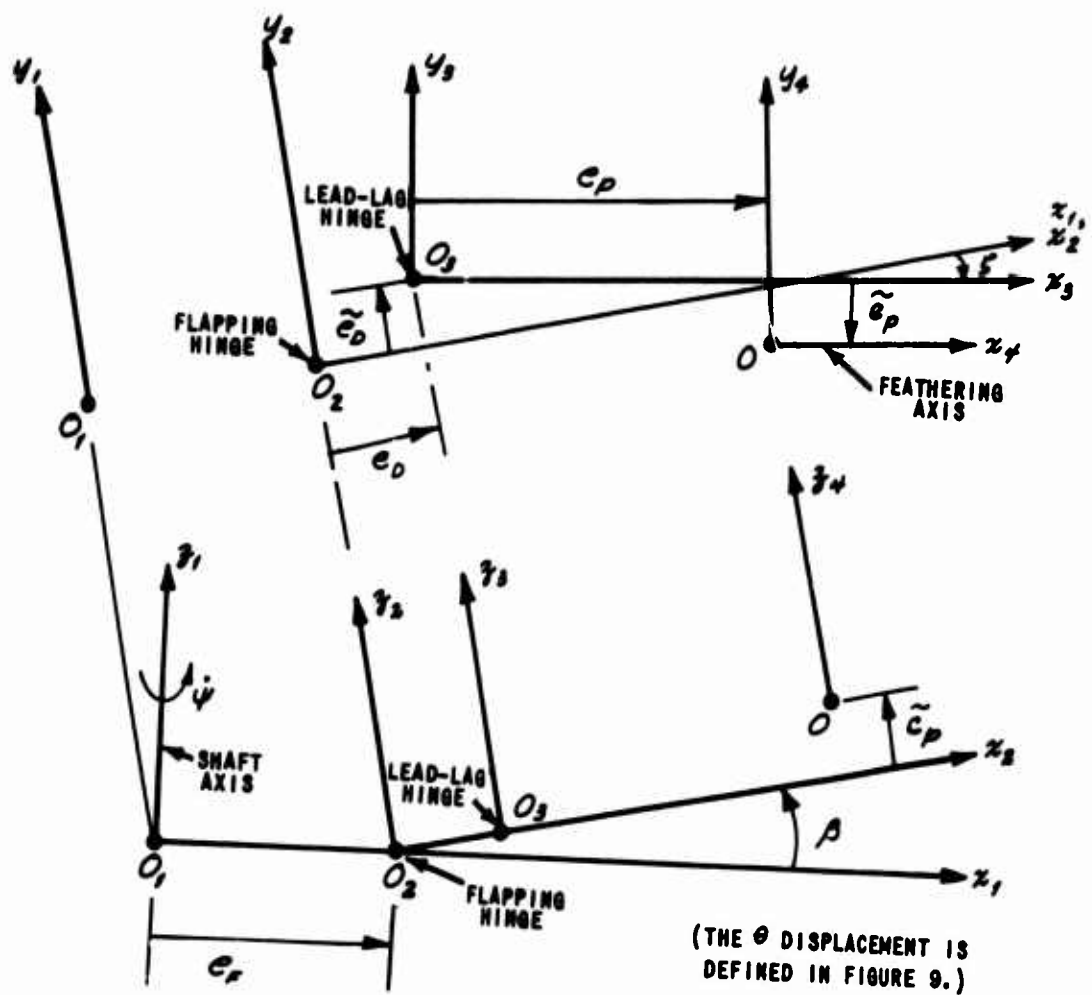
Figure 8. AXES AND HINGE-OFFSET DEFINITIONS FOR THE FLAPPING (β), LEAD-LAG (ζ), AND FEATHERING (θ) DEGREES OF FREEDOM.

The structural degrees of freedom are defined in terms of linear displacements of the elastic axis in the local chordwise and normal directions and of angular displacement about the elastic axis. These displacements are designated in Figure 9, for a given radial location on the blade,
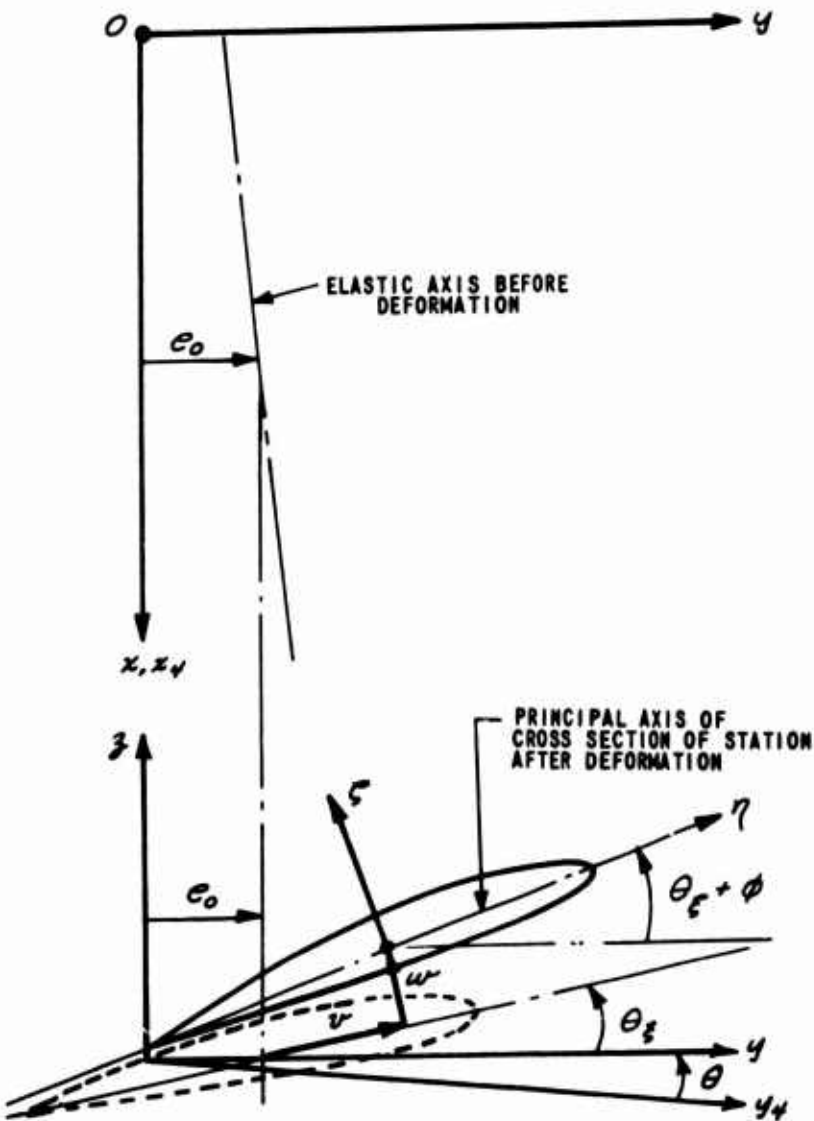
Figure 9. DEFINITION OF THE STRUCTURAL DEGREES OF FREEDOM (v, w, AND ϕ) AND THE FEATHERING DEGREE OF FREEDOM (θ).

as $v, w,$ and $\phi,$ respectively. Without any deformation of the blade, the elastic axis is assumed to be straight but not necessarily parallel to the feathering axis.[*] The location of the elastic axis with respect to the feathering axis, z_f, of the blade is given (as shown) by the dimension e_0, this dimension being a function of radial position along the blade. At any given radial position, a ξ-η-ζ axis system is used to define the radial, chordwise, and normal directions with respect to a plane tangent to the surface of the blade at a specified control point. Figure 10 shows the definition used for angle of attack in the two-dimensional "strip" analysis.

U_ζ — AIR VELOCITY RELATIVE TO THE BLADE ALONG THE POSITIVE ζ AXIS

U_η — AIR VELOCITY RELATIVE TO THE BLADE ALONG THE NEGATIVE η AXIS
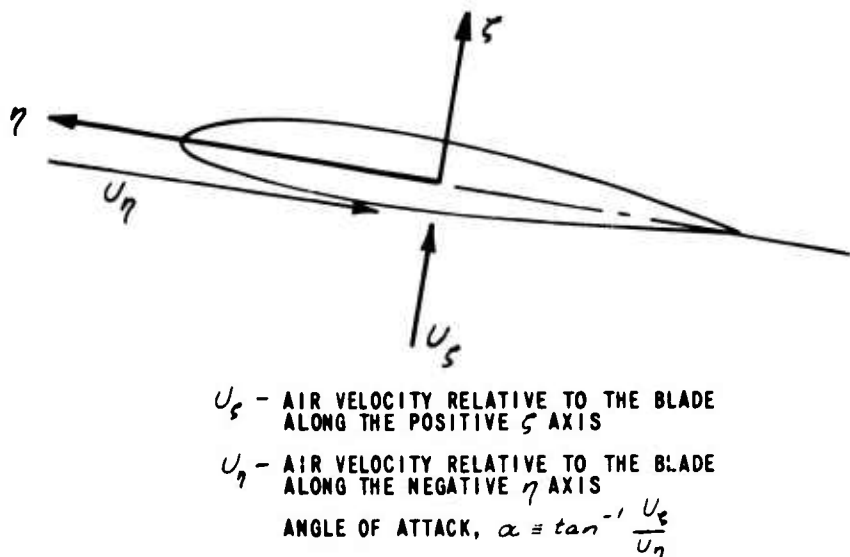
ANGLE OF ATTACK, $\alpha \equiv \tan^{-1} \dfrac{U_\zeta}{U_\eta}$

Figure 10.   DEFINITION OF ANGLE OF ATTACK APPLICABLE TO LOW-ADVANCE-RATIO CALCULATIONS.

---

[*] A slight inconsistency exists in the analysis as a result of assuming that the built-in twist of the blade is defined with respect to the elastic axis in deriving the structural equations of motion, whereas in the kinematic analysis, it was assumed that the built-in twist is defined with respect to the feathering axis. In actual practice, a blade is twisted about neither of these axes. This discrepancy is not considered to be significant.

In the three-dimensional analysis, U_f is defined to include the velocity induced by the free wake but does not include the velocity components caused by bound vorticity. (Note that the kinematic analysis required to express displacements and velocities in an appropriate reference system is given in Appendix I.)

WAKE MODEL

The wake model employed in TBL-II is similar to that utilized in TBL-I with a few minor exceptions. Although the TBL-II analysis contains higher frequency motions as a result of simulating blade flexibility, the vorticity shed parallel to the trailing edge of the blade, as a result of the time rate of change of bound vorticity on the blade, has been neglected as was done in TBL-I. In effect, a quasi-static approach is used in computing aerodynamic loadings, and this approach is equivalent to stating that the influence of the shed vorticity in the wake is second order in comparison with the influence of the trailing-vortex system.

The indexing procedure defined in Figure 11 is identical to that employed in TBL-I and serves as a convenient means of identifying the variables in the analysis. As before, m designates an instant of time; i, a blade of the rotor; j, the spanwise location of a control point; ib, the wake trailed by blade i; $\bar{m}$, an azimuthal position in the wake; and ℓ, a spanwise position in the wake or the spanwise location of a blade-segment end point. For computing the matrix of induced-velocity coefficients, the Biot-Savart law was applied as described in the appendix of Reference [12].

It was again assumed that only the γ-component of induced velocity need be retained in the analysis.

25
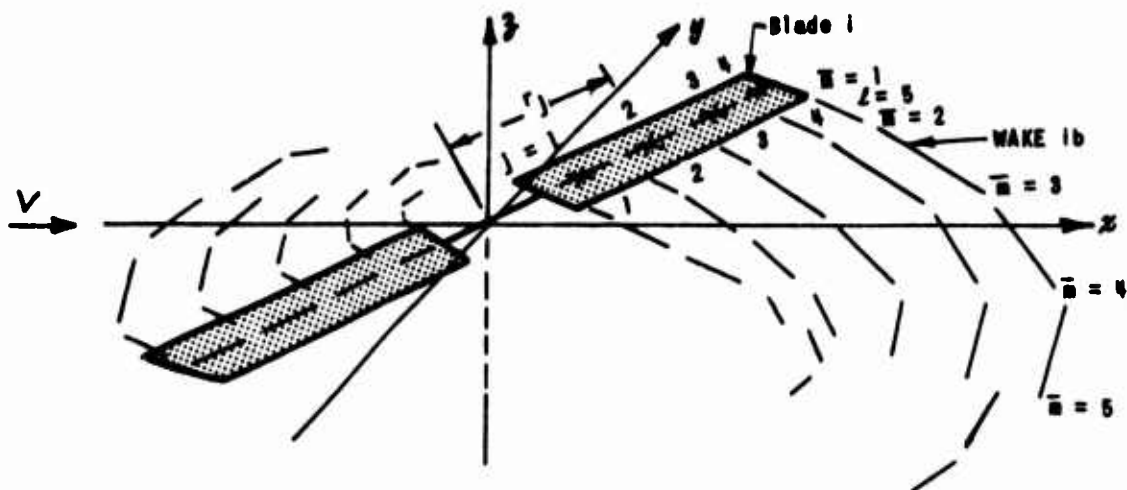
Figure 11.   INDEXING PROCEDURE USED TO DESIGNATE BLADE SEGMENTS,
CONTROL POINTS, AND WAKE LOCATIONS.

As was done in TBL-I, the wake geometry is arbitrarily spec-
ified. However, the specification procedure has been altered. In
TBL-II, the vertical transport velocity (assumed, as before, to be equal
to the momentum value of downwash) is continuously computed as a function
of the instantaneous value of the total thrust produced by the rotor. This
modification has greatly simplified the computational procedure in that it
is no longer necessary to predict in advance the transient variation in
the mean, induced downwash that will occur as a result of a control in-
put. In effect, the original "open-loop" procedure for specifying wake
geometry has been converted into a "closed-loop" procedure based on
the assumption that elements of trailing vorticity are transported in the
vertical direction with a constant velocity component equal to the momen-
tum-theory value of the downwash that existed at the instant that the vor-
tex element was trailed into the wake.

26

AERODYNAMIC MODEL

For reasons of obtaining a numerical check at low advance ratios, the computational program developed in TBL-II provided for two aerodynamic models. The first model was that developed in TBL-I, subsequently augmented to permit the use of nonlinear aerodynamic data applicable to a 360-degree range in angle of attack. The second model was derived from the bound-vortex and free-wake geometry that was adopted to represent a lifting surface which alternately changes from a high-aspect-ratio to a low-aspect-ratio surface. In both instances, it was assumed that the continuous distribution of vorticity on the blade, with respect to the radial coordinate and time, can be adequately defined by using a sufficient number of blade segments and azimuth intervals, over which segments and intervals the vorticity is assumed to be constant.

At each solution interval, the unknown bound circulations on the blade must have values such that the requirement for flow tangency is satisfied at each control point. The equations for the unknown circulations accordingly derive from the boundary condition. Since the velocities induced at the control points by either the free or bound vorticity can be expressed (by means of the Biot-Savart law) in terms of the prevailing geometry and the strengths of all vortex elements, the boundary condition reduces to equations that involve current and past circulation strengths and the specified geometry of the wake.

In solving the equation set resulting from the "strip" analysis, a nonlinear variation of lift coefficient with angle of attack requires that an iterative scheme be used. It was convenient to start the solution process by first solving a linearized formulation of the boundary condition.

The linear equations that result for the "strip" analysis (see Appendix in Reference [12]) can be indicated symbolically as

$$\left[\sigma_{ib,k}^{i,j} \right]_m \left\{ \Gamma_{m,i,j} \right\} = \left\{ \Gamma_{m,i,j}^{g} \right\}$$

27

where the column matrix, $\{\Gamma_{m,i,j}\}$, represents the unknown circulation strengths. The column matrix, $\{\Gamma'_{m,i,j}\}$, represents the portion of the circulation at each spanwise segment determined by all contributions to the local angle of attack, other than the contribution deriving from the unknown circulations. The square matrix, $\left[\sigma_{ib,1}^{i,j}\right]_m$, is derived from induced velocity coefficients that apply only to elements of wake vorticity adjacent to the blade. These elements are assumed to have the same strength as the unknown bound vorticity on the blade.

The "geometric" circulations, $\Gamma'_{m,i,j}$, are determined by the so-called "geometric" angles of attack which are functions of (1) the orientation and velocity of a given blade segment (namely, blade kinematics) and (2) the velocity induced by all elements of the wake, except those elements adjacent to the trailing edge of the blade. Thus, the downwash created by the wake is arbitrarily divided into two parts. The first part of the downwash, $\tilde{w}_T$, is given by the following summation

$$\tilde{w}_{T_{m,i,j}} = \sum_{ib=1}^{NB}\left\{\sum_{\bar{m}=3}^{MBLM}\sum_{\ell=1}^{LCN+1}\sigma_{ib,\bar{m},\ell}^{m,i,j}\left[\Gamma_{ib,m-\bar{m}+2,\ell} - \Gamma_{ib,m-\bar{m}+2,\ell-1}\right]\right.$$

$$\left. + \sum_{\bar{m}=MBLM+1}^{NAWRP}\bar{\Gamma}_{ib,m-\bar{m}+2}\left[\sigma_{ib,\bar{m},1}^{m,i,j} - \sigma_{ib,\bar{m},2}^{m,i,j}\right]\right\} ; \quad m \geq 2$$

where the summation from $\bar{m}=3$ to $\bar{m}=MBLM$ represents the nonrolled wake exclusive of the elements adjacent to the blade. It should be noted that all of the circulations, Γ, in the above expression are known since they are computed at an earlier time and thus correspond to what can be referred to as the "old" wake. The second part of the downwash is designated as $\tilde{w}_A$ and is given by the summation

$$\tilde{w}_{A_{m,i,j}} = \sum_{ib=1}^{NB}\sum_{\ell=1}^{LCN}\Gamma_{m,ib,\ell}\left[\sigma_{ib,2,\ell}^{m,i,j} - \sigma_{ib,2,\ell+1}^{m,i,j}\right]$$

28

where the circulations, Γ , in this expression are the unknown strengths of the elements of "new" wake adjacent to the blade.

On obtaining a solution to the linearized equation set, wherein Γ^g is defined as a function of $\tilde{w}_T$, the iterative process is initiated by computing $\tilde{w}_A$ and then correcting the angle of attack of each blade segment to reflect the influence of the adjacent ("new") wake. A new set of lift coefficients is obtained using the experimental data, and the bound circulations of the blade are redefined. By recalculating the downwash caused by the adjacent wake, $\tilde{w}_A$, this process is repeated until the changes computed in $\Gamma_{m,i,j}$ are either less than a specified percentage or less than a specified small number. (It should be noted that a Gauss-Seidel solution procedure is required, along with an averaging technique for Γ and $\tilde{w}_A$, in order to converge rapidly to a stable solution.)

The linear equations that result from the "three-dimensional" boundary condition (see Appendix II) can be indicated symbolically as

$$\left[\bar{\sigma}_{0_{ib,l}}^{i,j} \right]_m \left\{ \Gamma_{m,i,j} \right\} = \left\{ \tilde{w}_{m,i,j}^g \right\}$$

where the column matrix $\left\{ \Gamma_{m,i,j} \right\}$ represents, as before, the unknown circulation strengths. The column matrix $\left\{ \tilde{w}_{m,i,j}^g \right\}$ represents that portion of the velocity perpendicular to the blade (at the control point) resulting from the motion and displacement of the blade and the downwash created by the "old" wake. The square matrix, $\left[\bar{\sigma}_{0_{ib,l}}^{i,j} \right]$, represents the induced-velocity coefficients that yield the downwash created by all of the unknown vorticity, both bound and free, where the free vorticity is only that portion of the wake immediately adjacent to the trailing edge of the blade. If particular values of $\Gamma_{m,i,j}$ obtained from the solution of the above equation set should exceed a maximum value of circulation, calculated on the basis of a

29

two-dimensional stall condition, the vorticity deposited in the free wake is arbitrarily limited to the computed stall value. The induced velocity components, $\tilde{w}_A$, are then computed using the stall-limited value of circulation.

The remaining features of the aerodynamic model are concerned with the manner in which the computed circulations for the bound vortices representing the blade are converted to normal and tangential loadings in pounds per foot of radial distance and to pitching moments about a radial axis. In the two-dimensional "strip" analysis, experimental values of lift and drag are converted to a normal force and a chordwise force. Further, the location of the center of pressure is obtained from available experimental data as a combined function of angle of attack and Mach number. (See Appendix II for details.)

As was discussed previously, a fulfillment of the three-dimensional boundary condition yields circulatory forces that derive only from potential flow considerations. Accordingly, provision was made for adding a tangential (i.e., chordwise, for the high-aspect-ratio surface) viscous force to the circulatory forces which derive from the radial and tangential components of the bound vorticity representing the blade. In accordance with the Kutta-Joukowski law, the radial components of vorticity cause both a normal and a chordwise loading (in pounds per foot of rotor radius). However, the tangential elements of vorticity and the radial component of flow velocity cause a concentrated load at a given radial position. This load must subsequently be converted into a distributed loading having units of pounds per foot of rotor radius. It is assumed that the tangential location of the center of pressure for each radial segment is the same as that measured for the two-dimensional airfoil section at the angle of attack of that segment. In this regard, the angle of attack is defined in the plane normal to the spanwise axis of the blade segment. Not only does this provide

30

a valid approximation for the high-aspect-ratio wing, but it also
yields the proper tangential location for the center of pressure in
the low-aspect-ratio case.

STRUCTURAL MODEL

Lagrangian procedures were utilized to determine the equa-
tions of motion that yield the accelerations of the blades in their rigid
and elastic degrees of freedom. The resulting inertial and elastic
parameters increase geometrically as the number of degrees of
freedom used to represent the system is increased. Accordingly,
engineering judgment was applied to reduce the number of terms
that result from a mathematical expansion of the total kinetic and
potential energy of the system. This reduction was accomplished by
dropping terms acknowledged to be second order at various stages
of the expansion. However, considerable care had to be exercised
in order not to oversimplify prior to carrying out the required partial
derivatives.

An excellent example of the magnitude of the task and the
complexity of the result that is obtained upon choosing to define the
kinetic and potential energy in complete detail is given by Lemnios
in Reference [6]. Unfortunately, the equations derived in this latter
work could not be reduced to the equations required for the TBL-II
study. (In particular, the equations[*] presented in Reference [6]
did not include a degree of freedom corresponding to an angular-
displacement response of the rotor shaft.) For the purposes of
this study, it was necessary to express the Lagrangian of the system

---

[*]These equations are applicable to rotors assumed to have a flapping,
feathering, lagging, and servo-flap deflection degree of freedom,
including a single flatwise bending mode.

31

in terms of four rigid-blade degrees of freedom (i. e., ψ, β, ζ, and θ) and a finite number of degrees of freedom associated with blade flexibility. On assuming that a flexible blade can bend in both the flatwise and chordwise directions and can also twist about an axis defined as the elastic axis, a choice exists for representing the blades by means of a finite number of lumped mass and elastic segments or by means of a finite number of assumed radial functions. By assuming radial functions that correspond to the resonant vibration modes possessed by the rotor blade rotating in a vacuum, the number of radial functions required to represent the infinite number of elastic degrees of freedom with a given level of accuracy is significantly less than would be required if radial functions were assumed on a completely arbitrary basis.

For purposes of the TBL-II study, the elastic response of a rotary wing was assumed to be described by a finite number of coupled flatwise- and chordwise-bending modes plus a finite number of torsional modes. (Although the number of assumed modes should theoretically be a function of the highest frequency present in the disturbance function, in practice this number is very often determined by computational restrictions.) With reference to this study, it is clear that radial functions based on the vibration modes exhibited by the rotor at its normal revolution rate should give acceptable answers whenever the rotor is rotating at this rate or very close to this rate. When the rotor runs at revolution rates other than the normal value, the resonant frequencies and associated mode shapes are altered. In the TBL-II analysis, it is assumed that these mode shapes do not change to an appreciable extent as the revolution rate of the rotor is varied. Accordingly, it is assumed that the mode shapes calculated for the normal revolution rate remain good approximations of the resonant response characteristics of the rotor. Admittedly, this assumption can be viewed as being rather drastic if it is intended to make transient-response calculations in which the rotor approaches or achieves a near-zero or zero revolution

32

rate. It shall suffice to state here that assumed modes of constant character* are used to represent the structural dynamics of the rotor, and that the actual extent to which these assumed modes lead to inaccuracies at rotational speeds other than the nominal value cannot be stated without conducting an extensive investigation of this aspect of the problem. Further, it can be argued that the assumption of mode shapes should not be a matter of concern in light of the assumptions and approximations that are necessarily made to calculate the aerodynamic forces on the blade.

In deriving the Lagrangian of the rotor system, the potential energy of the system is assumed to derive only from the strain energy existing in each flexible blade, with the gravitational energy resulting from the displacements of the rigid blade being ignored. Further, no structural damping has been included in the formulation other than the structural damping assumed to exist in the torsion degree of freedom. It should be noted that the potential energy of the twisted-rotating beam has been defined in accordance with the theory outlined in Reference [19], as further discussed in Reference [8]. In view of the rather complete discussion in this latter reference, the details of this portion of the analysis are not included in this report. It should be noted, however, that the following assumptions have been made in deriving the strain energy of a twisted, rotating beam:

1. Elementary beam theory is applicable.

2. Rotor-blade cross sections are symmetrical with respect to the major neutral axis; hence, the c.g. of the cross section lies on the major neutral axis.

3. Gravity forces are negligible relative to centrifugal and elastic forces.

---

*Although the mode shapes remain fixed, the modal frequencies are a function of the revolution rate.

4. Elastic deformations of the rotor blade are small
with respect to the radius of the blade.

The derivation of the equations of motion for an articulated
rotor, which has the hinge-offset geometry diagrammed in Figure 6,
is presented in Appendix III. A specification of the boundary conditions
at the root of the blade and a designation of the allowable degrees of
freedom cause these equations to reduce to a form applicable to the
"rigid" rotor (i.e., no β and ζ degrees of freedom, with a cantilever
constraint at the hub) and to the teetering rotor (i.e., no ζ degree of
freedom, and an effective cantilever constraint for the symmetric
bending modes and an effective pin restraint for the antisymmetric
bending modes, including the flapping mode).

For the general case (i.e., the number of flexible response
modes are not specified), the equations of Lagrange yield that:

$$\frac{d}{dt}\left(\frac{\partial T}{\partial \dot{\psi}}\right) - \frac{\partial T}{\partial \psi} \qquad = \text{external torque about rotor shaft.}$$

$$\frac{d}{dt}\left(\frac{\partial T}{\partial \dot{\beta}_i}\right) - \frac{\partial T}{\partial \beta_i} \qquad = \text{external moment about flap hinge of blade } i.$$

$$\frac{d}{dt}\left(\frac{\partial T}{\partial \dot{\zeta}_i}\right) - \frac{\partial T}{\partial \zeta_i} \qquad = \text{external moment about lead-lag hinge of blade } i.$$

$$\frac{d}{dt}\left(\frac{\partial T}{\partial \dot{\theta}_i}\right) - \frac{\partial T}{\partial \theta_i} \qquad = \text{external moment about feathering axis of blade } i.$$

$$\frac{d}{dt}\left(\frac{\partial T}{\partial \dot{w}_i^{(r)}}\right) - \frac{\partial T}{\partial w_i^{(r)}} + \frac{\partial U}{\partial w_i^{(r)}} \qquad = \text{generalized force corresponding to } r^{th}\text{ bending mode of blade } i.$$

$$\frac{d}{dt}\left(\frac{\partial T}{\partial \dot{\phi}_i^{(s)}}\right) - \frac{\partial T}{\partial \phi_i^{(s)}} + \frac{\partial U}{\partial \phi_i^{(s)}} \qquad = \text{generalized force corresponding to } s^{th}\text{ torsion mode of blade } i.$$

34

The foregoing equations of motion for blade i are a coupled set since the inertial, centrifugal, and elastic forces (as expressed by the left-hand side) and the external forces (as expressed by the right-hand side) are functions of all of the degrees of freedom possessed by blade i. Further, the equations for blade i = 1 are coupled with the equations for blades i = 2, 3, 4,... through the ψ degree of freedom which is common to all blades. Thus, the total number of equations defining the response of an articulated rotor is equal to the number of rotor blades multiplied by the assumed number of blade degrees of freedom plus the shaft degree of freedom. If, for example, six bending modes and two torsion modes are assumed to describe the elastic response of a blade, then an articulated blade (i.e., one with a flapping, lagging, and feathering degree of freedom) would possess 11 degrees of freedom plus the ψ degree of freedom. A four-bladed rotor would be described by a coupled set of 45 equations of motion; a two-bladed rotor by a coupled set of 23 equations.

In order to minimize the numerical difficulties that accompany the simultaneous solution of large numbers of equations, the equation for the shaft-rotation degree of freedom was reduced to its simplest form and solved independently. The resulting, approximate solution for $\ddot{\psi}$ can then be substituted into the remaining equations, which can be solved in groups corresponding to a set for each blade. Thus, instead of determining the modal accelerations from a simultaneous solution of, say, 23 equations for a two-bladed rotor, these accelerations can be computed by performing an independent solution of two groups of equations consisting of 11 equations per blade. The lead-lag acceleration calculated for each blade can then be used to correct the approximate solution for the angular acceleration of the rotor shaft, and this process can be repeated to convergence.

In writing the equations of motion for a rotor, it is convenient to use a matrix notation where the indices m and i indicate an instant

35

of time and a blade, respectively. With the symbol q used to desig-
nate a generalized coordinate, i.e.,

$$\left\{ q \right\}_{m,i} \equiv \left\{ \begin{array}{c} q^{(1)} \\ q^{(2)} \\ \cdot \\ \cdot \\ \cdot \\ \cdot \\ \cdot \\ q^{(11)} \end{array} \right\} \equiv \left\{ \begin{array}{c} \beta \\ \zeta \\ \theta \\ w^{(1)} \\ \cdot \\ w^{(6)} \\ \phi^{(1)} \\ \phi^{(2)} \end{array} \right\} ,$$

the equations of motion for a given blade can be represented (symbolically)
as

$$\left[A \right]_{m,i} \left\{ \ddot{q} \right\}_{m,i} = \left\{ A_{\psi q} \right\} \ddot{\psi}_m + \left\{ \Lambda \right\}_{m,i} \tag{9}$$

where

$\left[A \right]_{m,i}$ is an 11 by 11 square matrix of inertia coefficients,

$\left\{ \ddot{q} \right\}_{m,i}$ is a column matrix of 11 generalized accelerations,

$\left\{ A_{\psi q} \right\}_{m,i}$ is a column matrix of 11 coefficients defining the inertial coupling between $\left\{ \ddot{q} \right\}$ and $\ddot{\psi}$, and

$\left\{ \Lambda \right\}_{m,i}$ is a column matrix of 11 quantities representing the combined forces resulting from centripetal and Coriolis accelerations, elastic deformations, and aerodynamic loadings.

The solution of Equation (9), yielding generalized accelerations, veloc-
ities, and displacements, can be expressed as follows:

36

$$\left\{ \ddot{q} \right\}_{m,i} = \left[A \right]_{m,i}^{-1} \left[\left\{ A_{\psi q} \right\} \ddot{\psi}_m + \left\{ \Lambda \right\}_{m,i} \right]$$

$$\left\{ \dot{q} \right\}_{m+1,i} = \int_{t_m}^{t_{m+1}} \left\{ \ddot{q} \right\}_{m,i} dt$$

$$\left\{ q \right\}_{m+1,i} = \int_{t_m}^{t_{m+1}} \left\{ \dot{q} \right\}_{m,i} dt$$

Figure 12 is a block diagram of the manner in which the right-hand side of Equation (9) was subdivided for ease of computation. The integrals comprising the coefficients in the indicated square and column matrices are tabulated in Table IV, to be found in Appendix III. The external force, $\left\{ GF \right\}_{m,i}$, shown in Figure 12, is the generalized force resulting from aerodynamic loadings, control-linkage forces, etc. The integrals yielding the generalized forces acting on each blade are given in Appendix IV.

On assuming six modes of coupled flatwise and chordwise bending, and two modes of torsion to represent the elastic response of a flapping, lagging, and feathering blade, one finds that 455 integrals must be evaluated to define the inertial, centrifugal, and elastic properties of a flexible, articulated blade. The tabulation of these 455 integrals has been omitted from this report since they represent only a detailed expansion of the integrals defined in Table IV.

However, it is pertinent to indicate the form of the inertia matrix, $\left[A \right]$, for the ith articulated blade prior to defining the equations of motion that apply to a two-bladed, teetering rotor. If the bending and flapping modes are derived as orthogonal modes, and if the two torsional modes are assumed to be orthogonal to each other,
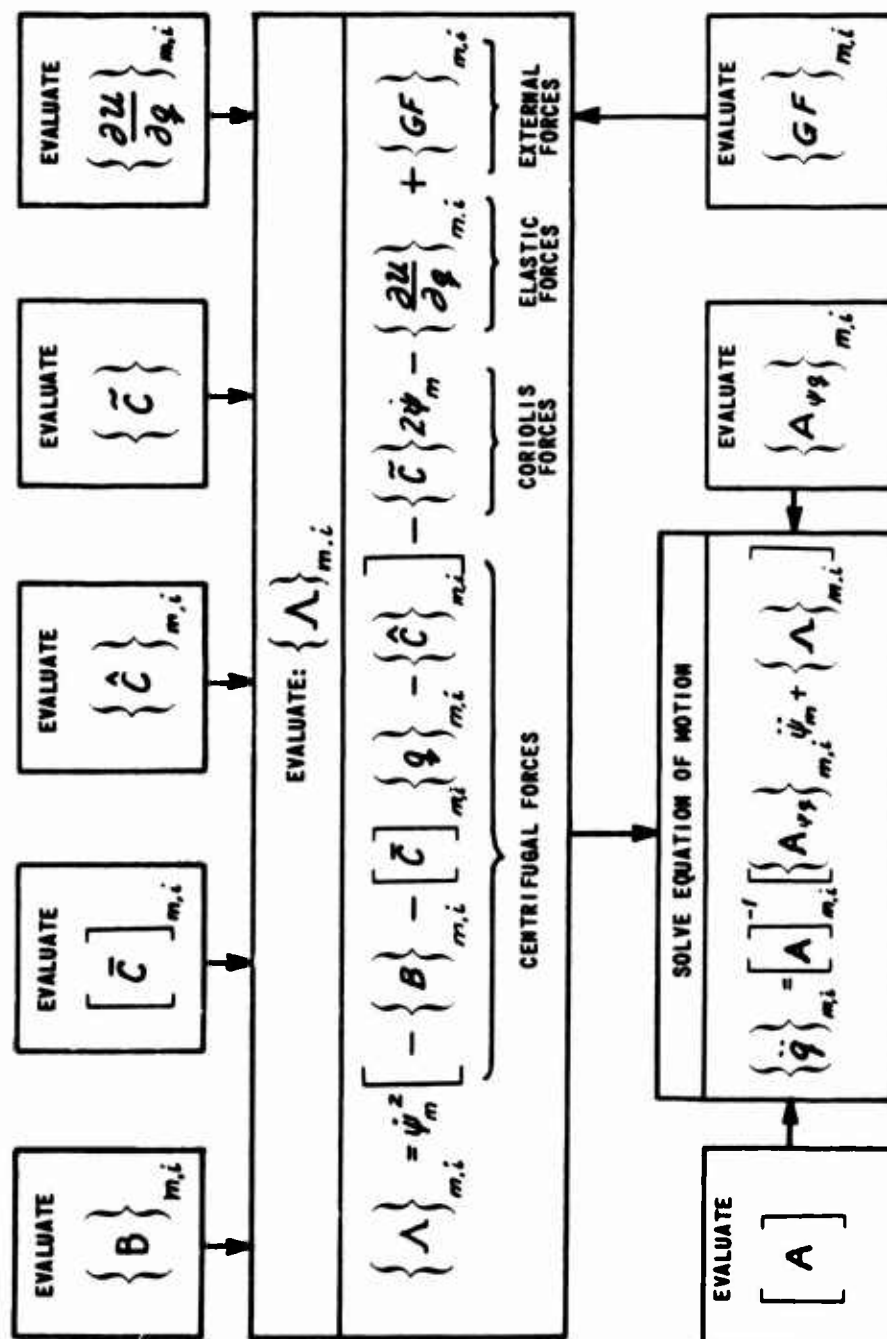
Figure 12. TBL-II EQUATIONS OF MOTION IN BLOCK-DIAGRAM FORM.

38

the inertia matrix for the ith articulated blade has the form indicated in Figure 13. Note that the generalized accelerations $\ddot{q}^{(4)}$ through $\ddot{q}^{(9)}$ are bending accelerations and the accelerations $\ddot{q}^{(10)}$ and $\ddot{q}^{(11)}$ are torsional accelerations.

In a teetering rotor, the lead-lag degree of freedom does not exist, and it is convenient to assume that the $q^{(4)}$, $q^{(5)}$, and $q^{(6)}$ degrees of freedom represent antisymmetric bending modes of the pinned, two-bladed rotor. On letting the $q^{(7)}$, $q^{(8)}$, and $q^{(9)}$ degrees of freedom represent symmetric bending modes of the rotor, and on summing the inertial, centrifugal, and elast c forces/moments over the entire rotor from blade tip to blade tip, equations of motion for a teetering rotor can be derived in terms of the same integrals used for the articulated blade. These equations are presented in Figure 14. It should be noted that only one torsion mode has been assumed to represent the elastic twist of the blades. It has further been assumed that each blade of a teetering rotor both pitches (against a flexible control link) and twists independently of the other blade. With these assumptions, a teetering rotor has 11 degrees of freedom, as is indicated in Figure 14. The kinematic constraints resulting from the assumed division of symmetric and antisymmetric modes require that

$$\ddot{q}_2^{(3)} = \ddot{\beta}_2 = -\ddot{\beta}_1 = -\ddot{q}_1^{(3)}$$

$$\ddot{q}_2^{(4)} = -\ddot{q}_1^{(4)}$$

$$\ddot{q}_2^{(5)} = -\ddot{q}_1^{(5)}$$

$$\ddot{q}_2^{(6)} = -\ddot{q}_1^{(6)}$$

$$\ddot{q}_2^{(7)} = \ddot{q}_1^{(7)}$$

$$\ddot{q}_2^{(8)} = \ddot{q}_1^{(8)}$$

$$\ddot{q}_2^{(9)} = \ddot{q}_1^{(9)}$$

$$
[A]_{m,i} \left\{ \ddot{q} \right\}_{m,i} =
\begin{bmatrix}
A_{1,1} & 0 & A_{1,3} & 0 & 0 & 0 & 0 & 0 & 0 & A_{1,10} & A_{1,11} \\
0 & A_{2,2} & A_{2,3} & A_{2,4} & A_{2,5} & A_{2,6} & A_{2,7} & A_{2,8} & A_{2,9} & A_{2,10} & A_{2,11} \\
A_{3,1} & A_{3,2} & A_{3,3} & A_{3,4} & A_{3,5} & A_{3,6} & A_{3,7} & A_{3,8} & A_{3,9} & A_{3,10} & A_{3,11} \\
0 & A_{4,2} & A_{4,3} & A_{4,4} & 0 & 0 & 0 & 0 & 0 & A_{4,10} & A_{4,11} \\
0 & A_{5,2} & A_{5,3} & 0 & A_{5,5} & 0 & 0 & 0 & 0 & A_{5,10} & A_{5,11} \\
0 & A_{6,2} & A_{6,3} & 0 & 0 & A_{6,6} & 0 & 0 & 0 & A_{6,10} & A_{6,11} \\
0 & A_{7,2} & A_{7,3} & 0 & 0 & 0 & A_{7,7} & 0 & 0 & A_{7,10} & A_{7,11} \\
0 & A_{8,2} & A_{8,3} & 0 & 0 & 0 & 0 & A_{8,8} & 0 & A_{8,10} & A_{8,11} \\
0 & A_{9,2} & A_{9,3} & 0 & 0 & 0 & 0 & 0 & A_{9,9} & A_{9,10} & A_{9,11} \\
A_{10,1} & A_{10,2} & A_{10,3} & A_{10,4} & A_{10,5} & A_{10,6} & A_{10,7} & A_{10,8} & A_{10,9} & A_{10,10} & 0 \\
A_{11,1} & A_{11,2} & A_{11,3} & A_{11,4} & A_{11,5} & A_{11,6} & A_{11,7} & A_{11,8} & A_{11,9} & 0 & A_{11,11}
\end{bmatrix}
\begin{Bmatrix}
\ddot{\beta} \\
\ddot{\zeta} \\
\ddot{\theta} \\
\ddot{q}^{(4)} \\
\ddot{q}^{(5)} \\
\ddot{q}^{(6)} \\
\ddot{q}^{(7)} \\
\ddot{q}^{(8)} \\
\ddot{q}^{(9)} \\
\ddot{q}^{(10)} \\
\ddot{q}^{(11)}
\end{Bmatrix}_{m,i}
$$

Figure 13 DEFINITION OF THE INERTIA MATRIX FOR THE ith ARTICULATED BLADE.

40

Figure 14. EQUATIONS OF MOTION FOR A TEETERING ROTOR.

where:

$$RHS^{(1)} = A_{\phi q_1}^{(1)} \ddot{\phi} + \Lambda_1^{(1)} - A_{\phi q_2}^{(1)} \ddot{\psi} - \Lambda_2^{(1)}$$

$$RHS^{(2)} = A_{\phi q_1}^{(3)} \ddot{\phi} + \Lambda_1^{(3)}$$

$$RHS^{(3)} = A_{\phi q_2}^{(3)} \ddot{\psi} + \Lambda_2^{(3)}$$

$$RHS^{(4)} = A_{\phi q_1}^{(4)} \ddot{\phi} + \Lambda_1^{(4)} - A_{\phi q_2}^{(4)} \ddot{\psi} - \Lambda_2^{(4)}$$

$$RHS^{(5)} = A_{\phi q_1}^{(5)} \ddot{\phi} + \Lambda_1^{(5)} - A_{\phi q_2}^{(5)} \ddot{\psi} - \Lambda_2^{(5)}$$

$$RHS^{(6)} = A_{\phi q_1}^{(6)} \ddot{\phi} + \Lambda_1^{(6)} - A_{\phi q_2}^{(6)} \ddot{\psi} - \Lambda_2^{(6)}$$

$$RHS^{(7)} = A_{\phi q_1}^{(7)} \ddot{\phi} + \Lambda_1^{(7)} + A_{\phi q_2}^{(7)} \ddot{\psi} + \Lambda_2^{(7)}$$

$$RHS^{(8)} = A_{\phi q_1}^{(8)} \ddot{\phi} + \Lambda_1^{(8)} + A_{\phi q_2}^{(8)} \ddot{\psi} + \Lambda_2^{(8)}$$

$$RHS^{(9)} = A_{\phi q_1}^{(9)} \ddot{\phi} + \Lambda_1^{(9)} + A_{\phi q_2}^{(9)} \ddot{\psi} + \Lambda_2^{(9)}$$

$$RHS^{(10)} = A_{\phi q_1}^{(10)} \ddot{\phi} + \Lambda_1^{(10)}$$

$$RHS^{(11)} = A_{\phi q_2}^{(10)} \ddot{\psi} + \Lambda_2^{(10)}$$

In addition, it should be noted that $q_i^{(\prime\prime)}$ is a disturbance variable, and therefore the initial conditions for the flap angles, $q_1^{(\prime)}$ and $q_2^{(\prime)}$, must reflect a preset coning angle, if such an angle exists in a teetering rotor.

COMPUTATIONAL PROCEDURE

GENERAL REMARKS

The TBL-II simulation outlined in the previous section was programmed (with the aid of FORTRAN IV) for solution on an IBM-7044 digital-computing facility. The significant expansion in the number of problem variables, relative to the number treated in TBL-I, required that calculations be restricted to a two-bladed rotor, namely, a teetering rotor or a "rigid" rotor. In general, the computational methodology followed that employed in TBL-I. Whereas the maximum number of radial segments used to represent a blade in TBL-I was 10, TBL-II provides for a total of 14 radial segments. This increase was deemed necessary to obtain accurate loadings at the root of a blade during high-advance-ratio operations in which the root of the blade becomes the leading edge of a surface of small aspect ratio.

The variable angular velocity, $\dot{\psi}$, that results when mechanical shaft torque is an input quantity integrates to nonrepeating azimuth positions; consequently, it is more difficult to judge when a steady-state operating condition is achieved than was the case for TBL-I. Rather than employ an interpolation scheme to determine whether blade response variables are repeating each 360 degrees of shaft rotation, steady state was defined to exist when the mean value of $\dot{\psi}$ (over one revolution of shaft rotation, approximate) reaches a steady value.

A Runge-Kutta integration subroutine is employed to integrate the computed modal accelerations to obtain modal velocities and displacements. Selection of the time intervals used in the integration process is guided by a rule of thumb which states that approximately 10 time intervals are required per cycle of response in order to obtain

an accurate integration. The time interval is thus governed by the natural frequency of the highest frequency mode included in the simulation.

In order to compute the response to a transient input of shaft torque, collective pitch, cyclic pitch, etc., it is necessary to integrate from a set of assumed initial conditions. This integration must proceed until the transient response resulting from the disturbance created by the assumed initial conditions disappears and steady, periodic loadings and blade motions are achieved. A premium is thereby placed on operating procedures wherein the time and expense of achieving an initial steady state is held to a minimum.

As was done in TBL-I, the program is first operated in a mode in which a constant induced inflow is assumed. With the wake model inactive (in the sense that induced-velocity coefficients are not evaluated), the computing time required to integrate from an assumed set of initial conditions to an approximate steady-state response is significantly reduced. Upon attainment of a steady-state response based on uniform inflow, the wake model is activated and computes induced velocities as a function of the approximate vortex strengths that were previously deposited in the airstream. The integration process continues until the circulation strengths in the wake become periodic and the rotor response is likewise periodic.

The computing time required for one calculation interval with the wake model operative and inoperative are 9.3 and 4.4 seconds, respectively. Although this saving is significant, it should be noted that in TBL-I a single calculation interval required only 2.5 seconds of machine time when the wake model was inoperative. This difference between TBL-I and TBL-II is attributable to the larger number of degrees of freedom and integrations associated with TBL-II.

44

Since the computing time associated with each operation of
the wake model is quite large, the computing program is instructed to
calculate a wake geometry and an induced velocity in the plane of the
rotor at specified azimuth intervals rather than at each of the small
time intervals required to perform an accurate integration. Provision
is also made for specifying a delay period between the achievement of
a steady state and the initiation of a change in any one of the independent
variables. The transient variation of these variables (e. g., shaft torque
or collective pitch) is treated as a ramp function for which the magnitude
and slope can be specified.

Various aspects of the computational procedure, other than
those discussed above, are the same as were employed in TBL-I (see
Reference 12).

PROBLEMS ENCOUNTERED

Considerable difficulties were encountered in starting up the
developed digital simulation when all of the degrees of freedom discussed
earlier were included in the simulation. Unfortunately, insufficient time
was available to determine whether the resulting unstable responses were
a result of programming errors or were caused by various other factors
such as the magnitude of the disturbance imposed by the assumed initial
conditions. Many calculation trials were made, however, and these have
indicated that the large inertial coupling between the feathering and
torsion degrees of freedom places a very severe requirement on the
initial conditions assumed for these two degrees of freedom. If, for
example, the feathering degree of freedom is assumed to possess an
initial displacement and velocity equivalent to that of the swashplate,
the acceleration computed for feathering at the first time interval is
very large, resulting in a torsional moment (from the large inertial
coupling) that, in turn, causes a large torsional acceleration. If the
initial departure from dynamic equilibrium is large, as was evidenced
by the feathering and torsional accelerations computed at the first time

interval, the rotor response proved to be unstable as a result of the direct influence of feathering and torsion on blade angles of attack and on the associated aerodynamic loading.

The expedient adopted to alleviate this difficulty consisted of the effective removal of the compliant control link between the swashplate and the blade. By this means, the feathering degree of freedom becomes an independent input variable rather than a response variable. Since the feathering accelerations are then prescribed to be the values determined by the tilt of the swashplate, the inertial coupling between torsion and feathering is automatically bounded to reasonable values. The dynamic system obtained on removal of the feathering degree of freedom exhibited less sensitivity to assumed initial conditions and, accordingly, was employed in the remainder of this study.[*]

Another computational matter worth discussing at this point relates to the determination of the unknown circulations from the simultaneous equations defining the boundary condition of flow tangency. Prior to the development of the aerodynamic model based on the abandonment of the Prandtl simplification, the solution of the simultaneous equations was iterated until the boundary condition was satisfied at all control points, even though some control points were located on blade segments experiencing angles of attack in excess of stall. In the calculations that utilized two-dimensional section data, this procedure was implemented by taking the solution of the linear equations, computing the resulting

---

[*]A subsequent discovery of the crucial importance of the quasi-static aerodynamic moment (caused by pitching and torsional velocities) in providing adequate damping for the stability of the torsional mode indicates that the above-discussed problem may not have existed had this damping moment been included in the equations of motion from the beginning of the study.

46

angles of attack, redefining the circulations, recomputing the angles
of attack, etc., until convergence was obtained.

In setting up the current procedure for computing the unknown
circulations, it was recognized that there is an inconsistency in demanding
that there be flow tangency at those sections where the blade is presum-
ably stalled. Accordingly, a procedure was adopted in which the linear
equations were solved once and the resulting circulations were truncated
if the local two-dimensional angle of attack exceeded a stall angle computed
as a function of the local Mach number. The local two-dimensional angle
of attack was first determined as a function of (a) blade geometry and
motion and (b) the velocity induced by the "old" wake. The additional
velocity induced by the adjacent wake elements was then computed using
the truncated circulations and, after making a single correction to the
local Mach number and the local angle of attack, the truncation process
was repeated. No attempt was made to iterate to values of circulation
that would insure flow tangency everywhere. Lacking any theory or
rationale which indicates how the circulation on the blades and in the
adjacent wake elements should readjust their strengths whenever certain
spanwise segments are stalled, there did not appear to be any alternative
other than to accept the above-described "open-loop" solution procedure.
This decision did, however, produce an unanticipated result; namely,
a fluctuation in calculated loadings where the fluctuation is caused by
the method of solution and results intermittently in oscillatory loadings,
with the frequency of this oscillation being the calculation frequency
(one calculation every 0.004 second or 250 calculation intervals per
second). Fortunately, this frequency is sufficiently high that the conse-
quences of this spurious high-frequency forcing are negligible, in that
this high-frequency excitation does not produce a significant response
in any of the assumed modes.

47

INPUT DATA

A separate computational program was used to evaluate the numerous integrals defined in the TBL-II analysis. Specific input data were required, making it desirable to select a rotor for which the necessary structural information was available. The further restrictions imposed by the capacity of available computing equipment led to the selection of the two-bladed rotor of the HU-1A helicopter.

Blade cross-section geometry and material properties, as supplied by the Bell Helicopter Company (Reference [22]), were analyzed at 11 spanwise stations to obtain the structural parameters defined in Appendix III. These results are tabulated in Table I. Existing data on the mass, $m(\zeta)$, and bending-stiffness, EI_{xx} and EI_{yy}, distributions (see Figure 15) were employed in a modal analysis (Reference [20]) to obtain mode shapes for three-symmetric and three-antisymmetric bending modes. The coupled flapwise-chordwise bending-mode shapes obtained for the nominal rotational speed of 314 rpm are presented in Figure 16, together with the two uncoupled torsional-mode shapes calculated by means of a Holzer analysis. Figure 17 shows the straight elastic axis that was assumed to approximate the computed elastic-axis location (see Table I) and also shows the location of the local c.g., the one-quarter chord, and the feathering axis relative to the elastic axis.

A lack of familiarity with the vibratory behavior of highly twisted, rotating blades, as yielded by a coupled flatwise- and chordwise-bending analysis, provided cause for questioning the data plotted in Figure 16. In order to produce a higher level of confidence in these results, calculations were made for a range of rotational speeds. These calculations served to demonstrate the manner in which the

TABLE I

STRUCTURAL PARAMETERS OF THE HU-1A
BLADE DETERMINED FROM CROSS-SECTION DATA

SPANWISE STATION in.	A ft^2	e_A ft	k_A^2 ft^2	B_2 ft^5	B_1 ft^6	μ $\dfrac{slugs\text{-}ft^2}{ft}$
42	5.62×10^{-2}	0.472	0.133	-2.07×10^{-3}	1.31×10^{-3}	0.04008
55	4.14×10^{-2}	0.451	0.155	-1.99×10^{-3}	1.17×10^{-3}	0.03440
65	3.50×10^{-2}	0.441	0.165	-1.86×10^{-3}	1.03×10^{-3}	0.03109
72.5	3.25×10^{-2}	0.443	0.165	-1.68×10^{-3}	0.948×10^{-3}	0.02874
85	3.31×10^{-2}	0.440	0.163	-1.79×10^{-3}	1.03×10^{-3}	0.02887
100	3.19×10^{-2}	0.412	0.148	-1.67×10^{-2}	1.00×10^{-3}	0.02541
120	3.06×10^{-2}	0.381	0.132	-1.41×10^{-3}	0.839×10^{-3}	0.02160
140	2.95×10^{-2}	0.354	0.116	-1.20×10^{-3}	0.796×10^{-3}	0.01840
155	2.97×10^{-2}	0.347	0.116	-1.29×10^{-3}	0.849×10^{-3}	0.01913
170	3.16×10^{-2}	0.338	0.114	-1.39×10^{-3}	0.870×10^{-3}	0.02346
240	4.31×10^{-2}	0.270	0.102	-2.06×10^{-3}	1.45×10^{-3}	0.02356

NOTE: SEE APPENDIX III FOR THE DEFINITION OF A, e_A, k_A^2, B_1, AND B_2.
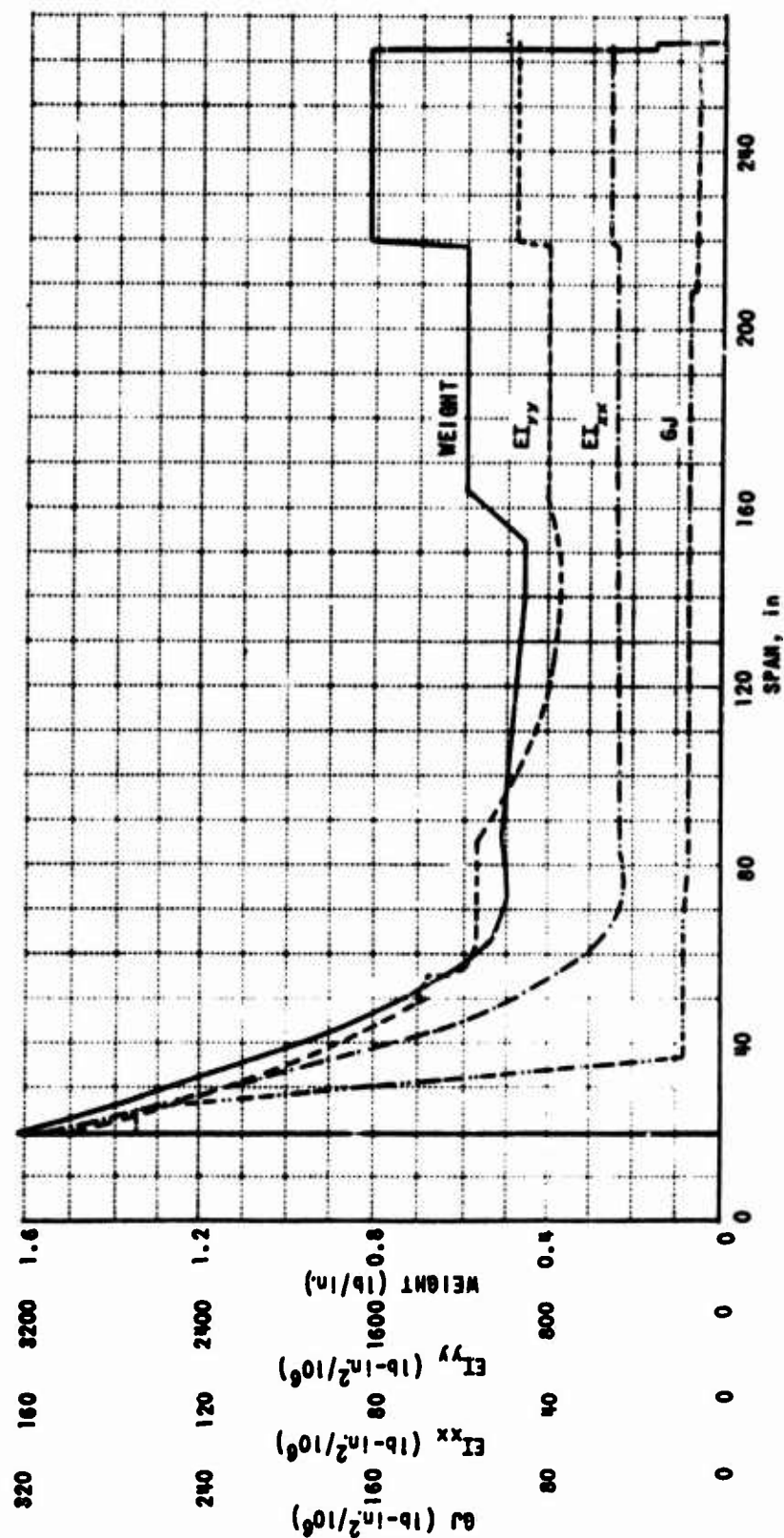
Figure 15. SPANWISE DISTRIBUTION OF WEIGHT, BENDING STIFFNESS, AND TORSIONAL STIFFNESS FOR THE HU-1A ROTOR BLADE.

50

MODE | FLATWISE SHAPE | CHORDWISE SHAPE

1st ANTISYMMETRIC BENDING
ω_n = 6.4106 cps

2nd ANTISYMMETRIC BENDING
ω_n = 14.267 cps

3rd ANTISYMMETRIC BENDING
ω_n = 25.099 cps

1st SYMMETRIC BENDING
ω_n = 6.5537 cps

2nd SYMMETRIC BENDING
ω_n = 5.4668 cps

3rd SYMMETRIC BENDING
ω_n = 17.304 cps

1st TORSION
ω_n = 25.8 cps

2nd TORSION
ω_n = 67.8 cps
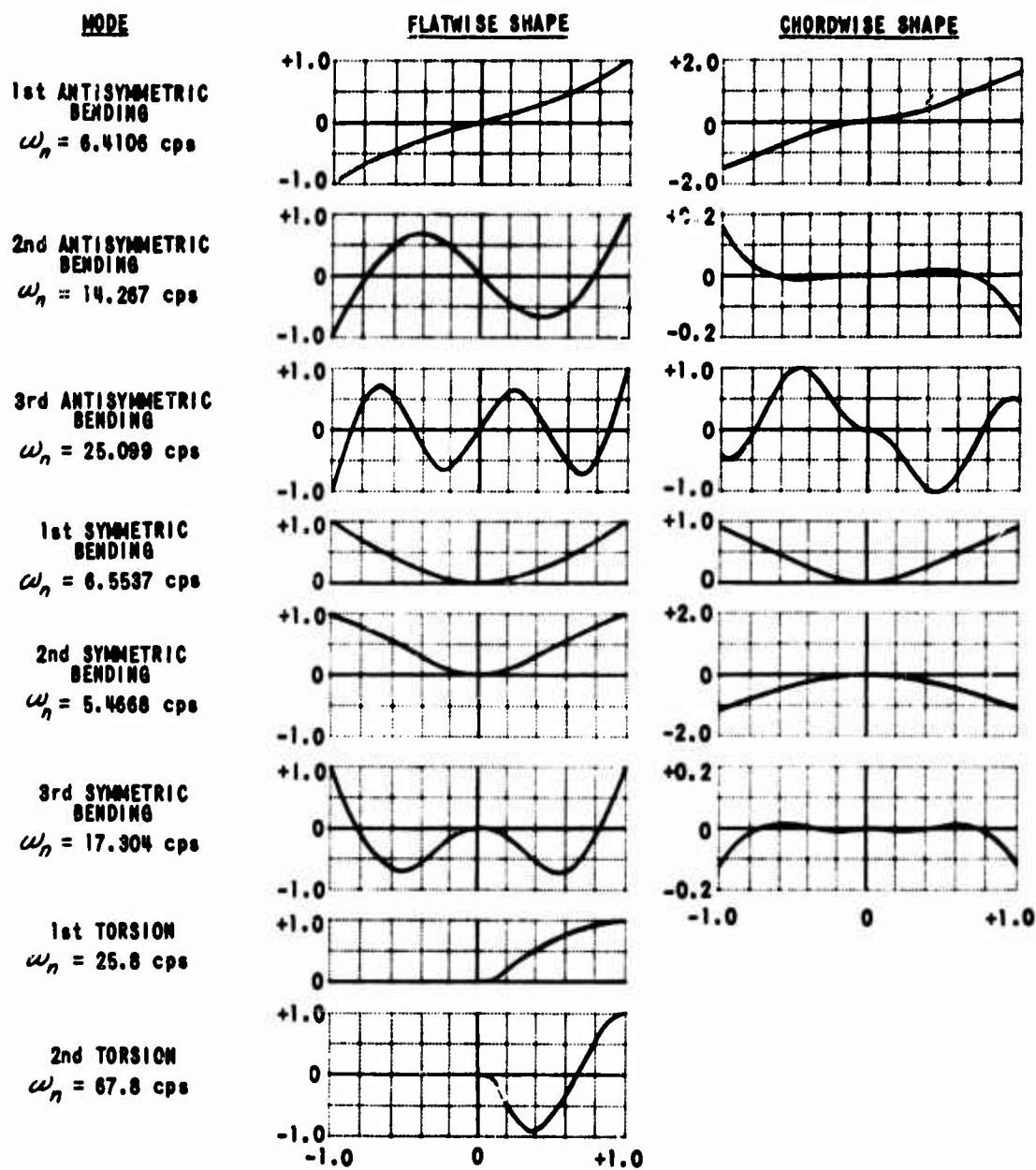
Figure 16.   SCHEMATIC DIAGRAM OF MODES USED TO DESCRIBE
MOTIONS OF A TWO-BLADED TEETERING ROTOR.

51
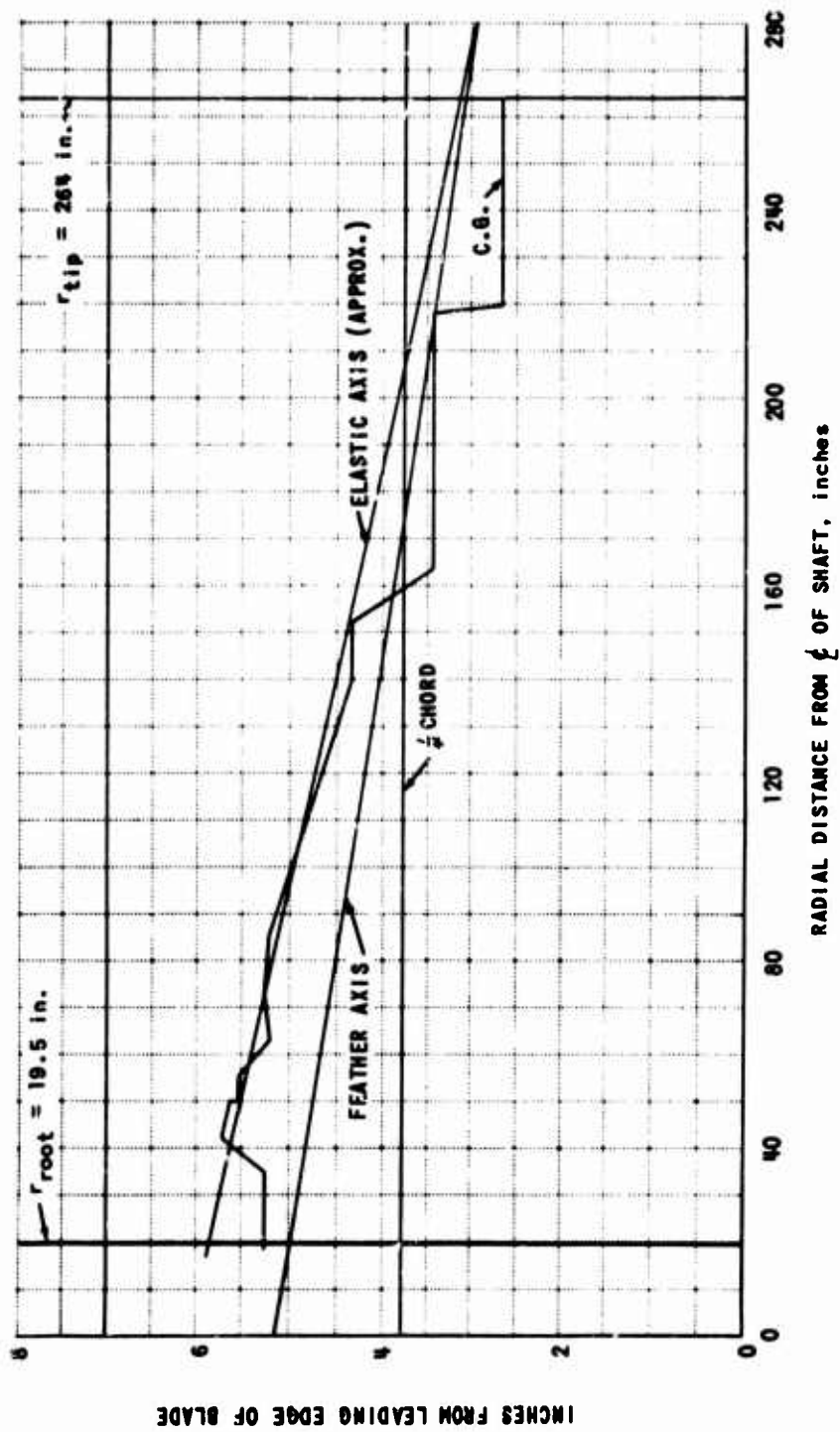
Figure 17. LOCATION OF ELASTIC AXIS, SECTIONAL CENTER OF GRAVITY, AND FEATHERING AXIS WITH RESPECT TO THE LEADING EDGE OF THE HU-1A BLADE.

52

coupled bending modes change their character as rotational speed is varied and provided assurance that the mode shapes computed for the 314-rpm case were realistic.

The modal frequencies obtained in these calculations are plotted in Figure 18. Note that both the first and second symmetric and antisymmetric bending modes change from a flatwise and chordwise mode to chordwise and flatwise modes, respectively. It is seen that the first and second symmetric modes approach each other in frequency and also change their chordwise to flatwise displacement ratio in the vicinity of 314 rpm, the nominal rotational speed of the HU-iA rotor. This particular result does raise a question as to whether uncoupled bending modes might have been better choices for assumed modes, since it appears, in theory, that it is preferable to assume mode shapes that do not change appreciably as the rotational speed of the rotor is varied. The data provided by the present program are not sufficient to determine a preferred procedure for choosing "assumed modes".
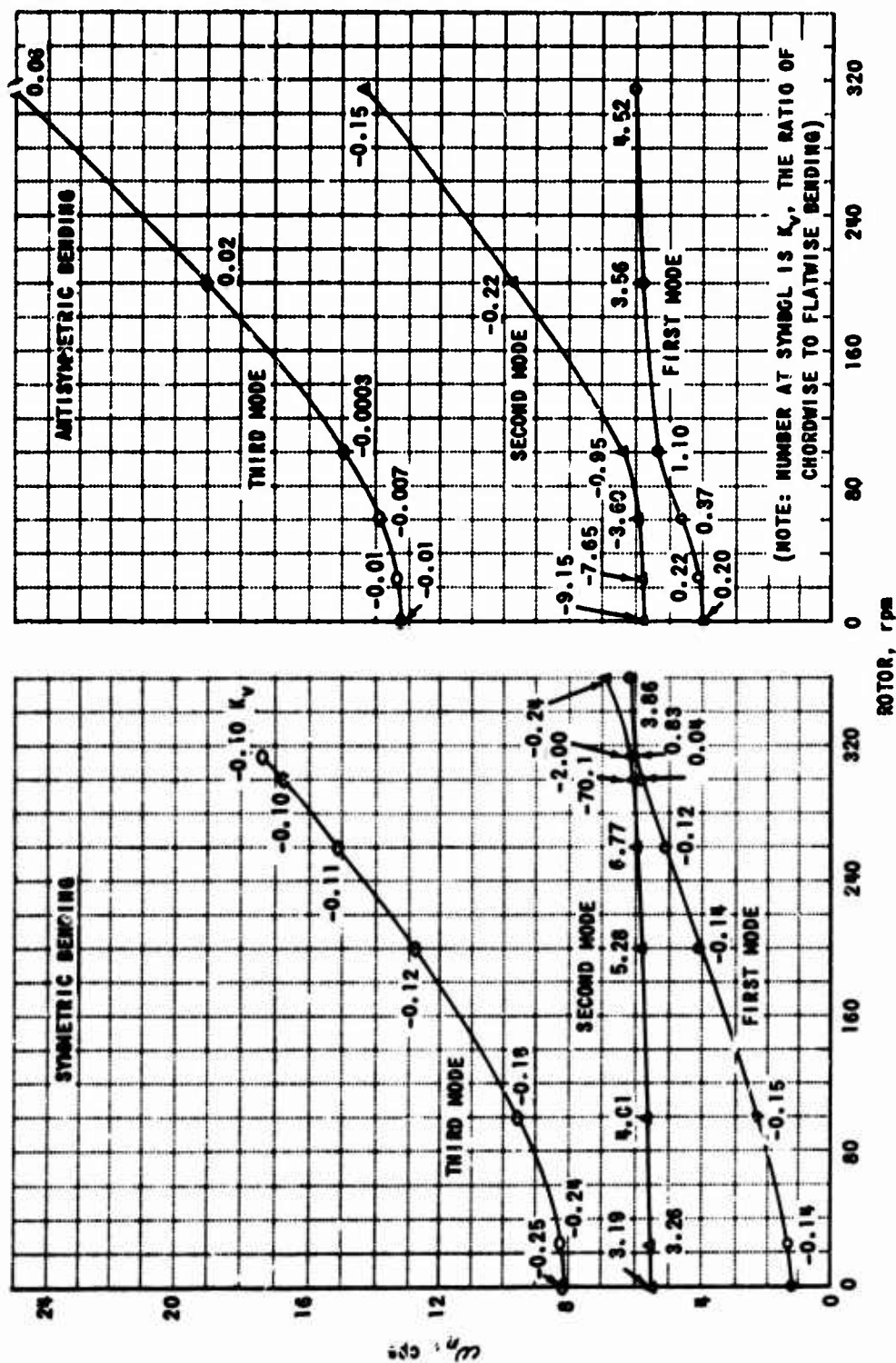
Figure 18. RESONANT FREQUENCIES OF COUPLED FLATWISE AND CHORDWISE BENDING VERSUS ROTOR RPM; HU-1A ROTOR BLADES. (ROOT CHORD IS AT ZERO-DEGREE COLLECTIVE PITCH)

54

RESULTS

EQUIVALENCE BETWEEN THE TWO AERODYNAMIC MODELS AT LOW ADVANCE RATIOS

In the section dealing with the aerodynamic model, it was shown that the vortex geometry, adopted in TBL-II to represent the bound vorticity on the blade, yields a realistic distribution of loadings on a low-aspect-ratio surface corresponding to a two-bladed rotor stopped at the 0 - 180-degree azimuth position. As is discussed in Appendix II, features were included in the model in order to yield, at low advance ratios, circulation strengths equivalent to the lift coefficient that is obtained from a "strip" analysis employing two-dimensional empirical airfoil data. In view of the heuristic nature of the steps taken to insure matching results from the two models at low advance ratios, questions did exist as to the level of agreement that would be obtained in actual computational practice.

Figure 19 shows that, for an advancing blade ($\mu = 0.26$) operating at angles of attack below the stall, excellent agreement is obtained between the spanwise distribution of loadings yielded by the two aerodynamic models. The minor differences noted at the root of the blade are due, in part, to the assumption that the negative component of radial flow experienced at $\psi = 142$ degrees causes the root to be, in effect, a trailing edge. The retreating blade, i.e., $\psi = 322$ degrees, happens to be encountering angles of attack in excess of the stall angle; therefore, the loadings computed on the basis of two-dimensional section data are less than those obtained from the solutions of the equations expressing the boundary condition, where these solutions have been limited to a specified value of maximum circulation. The differences noted for the retreating blade are, therefore, to be expected. It was concluded that the agreement between the two aerodynamic models is quite adequate at

55
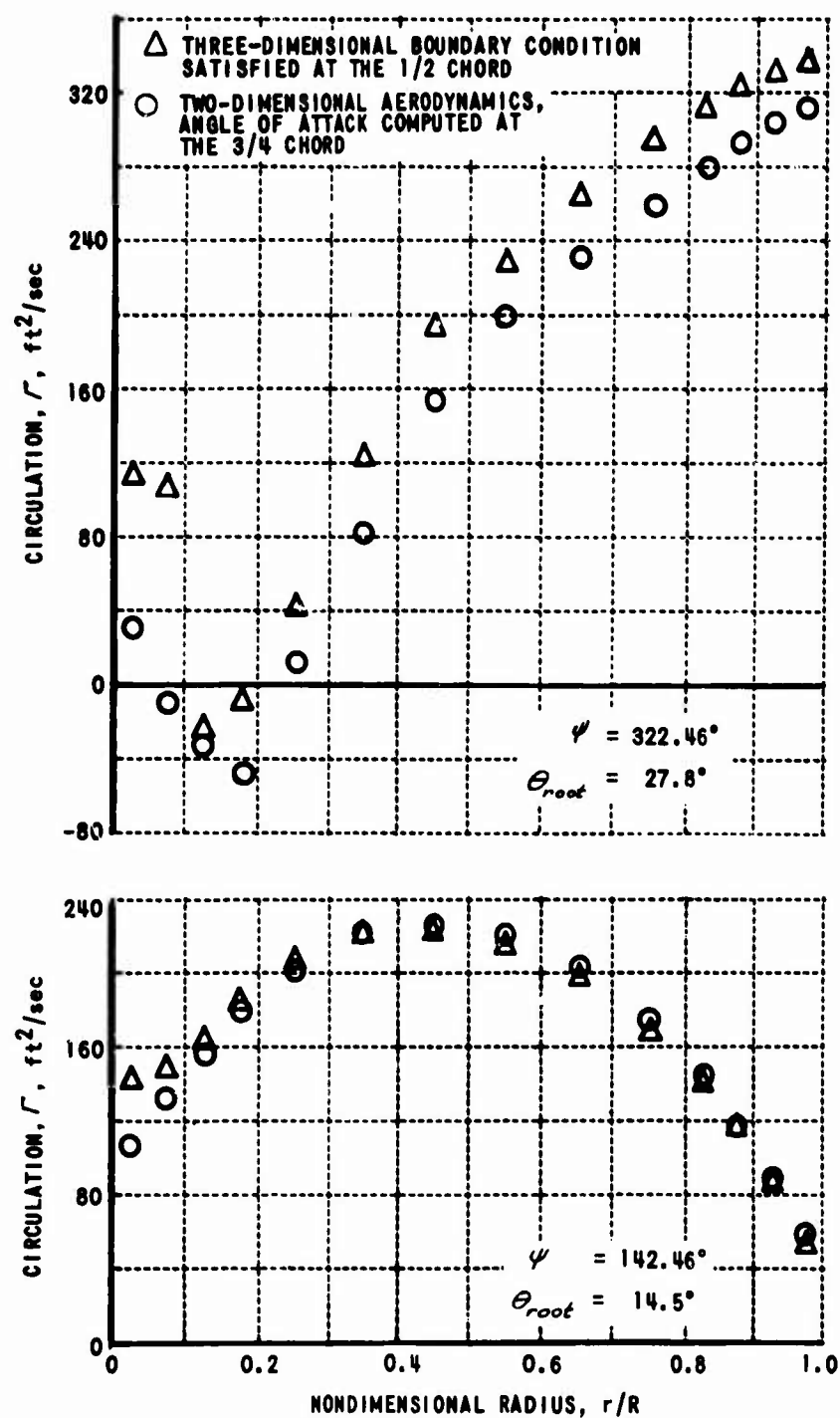
Figure 19. COMPARISON OF SPANWISE DISTRIBUTION OF CIRCULATION YIELDED BY TWO AERODYNAMIC MODELS, $\mu = 0.26$.

56

low advance ratios and, therefore, it is postulated that the aerodynamic analysis employed in this study has a rational basis for predicting load distributions on long, narrow blades irrespective of the local orientation of the total velocity vector and the magnitude of the radial component of this velocity vector.

Calculations made for an assumed rigid rotor stopped at the 0 - 180-degree azimuth position have pointed up, however, certain shortcomings of the wake model employed in the study. In particular, the methods used to define the location and strength of the rolled-up tip and root vortices produced at low advance ratios do not carry over, in a logical manner, for representing the roll-up process behind a low-aspect-ratio surface. The wake trailed behind the high-aspect-ratio surface is a function of the change in circulation (integrated over the chord) along the span, with the strengths of the root and tip vortex being equivalent to the maximum circulation achieved along the span. For the low-aspect-ratio surface, the adopted horseshoe-vortex representation yields the distribution of vorticity along the "chord" dimension. Consequently, the logic for assigning strengths to rolled-up elements of the sheet of vorticity trailed from the side edges of the airfoil is incorrect. Note that the variation in the strength of this vortex sheet is equivalent to the chordwise distribution of bound vorticity and that the strength of a single vortex element, representing a roll-up of this sheet, should be the integral of the chordwise distribution of vorticity. This is not the case in the adopted model. It appears that although the adjacent non-rolled elements of wake streaming back from the side edge of a low-aspect-ratio surface yields an appropriate geometry for representing its chordwise vorticity distribution, the rolled elements (two in number) have little justification, either with respect to their location or their strengths. Fortunately, the logic which is inappropriate to the low-aspect-ratio flow case gives these rolled-up elements a geometry and strength which, for the most part, make their influence self-canceling. In order to eliminate the steady-state loading error caused by this self-imposed

57

artifact, the steady-state computation procedure was modified to effectively eliminate the rolling-up process while the rotor was stopped at the 0 - 180-degree azimuth position. On initiating the transient, that is, engine torque is applied to start up the rotor, the rolling-up process necessarily reenters the calculation procedure. The wake geometry resulting from the roll-up logic built into the calculation procedure accordingly contributes an unknown level of error in calculating loadings at very high advance ratios when the rotor is in the vicinity of 0 - 180 degrees of azimuth. At azimuth locations in the vicinity of 90 - 270 degrees, the wake model operates in a satisfactory manner, irrespective of the magnitude of the advance ratio.

RESPONSE TO POWER LOSS AND A BRAKING TORQUE

Three transient responses were computed to examine the aerodynamic loadings and the structural motions of a two-bladed teetering and rigid rotor experiencing a power loss at a high-speed cruise condition. In order to obtain representative input data for shaft angle, cyclic pitch, etc., experimental values reported in Reference [24] for a forward flight speed of 111. 3 knots (μ = 0. 261) were employed. The tip-path plane computed for the teetering-rotor configuration (based on blade flapping only) was used to determine a shaft angle which would give the rigid rotor the same tip-path-plane orientation. In adjusting collective pitch on the rigid rotor to yield the same average lift produced by the teetering rotor, slight differences in average lift were accepted resulting in different steady-state torque requirements as tabulated in Table II.

Transient responses caused by both a 50- and 100-percent power loss were computed for the teetering-rotor configuration. Figure 20 indicates that the 50-percent power loss was applied in 0. 1 second; that is, in approximately one-half of a rotor revolution. The time history in Figure 20 is limited to 1. 3 seconds and shows one complete revolution of steady-state behavior prior to initiating the reduction in shaft torque.
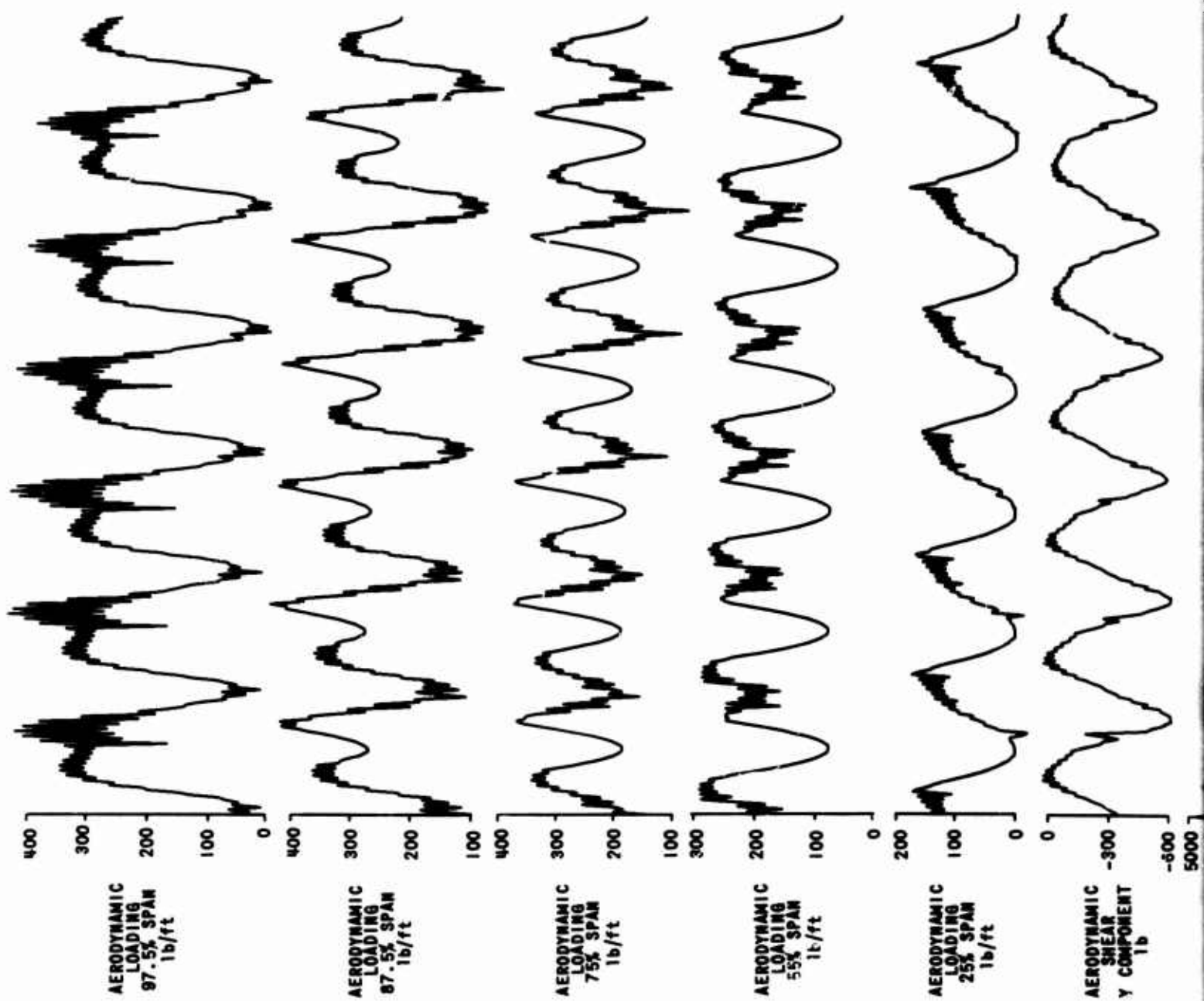
58

Figure 20. RESPONSE OF TEETERING ROTOR TO 50% POWER LOSS; $\mu = 0.26$, $\theta_c = 0.369$ RADIAN, $\alpha_s = 0.113$ RADIAN.
(a) AERODYNAMIC LOAD AND FORCE TIME HISTORIES.

TIP TWIST
1st TORSION
MODE, q(10)
rad

TIP DEFLECTION
3rd SYMMETRICAL
MODE, q(9)
ft

TIP DEFLECTION
2nd SYMMETRICAL
MODE, q(8)
ft

TIP DEFLECTION
1st SYMMETRICAL
MODE, q(7)
ft

TIP DEFLECTION
3rd ANTISYM.
MODE, q(6)
ft

TIP DEFLECTION
2nd ANTISYM.
MODE, q(5)
ft

TIP DEFLECTION
1st ANTISYM.
MODE, q(4)
ft

FLAP ANGLE, β
rad

61

Figure 20. RESPONSE OF TEETERING ROTOR TO 50% POWER LOSS: $\mu = 0.26$, $\theta_c = 0.369$ RADIAN, $\alpha_s = 0.113$ RADIAN. (b) BLADE DISPLACEMENTS AND BENDING MOMENTS; SHAFT-VELOCITY RESPONSE.

TABLE II
STEADY-STATE TRIM CONDITIONS;
POWER LOSS AND BRAKING TRANSIENTS

ROTOR CONFIGURATION	TEETERING (FULL THRUST)	RIGID (FULL THRUST)	RIGID (ZERO THRUST)
V - fps	188	188	188
α_s - rad	0.11395	0.10409	0
θ_o - rad	0.369	0.352	0.138
θ_{ts} - rad	-0.1278	-0.1278	-0.00872
θ_{tc} - rad	0.0498	0.0498	0.00417
Ω - rpm	313	313	313
μ	0.261	0.261	0.260
$\bar{Q}_o$ - ft-lb	7,500	6,650	1,800

The oscillations in loading occurring at the calculation frequency are spurious, as has been discussed earlier. In most cases, it is possible to distinguish between loading "spikes" that derive from sudden changes in the induced-velocity field and the oscillations that derive from the calculation procedure. In general, all of the plotted responses are self-explanatory. However, it should be noted that "Aerodynamic Shear-Y and Z Component" refers to the hub shear produced by aerodynamic loadings on one blade as measured in the shaft plane and perpendicular to the shaft plane, respectively.

Examination of the loadings plotted for five span locations does not reveal any unusual or surprising behavior. It is seen, however, that the mean response for the symmetric bending modes is much larger than would normally be anticipated for a preconed rotor. Investigation has shown that the conversion of the equations applicable to an articulated rotor to those applicable to a teetering rotor has inadvertently caused the influence of preconing on symmetric bending to be omitted. Specifically, it was found that the assumed orthogonality between flapping and symmetric bending does not hold for the steady, preconed component of flap angle. Although this omission of the influence of preconing on steady bending was

63

not discovered until all the calculations had been completed, it is believed that conclusions drawn with respect to either dynamic and/or transient phenomena are not significantly altered by the large values of mean bending and mean-bending moments that have been computed. This comment is believed to hold for the other cases studied as well as for the response time histories under discussion. In effect, the structural responses computed in this investigation apply to an unconed teetering rotor; the aerodynamic forces do, however, reflect the influence of 3 degrees of coning angle.

Figure 20 shows that the peak-to-peak amplitude of the symmetric-bending modes do not change appreciably following the power loss, although the mean deflections of the symmetric modes decrease with the decreased loading as would be expected. The peak-to-peak response in flapping and in the first antisymmetric mode increases with time as the rotor begins to slow down. The decrease in overall loadings causes a decrease in the mean flatwise bending moment (at 10-percent span) whereas the torque disturbance causes a significant increase in the peak-to-peak chordwise deflection of the blades resulting in an equivalent increase in the peak-to-peak chordwise bending moments. It should be noted that loading disturbances which cause increased excitation of the torsion mode (25.8 cps) result also in increased excitation of the third antisymmetric bending mode (25.1 cps).

Figure 21 shows that the 100-percent power loss was initiated at an azimuth position of 270 degrees, whereas the 50-percent power loss occurred at 120 degrees of azimuth. Further, the power loss was applied at the same rate as previously, thus requiring 0.2 second, or approximately one rotor revolution, to lose full power. The response produced by the 100-percent power loss is similar to that produced by the 50-percent power loss. However, it appears that greater high-frequency torsional and high-frequency flatwise-bending-moment responses are excited by the 100-percent power loss. In addition, the time history is
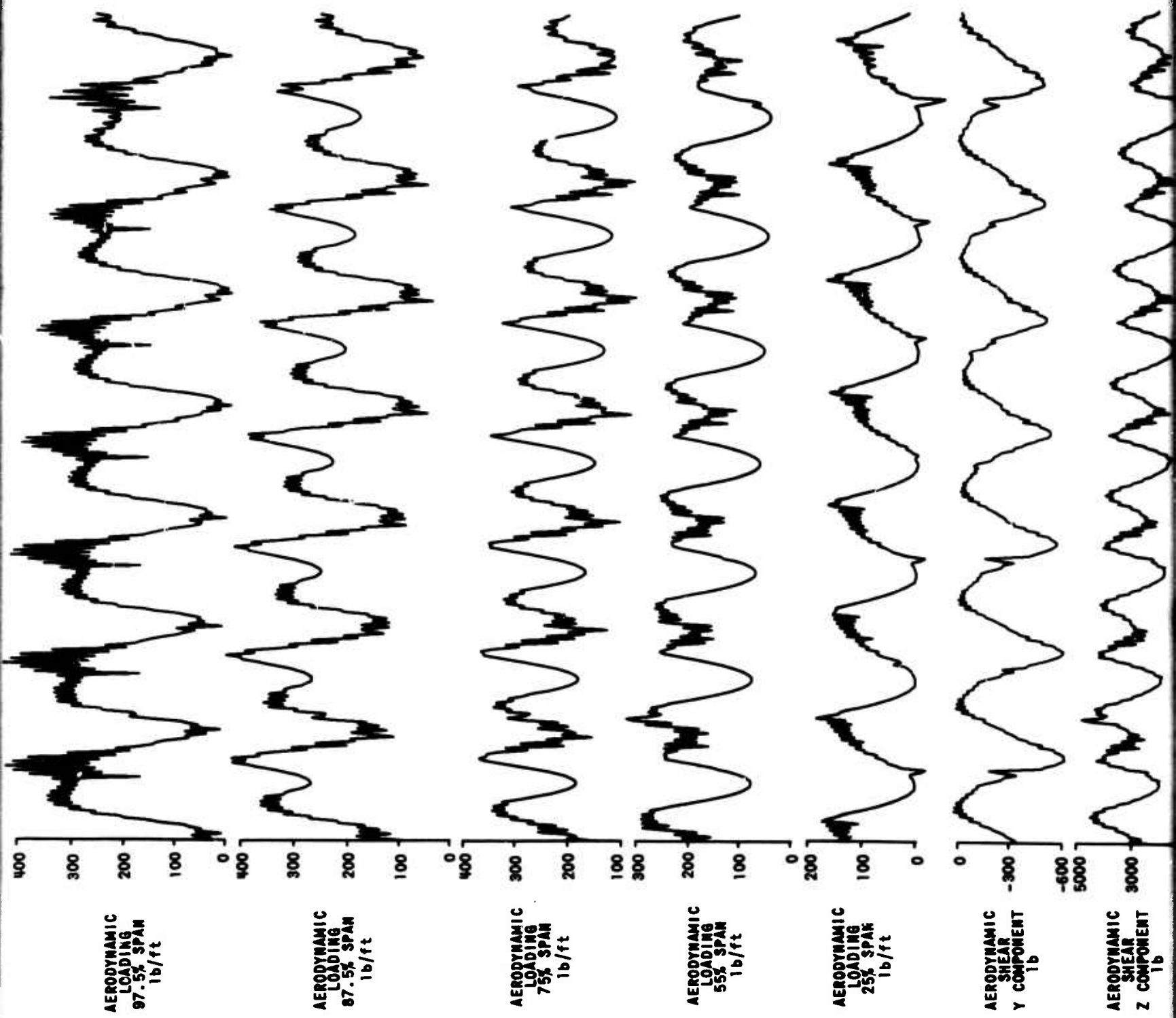
AERODYNAMIC
LOADING
97.5% SPAN
lb/ft

AERODYNAMIC
LOADING
87.5% SPAN
lb/ft

AERODYNAMIC
LOADING
75% SPAN
lb/ft

AERODYNAMIC
LOADING
55% SPAN
lb/ft

AERODYNAMIC
LOADING
25% SPAN
lb/ft

AERODYNAMIC
SHEAR
Y COMPONENT
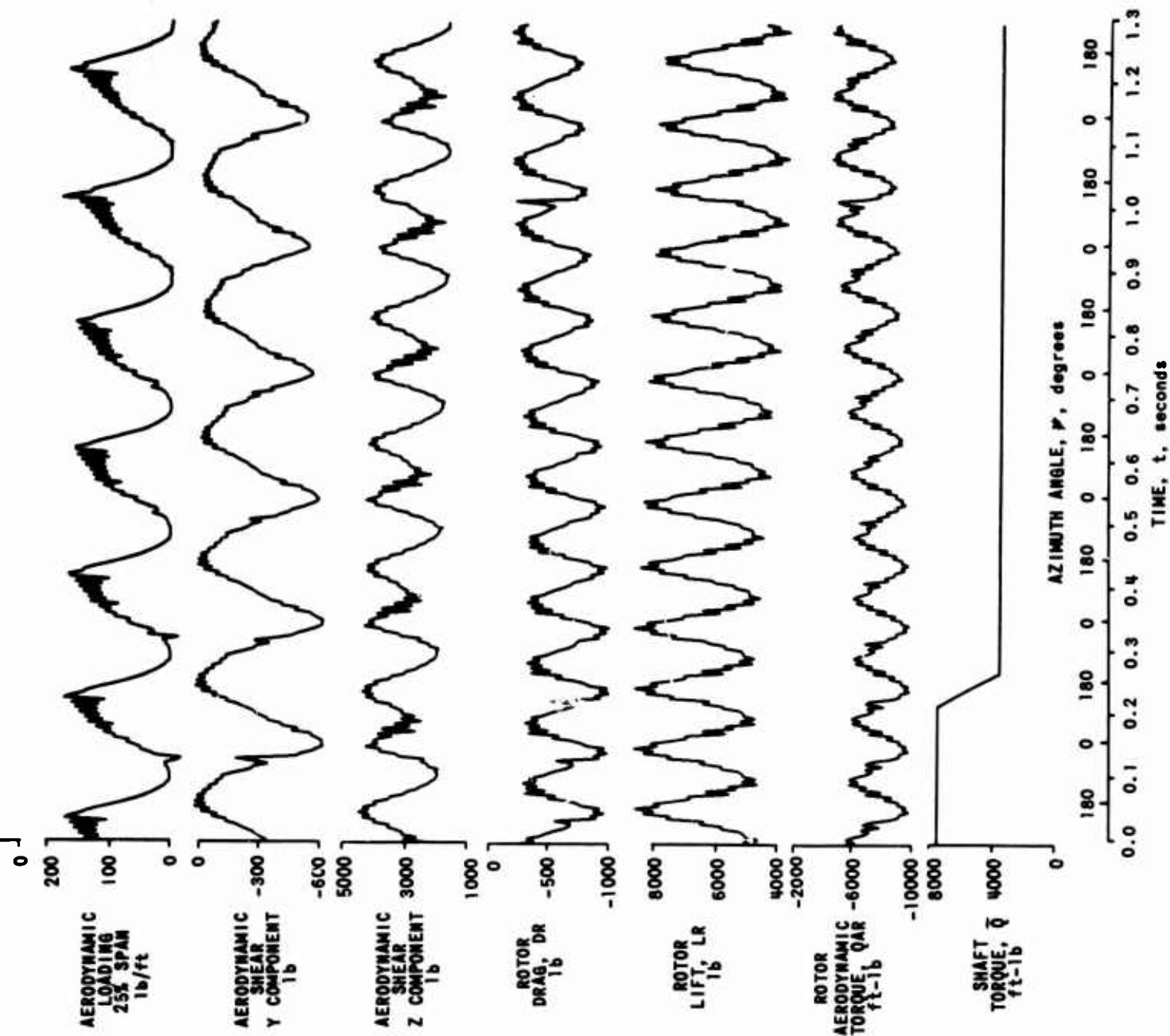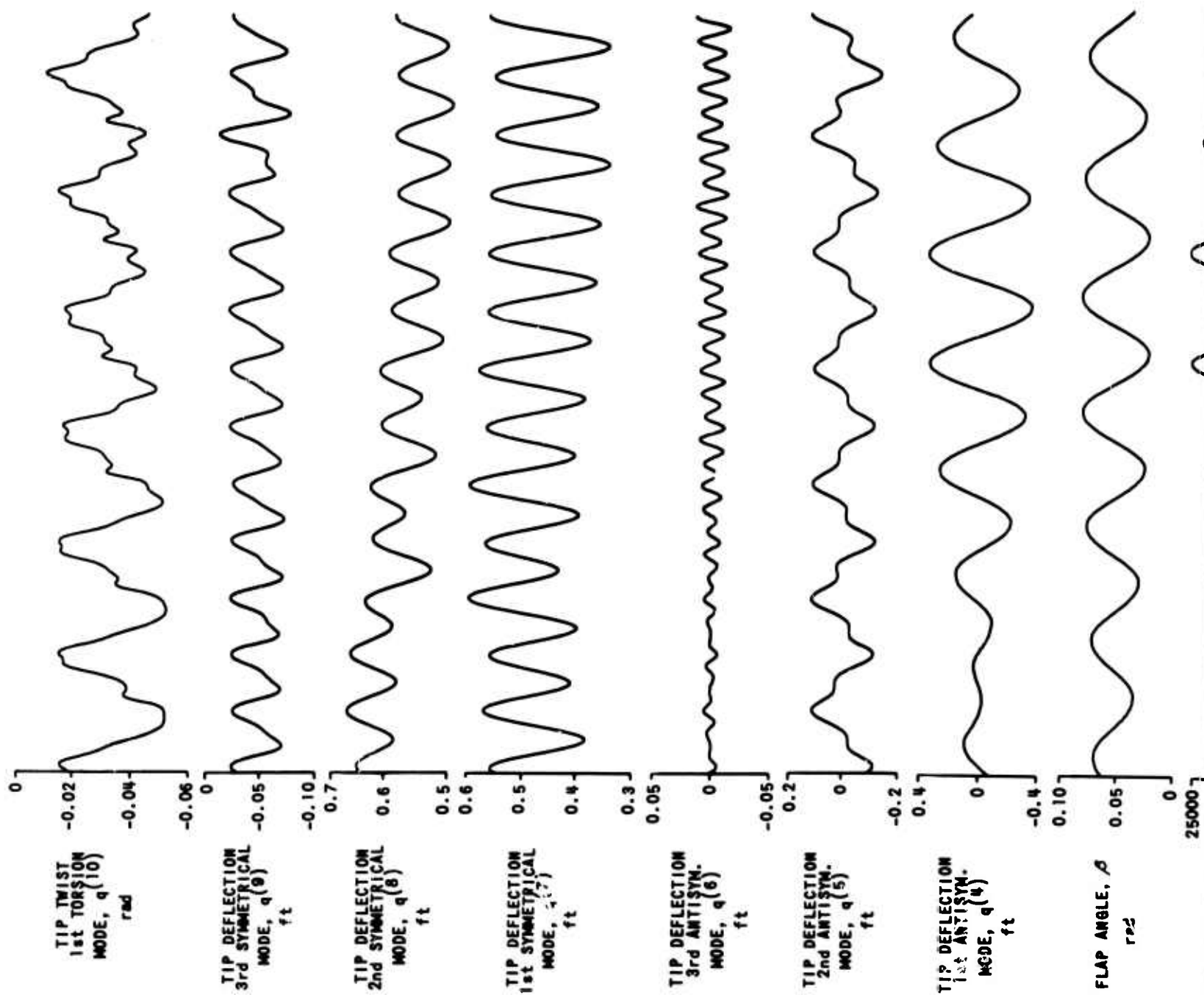lb

AERODYNAMIC
SHEAR
Z COMPONENT
lb

65

Figure 21. RESPONSE OF TEETERING ROTOR TO 100% POWER LOSS; $\mu = 0.26$, $\theta_c = 0.369$ RADIAN, $\alpha_s = 0.113$ RADIAN.
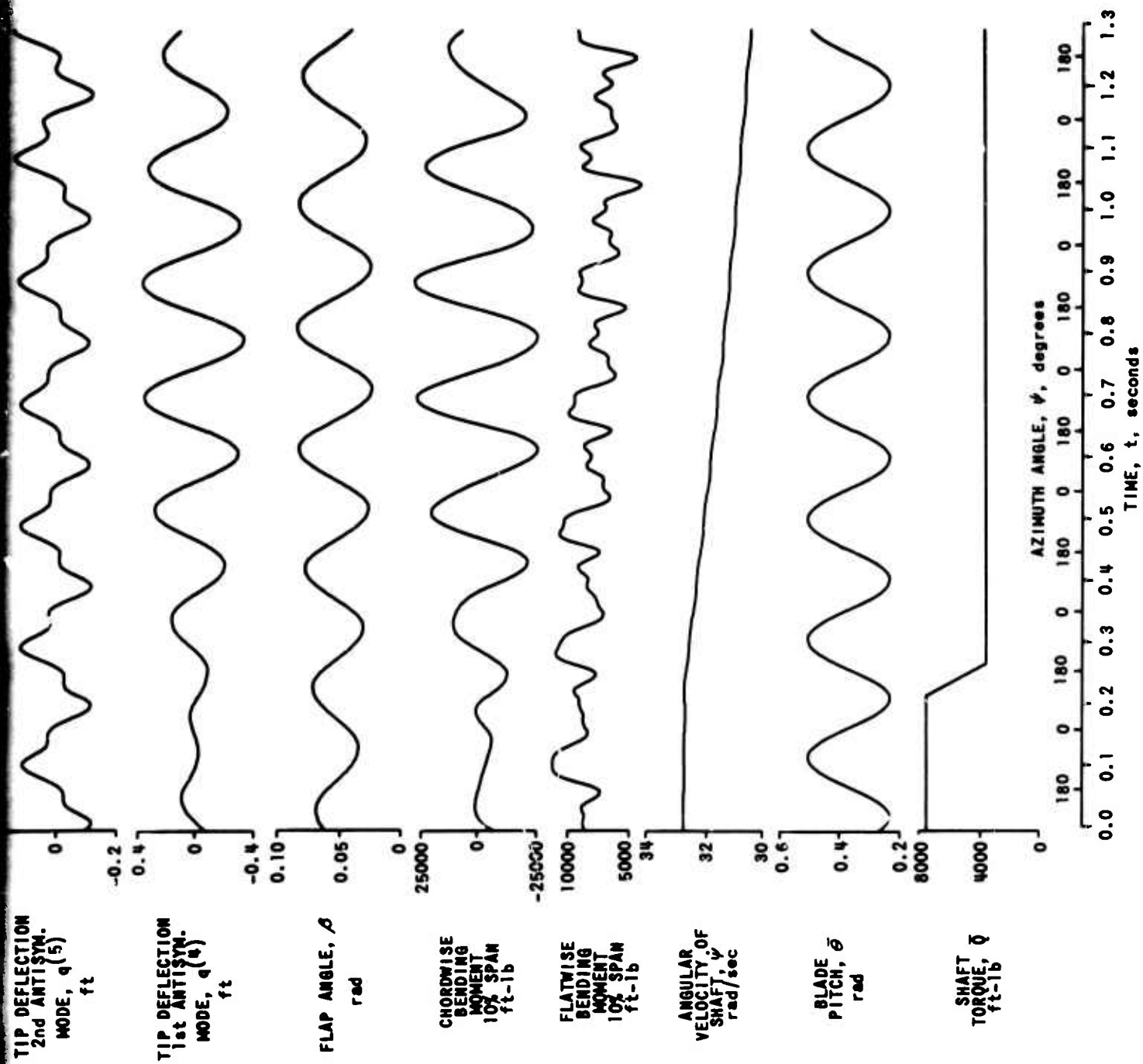(a) AERODYNAMIC LOAD AND FORCE TIME HISTORIES.

TIP TWIST
1st TORSION
MODE, $q(10)$
rad

TIP DEFLECTION
3rd SYMMETRICAL
MODE, $q(9)$
ft

TIP DEFLECTION
2nd SYMMETRICAL
MODE, $q(8)$
ft

TIP DEFLECTION
1st SYMMETRICAL
MODE, $q(7)$
ft

TIP DEFLECTION
3rd ANTISYM.
MODE, $q(6)$
ft

TIP DEFLECTION
2nd ANTISYM.
MODE, $q(5)$
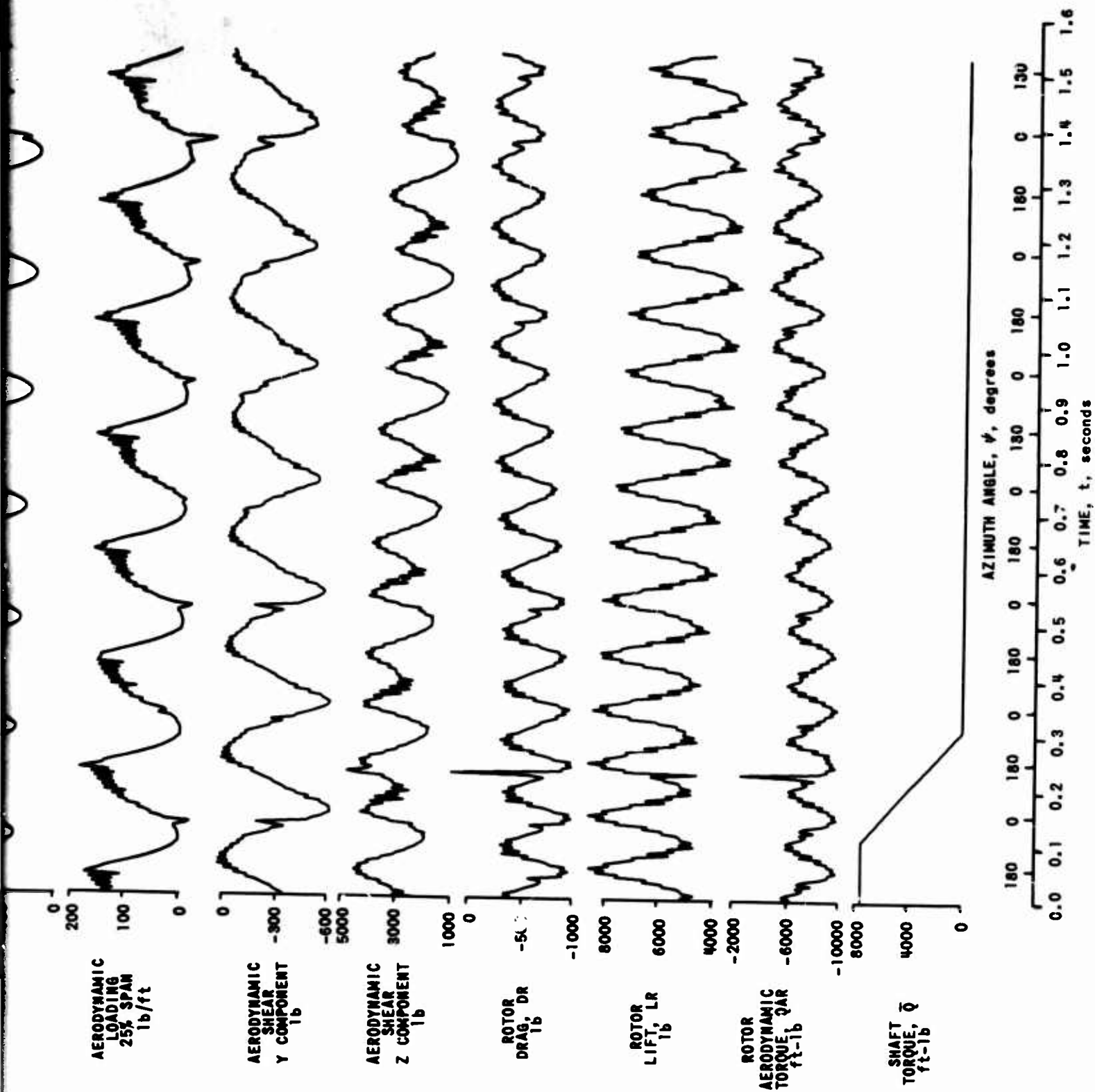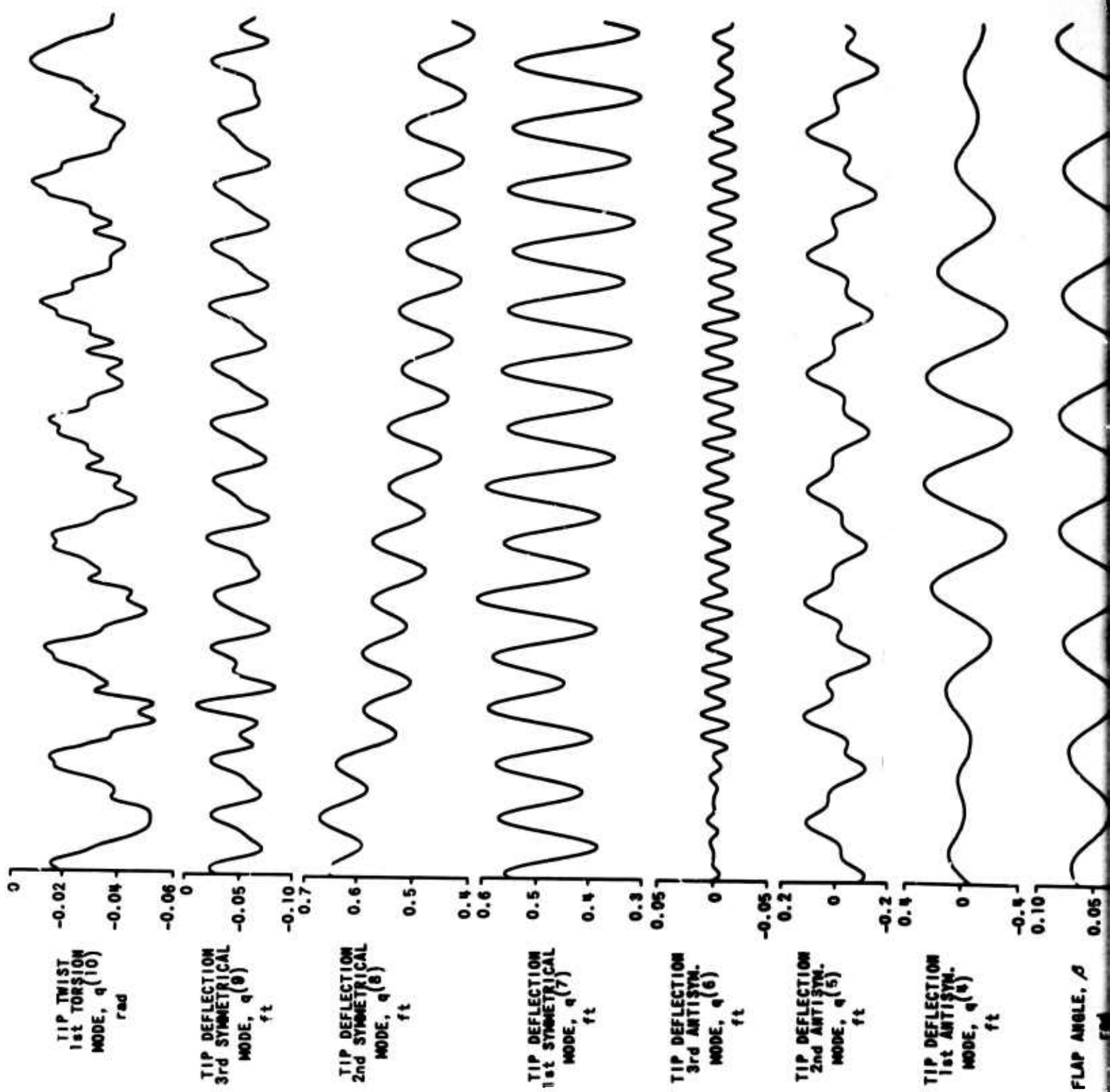ft

TIP DEFLECTION
1st ANTISYM.
MODE, $q(4)$
ft

FLAP ANGLE, β
rad

Figure 21. RESPONSE OF TEETERING ROTOR TO 100% POWER LOSS; $\mu = 0.26$, $\theta_c = 0.369$ RADIAN, $\alpha_s = 0.113$ RADIAN. (b) BLADE DISPLACEMENTS AND BENDING MOMENTS; SHAFT-VELOCITY RESPONSE.

long enough to show that the oscillation in the chordwise bending moment (excited by the change in shaft torque) finally begins to decay about 0.9 second after completion of the input disturbance.

Figure 22 indicates that loadings on the rigid rotor are very similar to those produced on the teetering rotor. The bending and torsional responses of the rigid blades are, however, significantly different from those experienced by the teetering rotor. Whereas first and second symmetric bendings on the teetering rotor are in phase with each other, resulting in increased flatwise displacements accompanied by decreased chordwise displacements, the first and second cantilever modes on the rigid rotor tend to be out of phase, with smaller components of second harmonic response being present. Nothwithstanding the out-of-phase addition of first and second bending, the resulting peak-to-peak excursions in flatwise and chordwise bending displacements and bending moments are substantially greater than those experienced by the teetering rotor. In fact, the periodic chordwise bending moment for the rigid rotor during steady-state flight is significantly greater than the chordwise bending-moment transient resulting from a power loss on the teetering rotor.

It should be noted that Figures 20, 21, and 22 present only a small portion of the data that are or can be obtained in the transient-response calculations performed in this study. Although the original plan called for presenting the inertial hub shears produced by each blade in addition to the aerodynamic shears, it was discovered that a required axis transformation was not introduced into the computation of the inertial shears; consequently, the computed results were in error. (This discovery was made sufficiently late in the program that time did not permit a correction of the noted deficiency.) Although the presented time histories give an adequate accounting of the loading changes that occur as a function of the azimuthal position of the blade, the spanwise distribution of loadings and the corresponding spanwise

distribution of bending displacements and moments are not adequately documented in this type of presentation. The spanwise distribution of loadings and the bent shape of the blade (flatwise and chordwise) are available in printed tabulations, but their bulk precludes their presentation in this report. It should be pointed out that the flatwise and chordwise bending moments were computed at only one span position, namely, 10 percent. It is felt that a complete examination of the influence of power loss and braking torques, in terms of the transient stresses imposed on rotor blades, would require, moreover, a thorough review of the spacial distribution of bending moments (flatwise and chordwise).

The response to a rapid and severe braking torque applied to the shaft of a rotor (operating at the zero-lift condition) is presented in Figure 23. In this instance, the wake is streaming back from the blades, remaining essentially in the plane of the rotor. The operation condition (defined in Table II) is assumed to be typical of a rotor mounted on a compound helicopter which is being supported by the lift on its fixed wing, just prior to removing power (required to turn the rotor at 100-percent rpm), and then braking the rotor to a stop. The impulses in loading caused by the close proximity of the wake to the blades are quite evident. It should be noted that some of these impulses are quite severe and constitute a very irregular spanwise distribution of loading.

When the collective pitch is set to yield a mean, nominal value of zero thrust, the loading outboard on the blades is negative, with the loading inboard being positive. As the rotor slows down, the negative loads outboard are reduced and the total rotor lift is seen to increase to a small, mean, positive value. At the end of the time history shown in the figure, the angular velocity of the rotor has dropped from an initial value of 32.81 radians per second to 18.98 radians per second. Thus, the advance ratio, μ, has increased from 0.26 to 0.45. Within this range of advance ratio, it appears that no unusual loading phenomena have been encountered other than the wake-disturbance effects that result from the absence of the usual downward transport velocity.

70

AERODYNAMIC
LOADING
97.5% SPAN
lb/ft

AERODYNAMIC
LOADING
87.5% SPAN
lb/ft

AERODYNAMIC
LOADING
75% SPAN
lb/ft

AERODYNAMIC
LOADING
55% SPAN
lb/ft

AERODYNAMIC
LOADING
25% SPAN
lb/ft

AERODYNAMIC
SHEAR
Y COMPONENT
lb
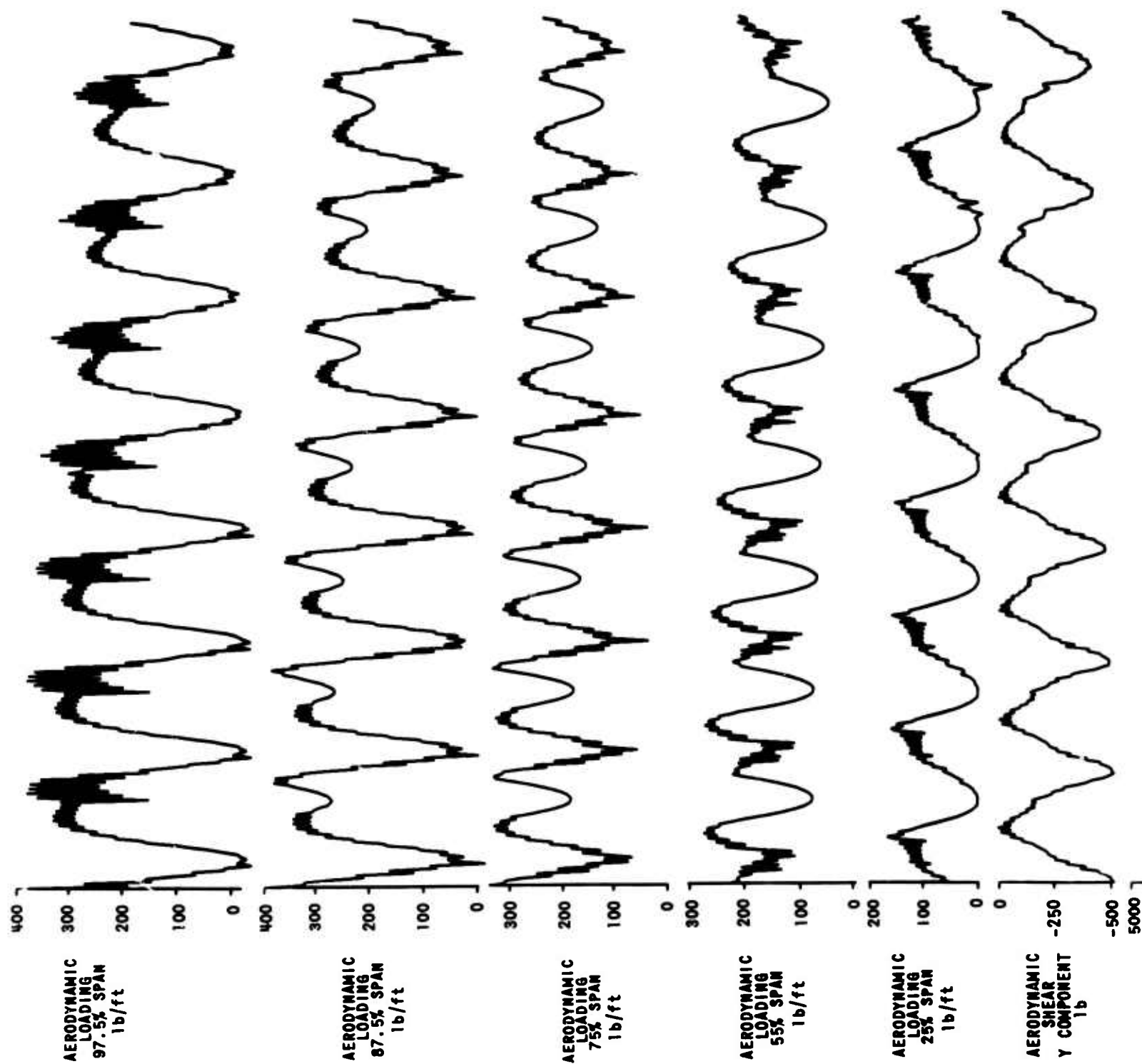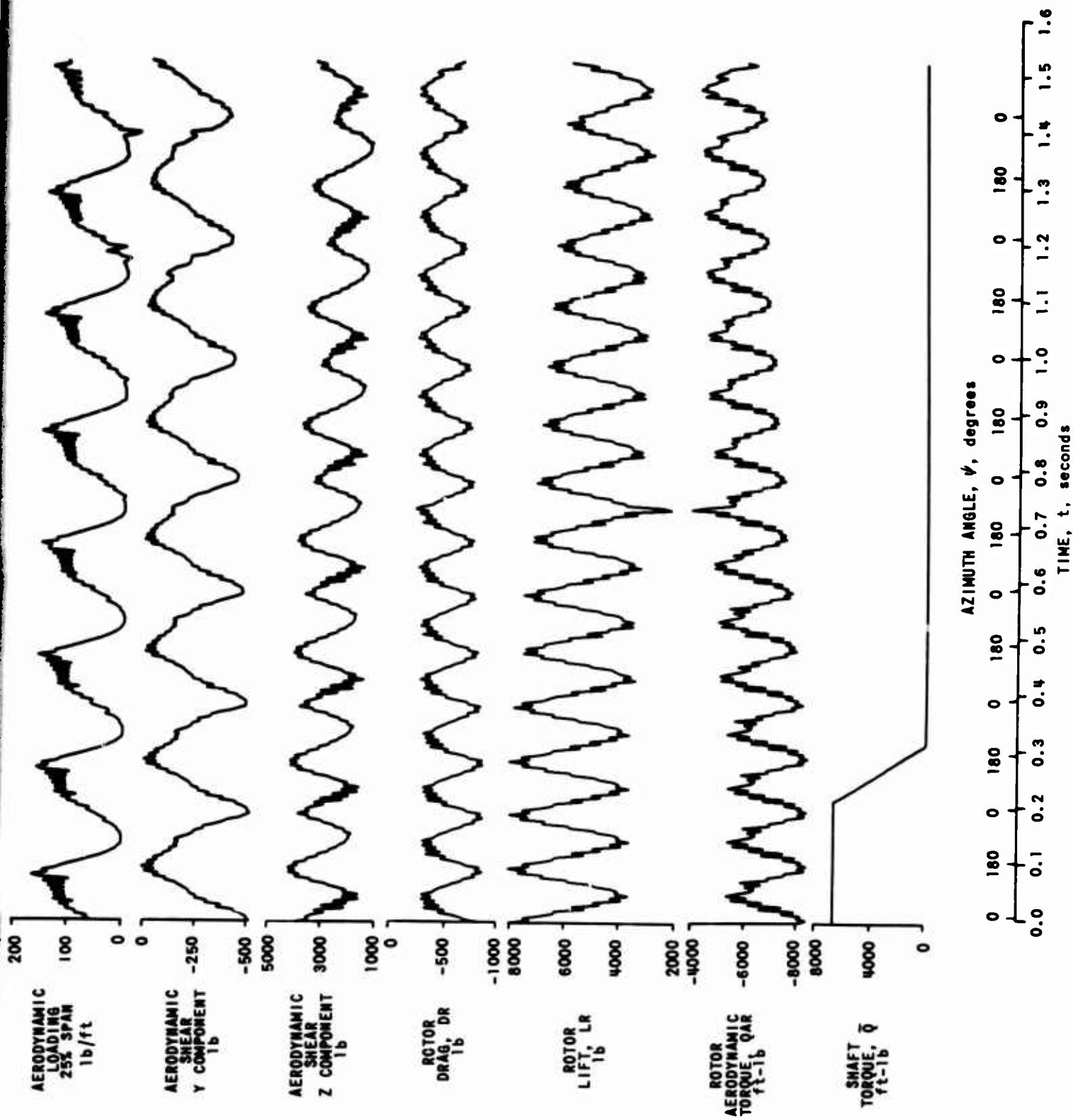
Figure 22. RESPONSE OF RIGID ROTOR TO 100% POWER LOSS; $\mu = 0.26$, $\theta_c = 0.352$ RADIAN, $\alpha_s = 0.104$ RADIAN.
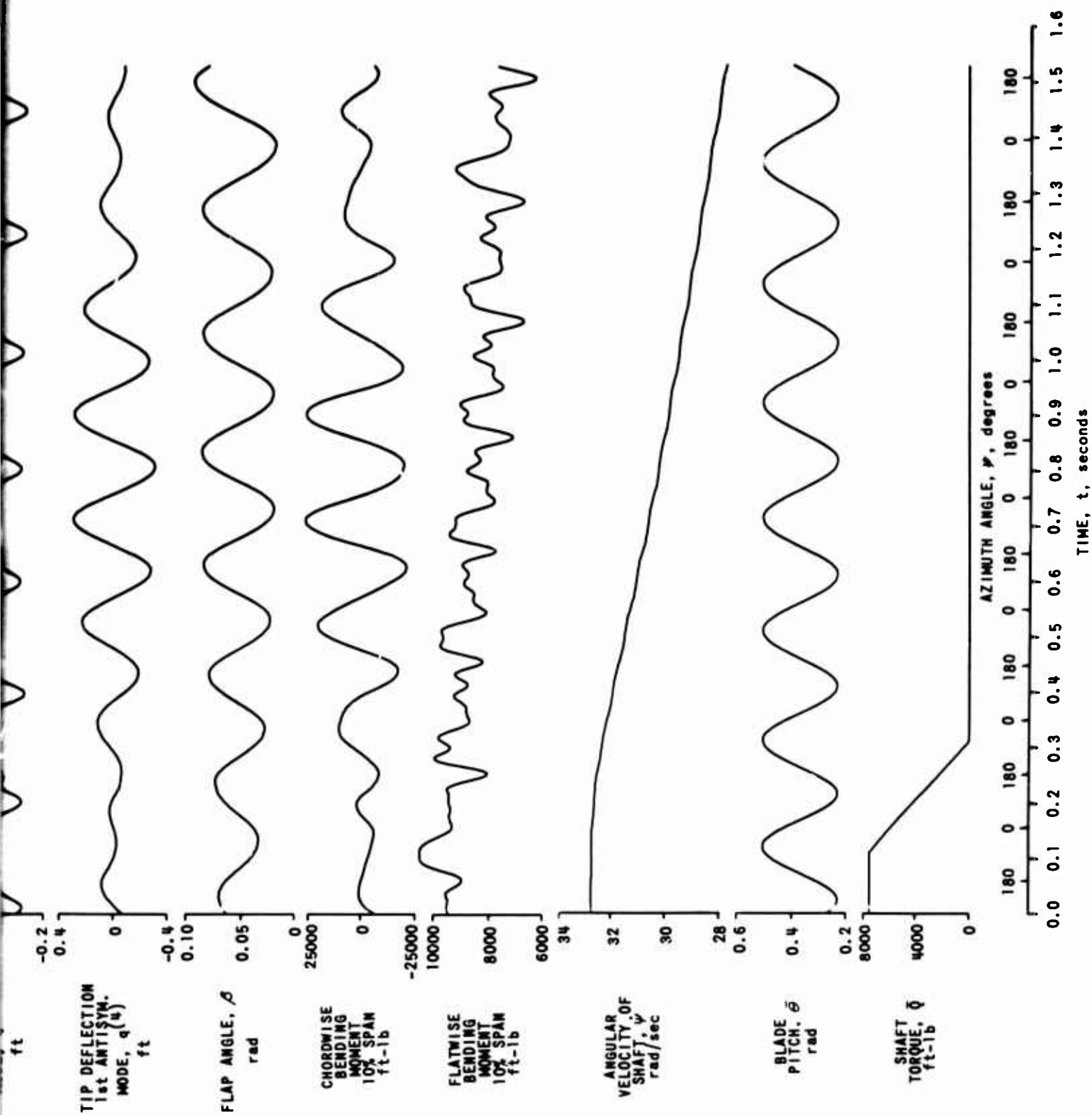(a) AERODYNAMIC LOAD AND FORCE TIME HISTORIES.

TIP TWIST
1st TORSION
MODE, $q(10)$
rad

TIP DEFLECTION
3rd CANTILEVER
MODE, $q(9)$
ft

TIP DEFLECTION
2nd CANTILEVER
MODE, $q(8)$
ft

TIP DEFLECTION
1st CANTILEVER
MODE, $q(7)$
ft

CHORDWISE
BENDING
MOMENT
10% SPAN
ft-lb

FLATWISE
BENDING
MOMENT
10% SPAN
ft-lb

73
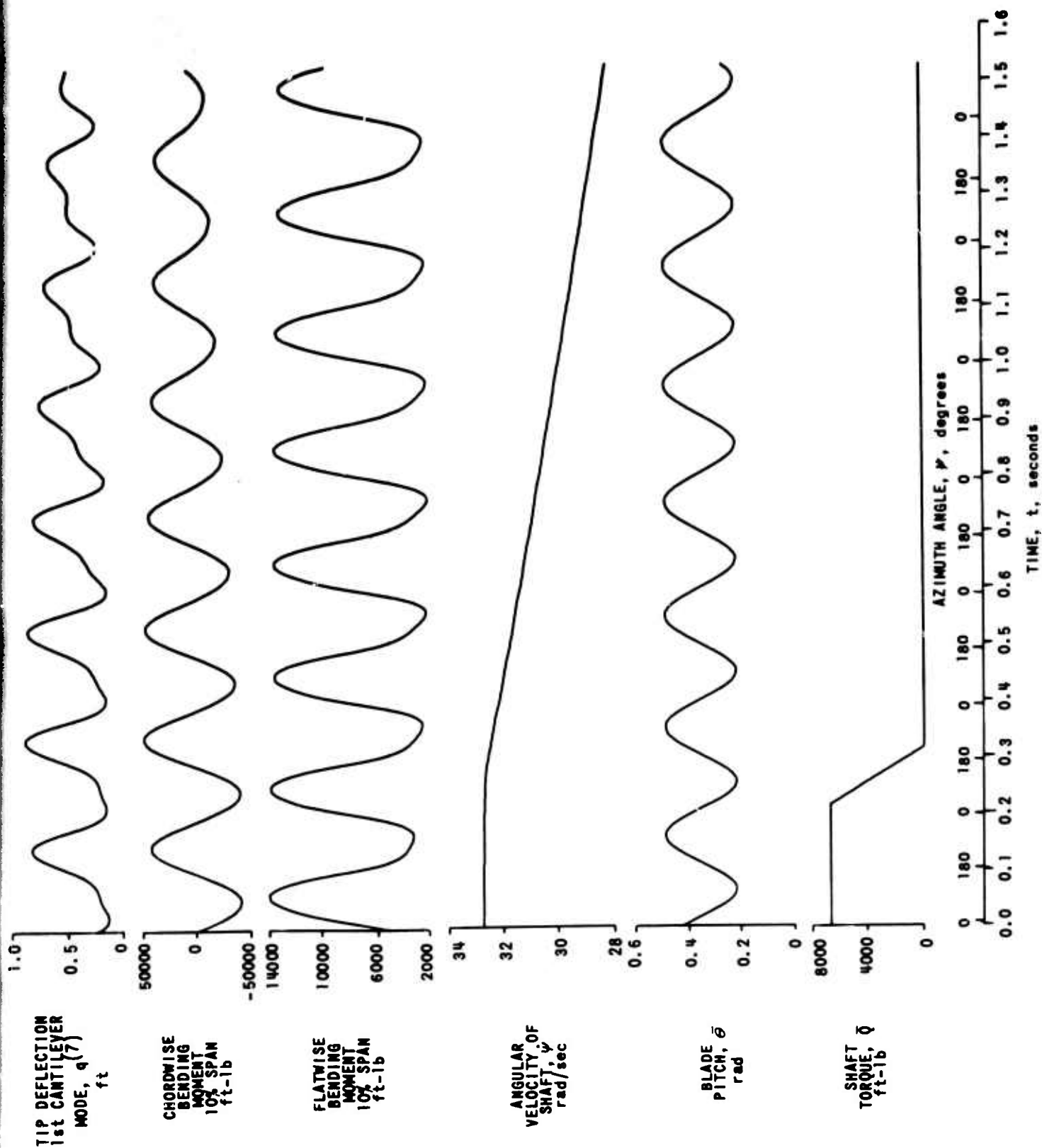
Figure 22. RESPONSE OF RIGID ROTOR TO 100% POWER LOSS; $\mu = 0.26$, $\theta_c = 0.352$ RADIAN, $\alpha_s = 0.104$ RADIAN.
(b) BLADE DISPLACEMENTS AND BENDING MOMENTS; SHAFT-VELOCITY RESPONSE.
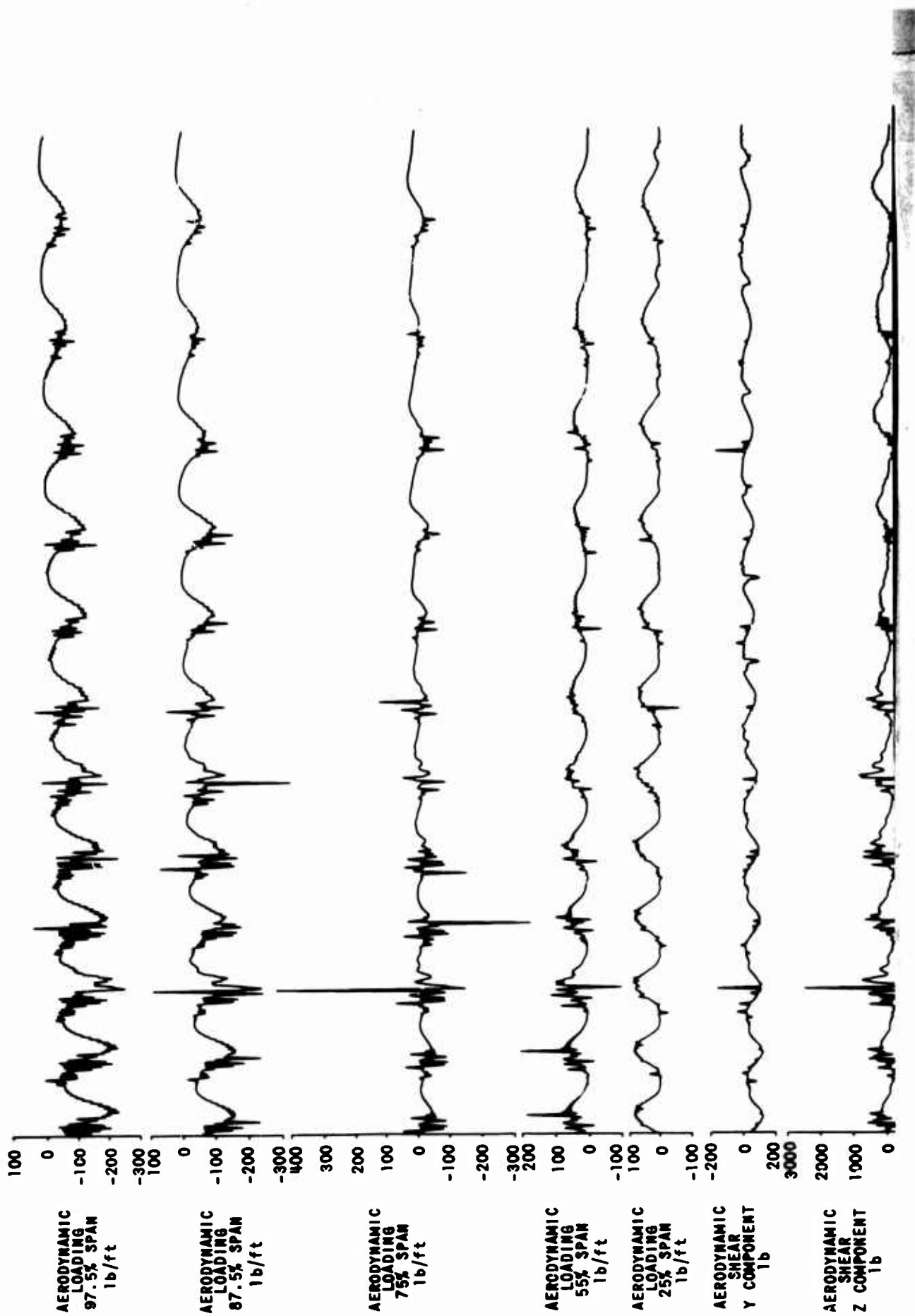
AERODYNAMIC
LOADING
97.5% SPAN
lb/ft

AERODYNAMIC
LOADING
87.5% SPAN
lb/ft

AERODYNAMIC
LOADING
75% SPAN
lb/ft

AERODYNAMIC
LOADING
55% SPAN
lb/ft

AERODYNAMIC
LOADING
25% SPAN
lb/ft

AERODYNAMIC
SHEAR
Y COMPONENT
lb

AERODYNAMIC
SHEAR
Z COMPONENT
lb

75

Figure 23. RESPONSE OF RIGID ROTOR AT ZERO THRUST TO LARGE BRAKING TORQUE; INITIAL ADVANCE RATIO = 0.26, θ_c = 0.138 RADIAN, α_s = 0 RADIAN.
(a) AERODYNAMIC LOAD AND FORCE TIME HISTORIES.

TIP TWIST
1st TORSION
MODE, q(10)
rad

0.02
0
-0.02

TIP DEFLECTION
3rd CANTILEVER
MODE, q(9)
ft

0
-0.04
-0.08

TIP DEFLECTION
2nd CANTILEVER
MODE, q(8)
ft

0.4
0
-0.4

TIP DEFLECTION
1st CANTILEVER
MODE, q(7)
ft

0.4
0
-0.4

CHORDWISE
BENDING
MOMENT
10% SPAN
ft-lb

25000
0
-25000

FLATWISE
BENDING
MOMENT
10% SPAN
ft-lb

4000
0
-4000

BLADE
PITCH, $\bar{\theta}$
rad

0.20
0.15
0.10

77
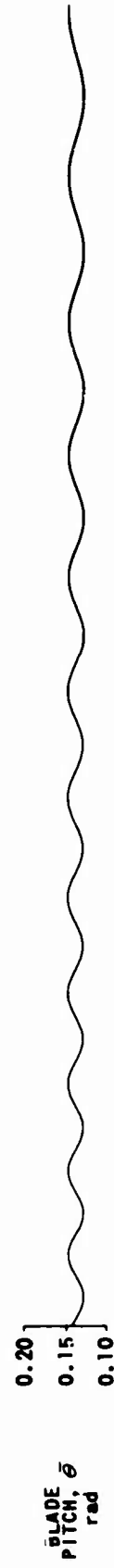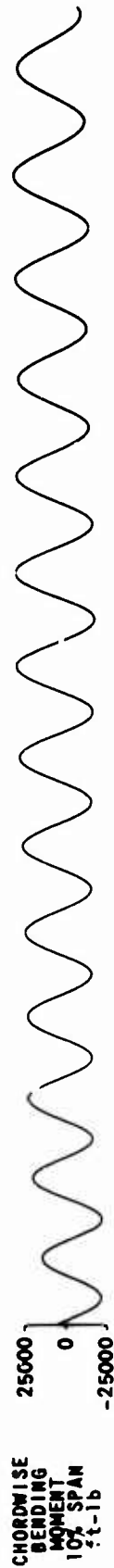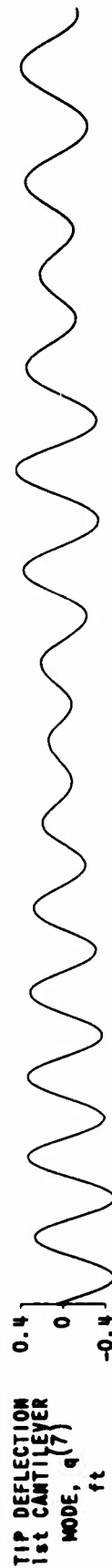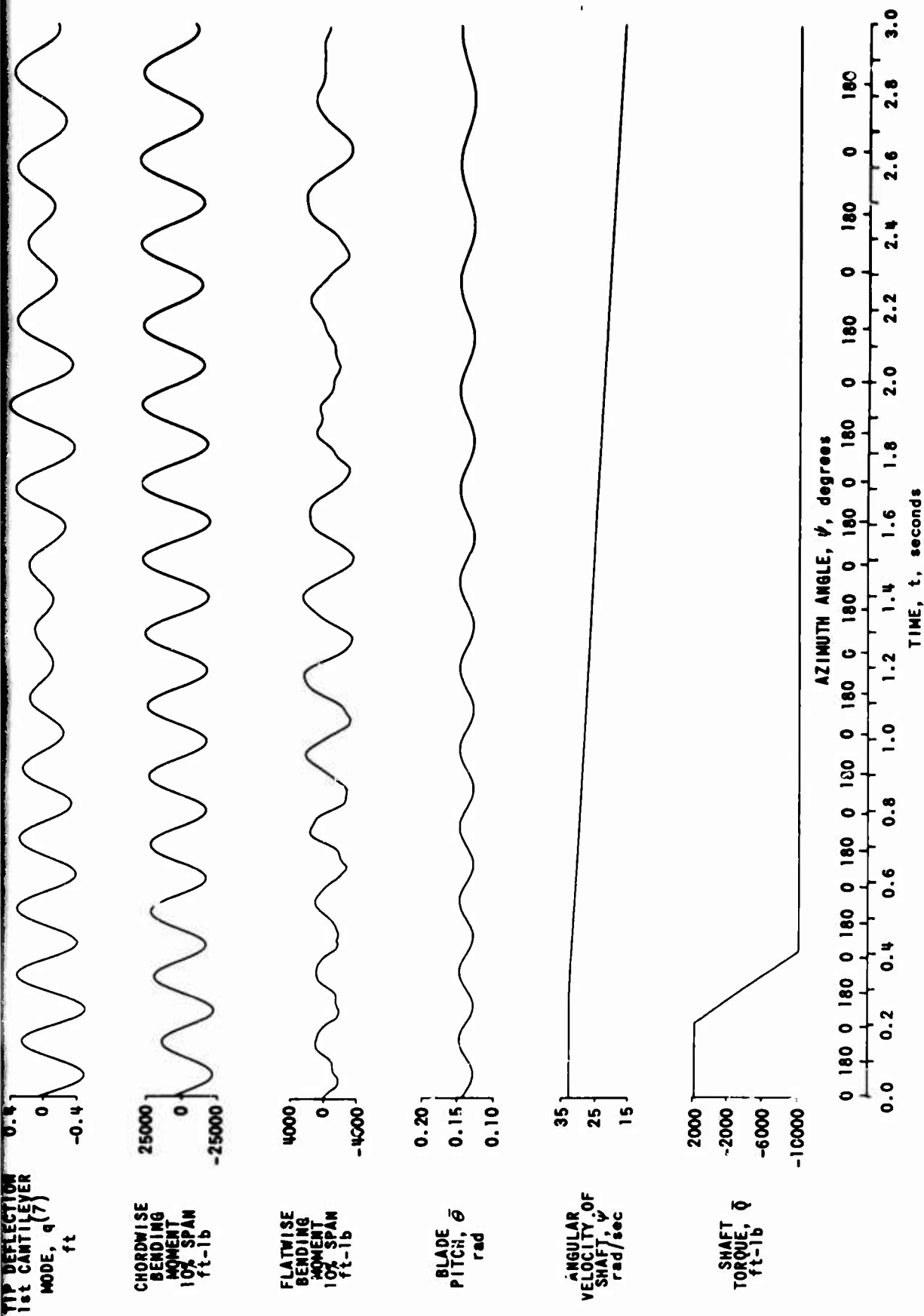
Figure 23. RESPONSE OF RIGID ROTOR AT ZERO THRUST TO LARGE BRAKING TORQUE; INITIAL ADVANCE RATIO = 0.26, θ_c = 0.138 RADIAN, α_s = 0 RADIAN. (b) BLADE DISPLACEMENTS AND BENDING MOMENTS; SHAFT-VELOCITY RESPONSE.

LOADINGS AND BLADE RESPONSE EXPERIENCED BY A RIGID ROTOR
IN THE "STOPPED" AND "START-UP" CONDITIONS

Figure 24 presents the loadings and displacements experienced by the rotor blade when it is stopped in the downstream position (0-degree azimuth) and then slowly rotated through one full rotor revolution. In this instance, it would have been desirable to plot also the results obtained for the blade which is stopped in the upstream position. However, the tape provided to the automatic-plotting routine contained results only for the reference blade; that is, the blade which is located at ψ = 0 degree when the rotor is assumed to be at ψ = 0 degree.

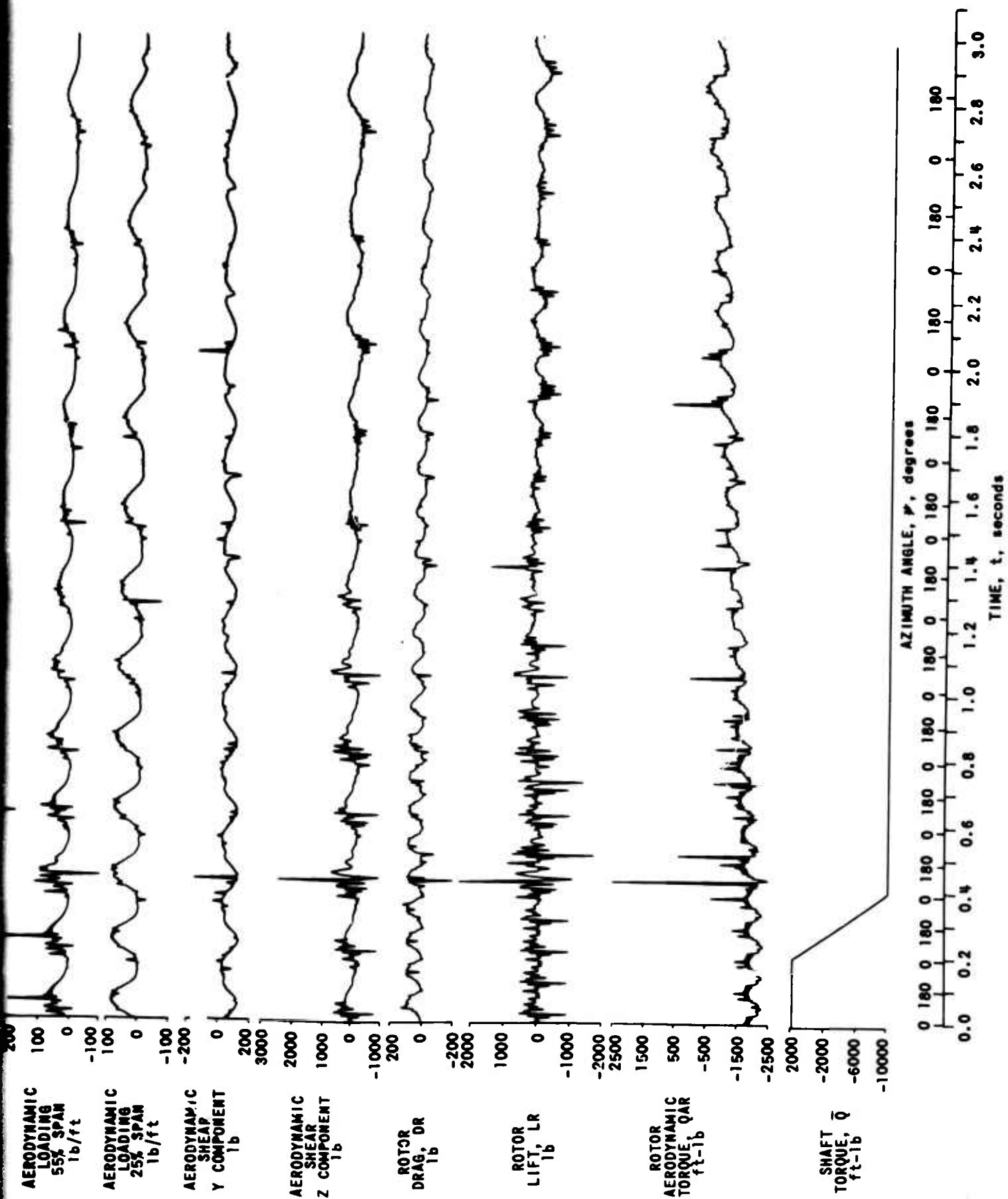It should be realized that the results shown for t = 0 second have been obtained by assuming zero values of blade displacement and velocity for the initial conditions. Since gravitational forces have been omitted, the blade does not bend due to its own weight and this means that the blade is initially straight when first exposed to the airstream. Since the assumed rigid rotor has 3 degrees of preconing and the shaft angle of attack is assumed to be zero, the forward blade is at 3 degrees positive angle of attack with respect to the airstream, and the downstream blade has a 3-degree negative angle of attack with respect to the airstream.[*] The loads and blade bending resulting from these initial conditions are permitted to reach a steady, equilibrium state prior to "unstopping" the rotor and applying a positive shaft torque to speed up the rotor.

Examination of Figure 24 indicates that any prior fears of the possibility of static divergence or dynamic instability appear to be unwarranted. Obviously, there is need to proceed to higher rotational

---

[*]It should be noted, however, that these blades have 12 degrees of negative twist with the collective pitch (as measured at the root chord) set to approximately 7.9 degrees.

79

speeds and to consider the changes that may result from representing the mode shapes more accurately than has been done here, before drawing firm and final conclusions on this point. Granting that the approximate aerodynamic analysis employed leads to inexact definition of the loadings, the evidence appears to support the conclusion that this specific rotor configuration is able to stop and start up without encountering an overstress condition.

It is instructive to examine Figure 24 in greater detail. Although, at $\psi = 0$ degree, the wake from the upstream blade is passing over the blade whose loading is plotted in this figure, it is seen that, notwithstanding this disturbance factor, the loading has the expected negative values at the 2.5- and 12.5-percent span locations which correspond to the forward chordwise portions of the resulting low-aspect-ratio surface. It appears that in the neighborhood of $\psi = 5$ degrees, the control point of the 87.5-percent span station passes in close proximity to a wake element originating from the forward blade as a result of the wake-definition logic which places a rolled-up element in space as if it had originated from the trailing edge (90-percent span location), thereby causing this rolled-up element to be located to the right of the shaft center line.

At $\psi = 90$ degrees, there is no component of radial flow, and the loading obtained is determined primarily by the twist distribution in the blade. Thus, the inboard sections have a positive loading and the outboard sections have a negative loading. On looking very closely, one can see a small discontinuity in loading at the 2.5- and 97.5-percent span stations when ψ is 90 degrees. This discontinuity is caused by the tip of the blade changing from a trailing to a leading edge (and vice versa for the root) as the component of radial flow switches from a positive to a negative value. As ψ approaches 180 degrees, the loading outboard on the blade changes from negative to positive, with the positive loadings on the inboard sections becoming smaller. At $\psi = 180$ degrees, a load distribution approaching that of a low-aspect-ratio surface is obtained,

AERODYNAMIC LOADING 97.5% SPAN lb/ft

AERODYNAMIC LOADING 87.5% SPAN lb/ft

AERODYNAMIC LOADING 75% SPAN lb/ft

AERODYNAMIC LOADING 55% SPAN lb/ft

AERODYNAMIC LOADING 25% SPAN lb/ft

AERODYNAMIC LOADING 12.5% SPAN lb/ft

AERODYNAMIC LOADING 2.5% SPAN lb/ft

AERODYNAMIC SHEAR Y COMPONENT lb

AERODYNAMIC SHEAR Z COMPONENT

81
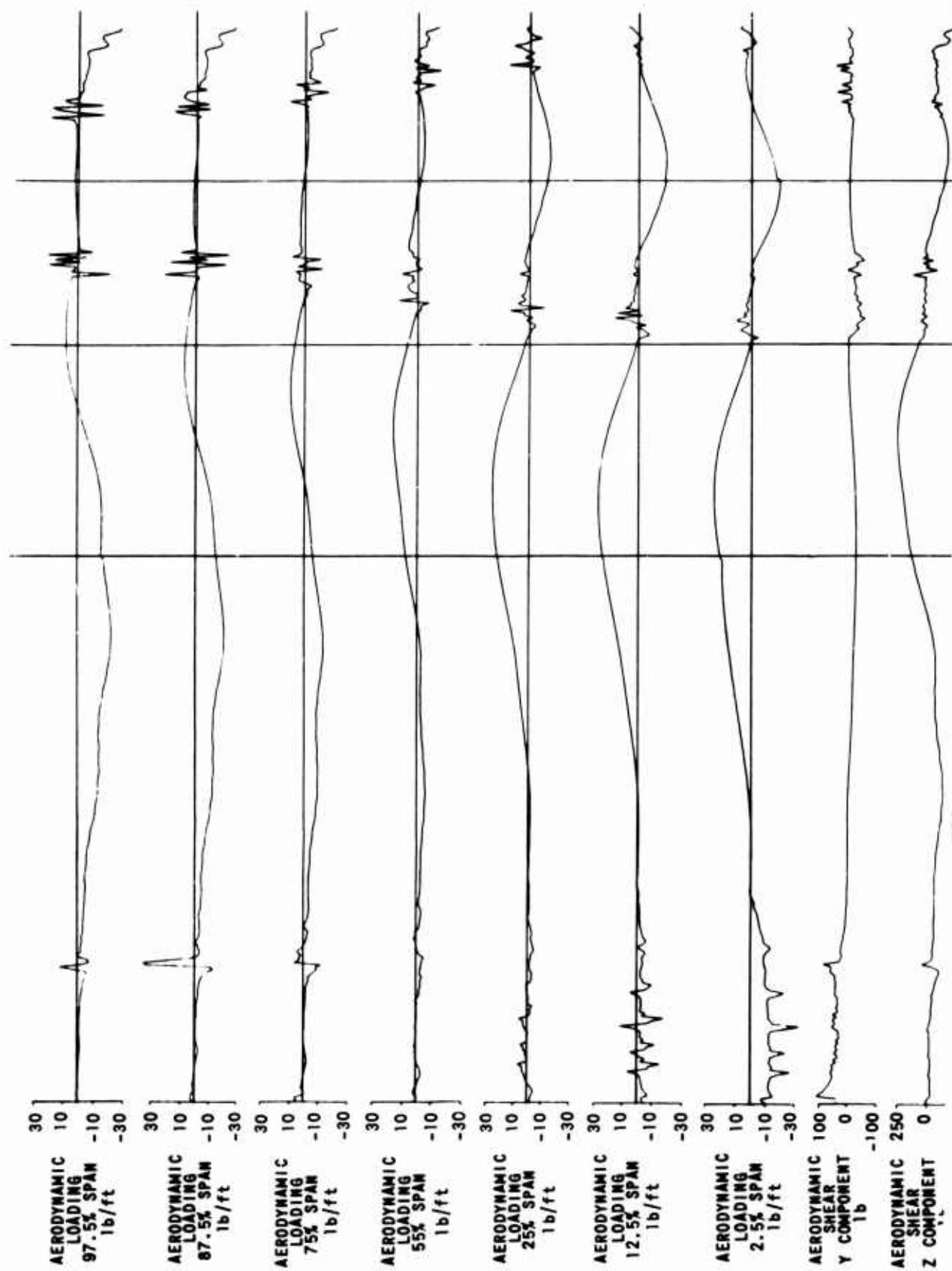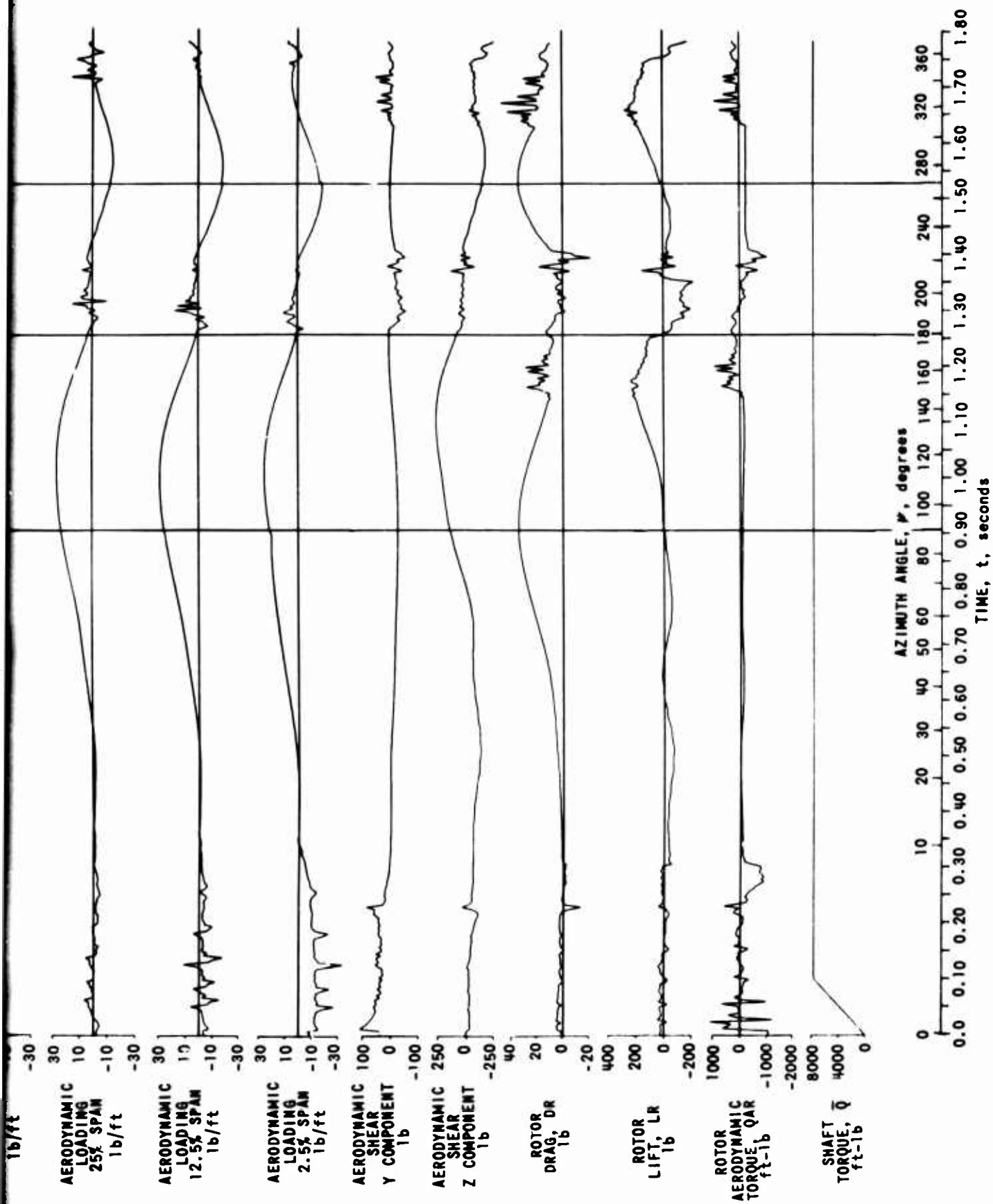
Figure 24. RESPONSE OF STOPPED, RIGID ROTOR TO INPUT OF POSITIVE SHAFT TORQUE; $\theta_c = 0.138$ RADIAN, $\alpha_s = 0$ RADIAN.

(a) AERODYNAMIC LOAD AND FORCE TIME HISTORIES.
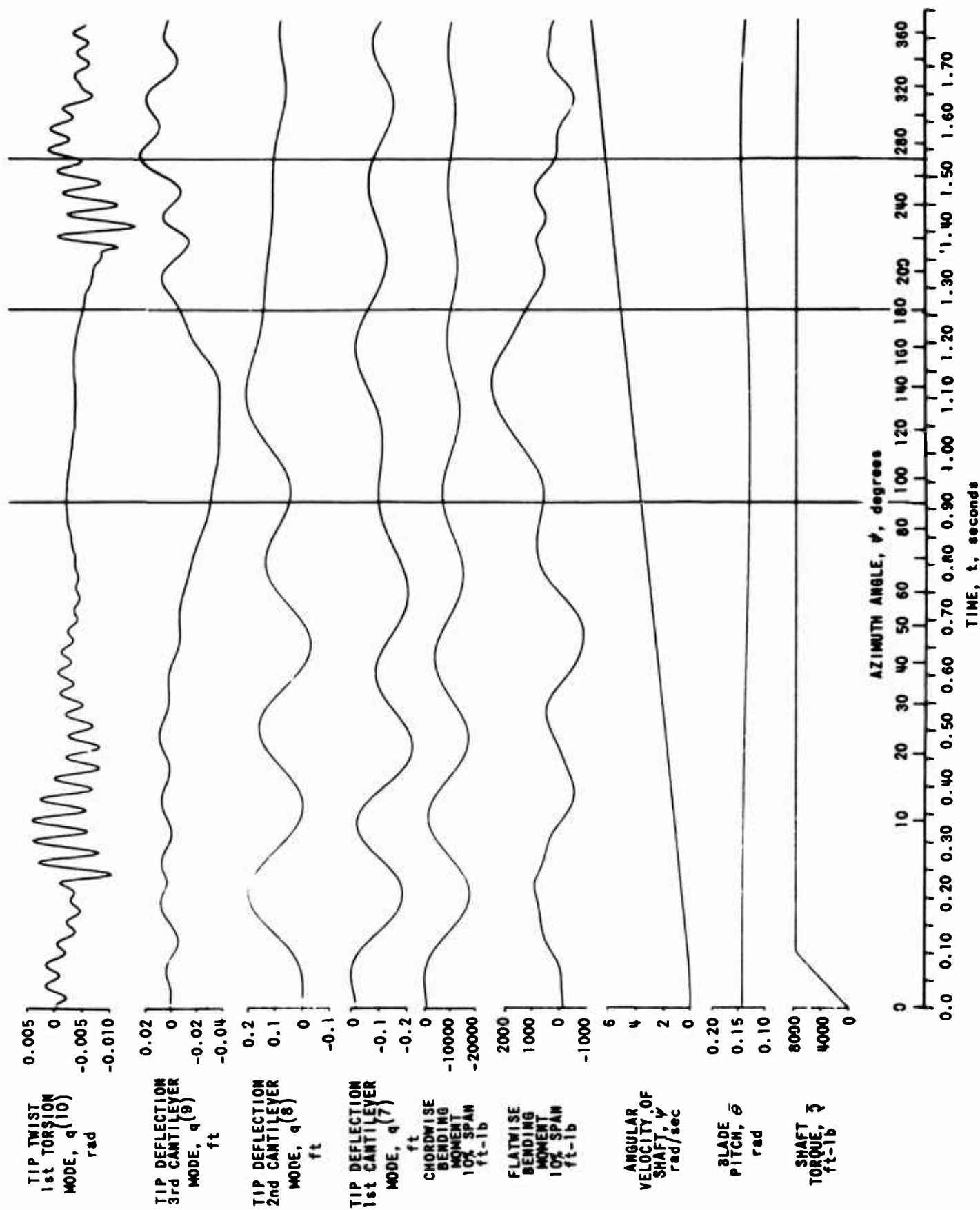
Figure 24. RESPONSE OF STOPPED, RIGID ROTOR TO INPUT OF POSITIVE SHAFT TORQUE; $\theta = 0.138$ RADIAN, $\alpha = 0$ RADIAN.

83

Figure 24. RESPONSE OF STOPPED, RIGID ROTOR TO INPUT OF POSITIVE SHAFT TORQUE; θ_c = 0.138 RADIAN, α_s = 0 RADIAN. (b) BLADE DISPLACEMENTS AND BENDING MOMENTS; SHAFT-VELOCITY RESPONSE.

83

except that the existing value of $\dot{\psi}$ = 5.2 radians per second causes positive loadings in the vicinity of midspan. The cause of the high-frequency change in loadings occurring between ψ = 180 and 360 degrees, when the loadings are in the vicinity of zero, is not clear. At ψ = 270 degrees, however, the calculated loadings are exactly what one would expect as a result of the angular velocity of the rotor building up to 6.4 radians per second at this point.

Note that rotor drag is small when the rotor is in the vicinity of ψ = 0 and 180 degrees and is at the expected peak when ψ = 90 and 270 degrees. Note, further, that shifts in the chordwise center of pressure explain, in part, the torsional response (however small) which is noted in Figure 24. Starting at time equal to zero, the initial torsional response is due to fluctuations in loadings on the leading portion of the downstream blade with the c.p. of these loadings being around midchord. The larger torsional response ensuing at t = 0.2 second is the result of the sharp change in loading at the 87.5-percent span location. (Here, the contribution to the generalized force in torsion is much greater than is produced by moments at inboard stations.) Later, at ψ in the vicinity of 210 degrees, the chordwise c.p. is moving from the midchord to the three-quarter chord, and the small fluctuations in loading at the blade tip provide sufficient moment excitation to excite the torsional mode of the blade again.

85

CONCLUSIONS

The following conclusions are drawn as a result of this study:

1. It is feasible to simulate the dynamics of a rotor-wake system by means of numerical integration of the applicable equations of motion. However, it would be preferable to employ a hybrid of digital- and analog-computing means to implement the desired calculations in a more efficient manner.

2. The efforts made in this study to develop an aerodynamic model to generate valid aerodynamic loadings, irrespective of whether the flow is primarily tangential or radial with respect to the lifting surface, are considered successful. Additional refinements are indicated for the wake model in order to represent properly the roll-up of wake vorticity trailed under conditions of predominantly radial flow.

3. It appears that no aerodynamic and/or structural response phenomena of unusual nature occur during power loss and braking transients for the rotors treated in this study. This conclusion could presumably be modified by performing a more extensive examination of the bending moment distributions along the span.

4. The aerodynamic loadings and structural displacements produced on a rotor stopped at 0 - 180 degrees and then turned through one rotor revolution are small and bounded.

RECOMMENDATIONS

1. The refinement of the developed digital-computing program to obtain a more efficient calculation procedure should be performed by personnel bearing helicopter-design responsibilities.

2. There is need for extending the current understanding of the aerodynamic behavior of lifting surfaces having geometry and flow orientation typical of rotary wings in forward flight. This extension should be concerned with both steady and unsteady flow processes.

3. Calculations should be made to determine the extent to which the fulfillment of a three-dimensional boundary condition and the employment of a wake model would explain discrepancies existing between the performance of rotary wings, as measured and as predicted by calculation procedures employing "strip" the ~· ~~d the traditional assumption of uniform inflow.

4. The analysis and digital-computing program developed in this study should be employed to investigate problems of rotor stability at the high advance ratios that will result from an attempt to achieve higher forward flight speeds. Conclusions drawn by others relative to instability phenomena, deriving either from mechanical or aerodynamic sources or a combination of these, should be put to the test with the assistance of the developed program.

5. Efforts should be initiated to augment the transient-blade-
    loads program for purposes of examining the spacial and
    temporal distribution of loadings and stresses encountered
    by rotary wings upon entry into a vertical gust.

REFERENCES

1. Blankenship, B. L. and Harvey, K. W., "A Digital Analysis fo. Helicopter Performance and Rotor Blade Bending Moments", Journal of the American Helicopter Society, Volume 7, No. 4, October 1962.

2. Gerstenberger, W. and Wood, E. R., "Analysis of Helicopter Aeroelastic Characteristics in High-Speed Flight", American Institute of Aeronautics and Astronautics Journal, Volume 1, No. 10, October 1963.

3. Berman, A., "A New Approach to the Solution of Rotor Blade Dynamics Problems", Journal of the American Helicopter Society, Volume 10, No. 3, July 1965.

4. Piziali, R. A., Method for Solution of the Aeroelastic Response Problems for Rotating Wings, Presented at a Symposium on the Noise and Loading Actions on Helicopter V/STOL Aircraft and Ground Effect Machines, August 30 - September 3, 1965 (To appear in the Journal of Sound and Vibration).

5. Harrison, J. M. and Ollerhead, J. B., The Nature of Limitations Imposed on the Performance of a Helicopter Rotor, Presented at a Symposium on the Noise and Loading Actions on Helicopter V/STOL Aircraft and Ground Effect Machines, August 30 - September 3, 1965 (To appear in the Journal of Sound and Vibration).

6. Lemnios, A. Z., "A Nonlinear Aeroelastic Loads Analysis of Rotary Wings", Proceedings of AIAA Symposium on Structural Dynamics and Aeroelasticity, August 30 - September 1, 1965.

7. Duhon, J. M., Harvey, K. W. and Blankenship, B. L., "Computer Flight Testing of Rotorcraft", Journal of the American Helicopter Society, Volume 10, No. 4, October 1965.

8. Trenka, A. R., Development of a Method for Predicting the Performance and Stresses of VTOL-Type Propellers, U. S. Army Aviation Materiel Laboratories, USAAVLABS Technical Report 66-26.

9. Willmer, M. A. P., The Loading of Helicopter Blades in Forward Flight, Aeronautical Research Council R & M 3318, April 1959.

10.   Piziali, R. A. and DuWaldt, F. A., Computation of Rotary Wing Air Loads and Comparison with Experimental Results, Proceedings of the American Helicopter Society Eighteenth Annual National Forum, 1962.

11.   Miller, R. H., "On the Computation of Airloads Acting on Rotor Blades in Forward Flight", Journal of the American Helicopter Society, Volume 7, No. 2, 1962.

12.   Segel, L., Air Loadings on a Rotor Blade as Caused by Transient Inputs of Collective Pitch, U. S. Army Aviation Materiel Laboratories, USAAVLABS Technical Report 65-65, October 1965. [See also: "A Method for Predicting the Non-Periodic Air Loads on a Rotary Wing", Journal of Aircraft, Volume 3, No. 6, 1966.]

13.   Sweet, G. E. and Jenkins, J. L., Jr., "Results of Wind Tunnel Measurements on a Helicopter Rotor Operating at Extreme Thrust Coefficients and High Tip Speed Ratios", American Helicopter Society Journal, Volume 8, No. 3, July 1963.

14.   Arcidiano, P. J., "Aerodynamics of a Model Helicopter Rotor Operating under Nominally Stalled Conditions in Forward Flight", American Helicopter Society Journal, Volume 9, No. 3, July 1964.

15.   Gersten, K., Nonlinear Airfoil Theory for Rectangular Wings in Incompressible Flow, National Aeronautics and Space Administration, NASA RE 3-2-59W, February 1959.

16.   Holme, O. A., Measurements of the Pressure Distribution on Rectangular Wings of Different Aspect Ratios, Aeronautical Research Institute of Sweden (FFA), Report No. 32, 1950.

17.   Marshall, W. S. D., The Distribution of Pressure Over the Surface of Wings of Small Aspect Ratio, The College of Aeronautics (Cranfield), Report No. 52, February 1952.

18.   Jones, R. T., Properties of Low Aspect Ratio Pointed Wings at Speeds Below and Above the Speed of Sound, National Advisory Committee for Aeronautics, Report No. 835, 1946.

19.   Houboult, J. C. and Brooks, G. W., Differential Equations of Motion for Combined Flapwise Bending, Chordwise Bending, and Torsion of Twisted Nonuniform Rotor Blades, National Advisory Committee for Aeronautics, Technical Note 3905, February 1957.

20. Targoff, W. P, The Bending Vibrations of a Twisted Rotating Beam, Wright Air Development Center, WADC Technical Report 56-27, December 1955.

21. Lamnios, A. Z. and Smith, A., High Speed Rotor Research, Part I - Tensor Techniques in Rotor Analyses, Kaman Aircraft Corporation Research Note 64-6, July 8, 1964.

22. HU-IA Rotor Blade Drawings (Sent to Cornell Aeronautical Laboratory, Inc. via a personal communication from F. Burpo, dated March 16, 1966).

23. Bisplinghoff, R. L., Ashley, H., and Halfman, R. L., Aeroelasticity, Addison Wesley Publishing Company, Inc., Reading, Massachusetts, 1955.

24. Bell Helicopter Company, Measurement of Dynamic Air Loads on a Full-Scale Semirigid Rotor, U. S. Army Transportation Research Command, TCREC Technical Report 62-42, December 1962.

APPENDIX I

THE KINEMATICS OF ROTOR BLADES FREE TO FLAP, LAG, PITCH, BEND, TWIST, AND ROTATE WITH A VARIABLE ANGULAR VELOCITY

The objective of this appendix is to document the significant kinematic relationships that are utilized in (1) performing wake calculations, (2) solving for the unknown bound circulations, and (3) deriving the equations of motion that yield the accelerations in each assumed generalized coordinate. In the third task, the evaluation of kinetic and potential energies of the rotor system utilized an approach that was based on assumptions (e. g., the location of the elastic axis, the axis of built-in twist, etc.) that were slightly different from those adopted to compute the displacement and velocities of points relative to the x-y-z axis system defined in Figure 7. These different assumptions stemmed, in part, from the uncertainties that existed with respect to actual construction practice and, in part, from the different procedures that were used to derive kinematic relationships in these separate instances.

In order to derive the x-y-z position (see Figure 7 for the definition of this axis system) of points on a blade as defined by their ζ, η location (see Figure 9), use was made of the axis-transformation procedure referred to in Reference 6 and outlined in more detail in Reference 21. The procedure is implemented by starting with a point on the blade and moving inboard to the hub by successive translations and rotations based on all of the generalized displacements assumed to exist in deriving the equations of motion of the rotor. The degrees of freedom assumed for this analysis require the following transformations:

1. Rotation of the blade about the elastic axis to eliminate the twist due to torsion.

2. Translation of the blade to remove bending displacements in the flapwise and chordwise directions (shortening of the blade in ζ direction is neglected).

3. Translation of the elastic axis to the feathering axis.

4. Rotation of the blade about the feathering axis to eliminate the built-in twist.[*]

5. Translation of the η axis to that position along the blade span assumed to be the origin of the ζ axis.

6. Rotation of the root chord about the feathering axis to a plane parallel to the shaft plane.

7. Translation of the origin of the feathering axis to the drag hinge.

8. Rotation about the drag hinge such that the feathering axis is parallel to the radial direction.

9. Translation of the origin to the flap hinge.

10. Rotation about the flap hinge such that the feathering axis is parallel to the shaft plane.

11. Translation of the origin from the flap hinge to the center of the rotor shaft.

---

[*]It should be recalled that this assumption is incorrect. The practical consequences, however, are not believed to be significant.

12. Rotation of the axes (established by the previous transformation) about the rotor shaft to line up with the nonrotating axis system $(x, -y, -z)$ defined in Figure 7.

13. Rotation of the $x, -y, -z$ axes about the y axis to obtain the "wind-axis" system.

On making the usual small-angle assumptions, and on dropping second-order terms, the following general expressions for blade coordinates are yielded by the above-outlined transformation procedure:

$$x(\xi, \eta) = \cos\psi \left[e_H + \xi \right] - \sin\psi \left[\tilde{e}_D - \tilde{e}_p + e_o + \eta - \zeta(e_p + \xi) \right]$$
$$- \alpha_s \beta \left[e_1 + \xi \right] - \alpha_s \left[(e_o + \eta)(\theta + \theta_s) + w + \phi\eta \right],$$

$$y(\xi, \eta) = \sin\psi \left[e_H + \xi \right] + \cos\psi \left[\tilde{e}_D - \tilde{e}_p + e_o + \eta - \zeta(e_p + \xi) \right],$$

$$z(\xi, \eta) = \alpha_s \cos\psi \left[e_H + \xi \right] - \alpha_s \sin\psi \left[\tilde{e}_D - \tilde{e}_f + e_o + \eta - \zeta(e_p + \xi) \right]$$
$$+ (e_o + \eta)(\theta + \theta_s) + w + \phi\eta + \beta \left[e_1 + \xi \right].$$

These expressions are utilized to determine the coordinates of control points and the end points of vortex elements, both fixed and free, in the $x\cdot y\cdot z$ space. For example, the $x\cdot y\cdot z$ location of the three-quarter chord point located in blade i at the center of blade segment j and at time m is given by

$$x_{m,i,j} = \cos\psi_{m,i} \left[e_H + \xi_j \right] - \sin\psi_{m,i} \left[\tilde{e}_D - \tilde{e}_p + e_{o_j} + \bar{\eta}_j - \zeta_{m,i}(e_p + \xi_j) \right]$$
$$- \alpha_s \beta_{m,i} \left[e_1 + \xi_j \right] - \alpha_s \left[e_{o_j} \hat{\theta}_{m,i,j} + \bar{\eta}_j \tilde{\theta}_{m,i,j} + w_{m,i,j} \right],$$

$$y_{m,i,j} = \sin\psi_{m,i} \left[e_H + \xi_j \right] + \cos\psi_{m,i} \left[\tilde{e}_D - \tilde{e}_p + e_{o_j} + \bar{\eta}_j - \zeta_{m,i}(e_p + \xi_j) \right],$$

$$z_{m,i,j} = \alpha_s \cos\psi_{m,i} \left[e_H + \xi_j \right] + e_{o_j} \hat{\theta}_{m,i,j} + \bar{\eta}_j \tilde{\theta}_{m,i,j} + w_{m,i,j}$$
$$+ \beta_{m,i} \left[e_1 + \xi_j \right] - \alpha_s \sin\psi_{m,i} \left[\tilde{e}_D - \tilde{e}_p + e_{o_j} + \bar{\eta}_j - \zeta_{m,i}(e_p + \xi_j) \right],$$

94

where

$$\bar{\theta}_{m,i,j} = \theta_{m,i} + \theta_j + \phi_{m,i,j}$$

$$\hat{\theta}_{m,i,j} = \theta_{m,i} + \theta_j$$

$\bar{\eta}_j \quad = \quad \eta$ distance from elastic axis to three-quarter chord at center of blade segment j.

$\theta_j \quad = \quad$ lumped value of θ_ζ, i.e., value of built-in twist at center of segment j relative to chord at $\zeta = 0$.

$\phi_{m,i,j} =$ blade twist due to torsion at time m, blade i, station j.

$\theta_{m,i} \quad =$ pitch angle of blade chord, at $\zeta = 0$, with respect to the shaft plane; blade i at time m.

The coordinates of the wake are defined in a fashion similar to that outlined in the appendix of Reference [12]. Since the rotor in TBL-II rotates with a variable angular velocity, the time increment used for convecting the wake is $t_m - t_{m-1}$, rather than $\frac{2\pi}{\Omega NA}$, as was used in TBL-I.

In addition to determining the coordinates of the blade in x-y-z space, it is necessary to determine the velocities of given points on the blade with respect to inertial space. Since these velocities are used to compute the angles of attack used in the "strip" analysis and to obtain the velocity component normal to the blade when satisfying the "three-dimensional" boundary condition, it is more convenient to work in the

95

shaft-axis system. Coordinates $x_1(\xi, \eta)$, $y_1(\xi, \eta)$, and $\mathfrak{z}_1(\xi, \eta)$ are thus differentiated to obtain $\dot{x}_1(\xi, \eta)$, $\dot{y}_1(\xi, \eta)$, and $\dot{\mathfrak{z}}_1(\xi, \eta)$.

If the radial, tangential, and normal velocities of a point on a blade relative to still air are designated as U_ξ', U_η', and U_ζ' (ξ, η, and ζ are axes located in a plane tangent to the blade surface at the selected point), these velocities are given by

$$U_\xi' = \bar{q} \cdot \hat{e}_\xi$$
$$U_\eta' = \bar{q} \cdot \hat{e}_\eta \qquad\qquad (10)$$
$$U_\zeta' = \bar{q} \cdot \hat{e}_\zeta$$

where $\hat{e}_\xi$, $\hat{e}_\eta$, and $\hat{e}_\zeta$ are unit vectors oriented along the respective ξ, η, and ζ axes, and $\bar{q}$ is the total velocity vector of a point on the blade as defined in the shaft-axis system, $x_1 - y_1 - \mathfrak{z}_1$. If $\tilde{u}$, $\tilde{v}$, and $\tilde{w}$ are designated as components of the velocity that is induced by the rotor wake in $x - y - \mathfrak{z}$ space and α_s is taken as a small angle, Figure 7 shows that

$$\bar{q} = (\dot{x}_1 - V - \tilde{u} - \tilde{w}\alpha_s)\bar{\imath} + (\dot{y}_1 - \tilde{v})\bar{\jmath} + (\dot{\mathfrak{z}}_1 + V\alpha_s - \tilde{w} + \tilde{u}\alpha_s)\bar{k}$$

where V is the forward velocity of the hub along the negative x axis. Equation (10) can be employed to obtain the desired velocity components by noting that

$$\hat{e}_\zeta = \frac{1}{h_\zeta}\left[\frac{\partial x_1}{\partial \zeta}\bar{\imath} + \frac{\partial y_1}{\partial \zeta}\bar{\jmath} + \frac{\partial \mathfrak{z}_1}{\partial \zeta}\bar{k}\right]$$

$$\bar{e}_\eta = \frac{1}{h_\eta}\left[\frac{\partial x_1}{\partial \eta}\bar{\imath} + \frac{\partial y_1}{\partial \eta}\bar{\jmath} + \frac{\partial \mathfrak{z}_1}{\partial \eta}\bar{k}\right]$$

$$\hat{e}_\zeta = \hat{e}_\xi \times \hat{e}_\eta$$

96

where

$$h_\xi^2 = \left(\frac{\partial x_1}{\partial \xi}\right)^2 + \left(\frac{\partial y_1}{\partial \xi}\right)^2 + \left(\frac{\partial z_1}{\partial \xi}\right)^2$$

and

$$h_\eta^2 = \left(\frac{\partial x_1}{\partial \eta}\right)^2 + \left(\frac{\partial y_1}{\partial \eta}\right)^2 + \left(\frac{\partial z_1}{\partial \eta}\right)^2.$$

On differentiating the coordinates $x_1(\xi,\eta)$, $y_1(\xi,\eta)$ and $z_1(\xi,\eta)$ both with respect to time and with respect to ξ and η, and on neglecting second-order terms, the following expressions are obtained for U_ξ, U_η, and U_ζ, where these unprimed components designate air velocities relative to the blade rather than blade velocities relative to still air:

$$U_{\xi_{m,i,j}} = V\cos\psi_{m,i} + V\zeta_{m,i}\sin\psi_{m,i} - \left[\beta_{m,i} + \frac{\partial w}{\partial \xi}\right)_{m,i,j}\left[V\alpha_s - \tilde{w}_{m,i,j}\right]$$
$$- \frac{\partial w}{\partial \xi}\bigg)_{m,i,j}\left[\dot{\beta}_{m,i}(e_1 + \xi_j) + \dot{w}_{m,i,j}\right]$$

$$U_{\eta_{m,i,j}} = \cos\tilde{\theta}_{m,i,j}\left[\bar{U}_{m,i,j} - V\zeta_{m,i}\cos\psi_{m,i}\right]$$
$$+ \sin\tilde{\theta}_{m,i,j}\left[V\beta_{m,i}\cos\psi_{m,i} + \dot{\beta}_{m,i}(e_1 + \xi_j) + V\alpha_s\right]$$
$$+ \dot{v}_{m,i,j} - \dot{\theta}_{m,i}w_{m,i,j} - \sin\tilde{\theta}_{m,i,j}\tilde{w}_{m,i,j}$$

$$U_{\zeta_{m,i,j}} = \sin\tilde{\theta}_{m,i,j}\bar{U}_{m,i,j} - (e_{0j} + \bar{\eta}_j)\dot{\theta}_{m,i} - \dot{w}_{m,i,j} - \bar{\eta}_j\dot{\phi}_{m,i,j}$$
$$- \cos\tilde{\theta}_{m,i,j}\left[V\bar{\beta}_{m,i,j}\cos\psi_{m,i} + \dot{\beta}_{m,i}(e_1 + \xi_j) + V\alpha_s\right] + \cos\tilde{\theta}_{m,i,j}\tilde{w}_{m,i,j}$$

where

$$\bar{U}_{m,i,j} = \dot{\psi}_{m,i}(e_H + \xi_j) - \dot{\zeta}_{m,i}(e_p + \xi_j) + V\sin\psi_{m,i}$$

and

$$\bar{\beta}_{m,i} = (e_{0j} + \bar{\eta}_j)\frac{\partial \theta_\xi}{\partial \xi} + \frac{\partial w}{\partial \xi}\bigg)_{m,i,j} + \bar{\eta}_j\frac{\partial \phi}{\partial \xi}\bigg)_{m,i,j} + \beta_{m,i}.$$

Note that the above velocity components have been expressed in terms of an $\xi\text{-}\eta\text{-}\zeta$ set of axes whose origin is located at an i,j control point. If $\bar{\eta}_j$ is assumed to be a distance from the elastic axis to a three-quarter

97

chord point, then, for the "strip" analysis, the angle of attack at the three-quarter chord can be expressed as

$$\alpha_{m,i,j} = \tan^{-1} \frac{U_{\zeta_{m,i,j}}}{U_{\eta_{m,i,j}}} \ .$$

The boundary condition for the "three-dimensional" analysis is given by

$$U_{\zeta_{m,i,j}} + \widetilde{w}_{b_{m,i,j}} = 0$$

where

$\widetilde{w}_{b_{m,i,j}}$ = velocity induced by the bound circulation on
blade i at the i,j control point .

The elastic-blade degrees of freedom, v, w, and ϕ, are assumed to be represented by a superposition of assumed-mode shapes. Combined flapwise- and chordwise-bending modes can be represented as

$$w_{m,i,j} = \sum_p w_{m,i}^{(p)} f_w^{(p)}(j)$$

$$v_{m,i,j} = \sum_p w_{m,i}^{(p)} k_v^{(p)} f_v^{(p)}(j)$$

where

$f_w^{(p)}(j)$, $f_v^{(p)}(j)$ are the flapwise- and chordwise-displacement mode
shapes, respectively, for the pth mode.

$k_v^{(p)}$ is the ratio of the chordwise displacement of the blade tip
to the flapwise displacement of the blade tip for the pth mode

and

$w_{m,i}^{(p)}$ is the flapwise displacement of the blade tip in the pth mode.

Blade torsion is represented as

$$\phi_{m,i,j} = \sum_q \phi_{m,i}^{(q)} f_\phi^{(q)}(j)$$

where

$f_{\phi(j)}^{(q)}$ is the mode shape of the qth torsion mode

and

$\phi_{m,i}^{(q)}$ is the torsional displacement of the blade tip in the qth mode.

Blade response variables such as $\phi_{m,i,j}$, $\frac{\partial \omega}{\partial \xi}\big)_{m,i,j}$, and $\frac{\partial \phi}{\partial \xi}\big)_{m,i,j}$ follow directly from the above-stated modal definitions.

APPENDIX II

AN AERODYNAMIC MODEL FOR CALCULATING LOADINGS ON ROTOR BLADES OPERATING AT HIGH ADVANCE RATIOS

The horseshoe-vortex representation employed in TBL-I constituted, in essence, a classical lifting-line approach for evaluating the spanwise distribution of circulation on a high-aspect-ratio surface. In accordance with the Prandtl simplification, the lifting line located in a given spanwise segment of the blade is considered to extend to plus and minus infinity in stating the boundary condition to be satisfied at the three-quarter chord of that same segment. The net result of this approximation is that the loading on a given spanwise segment is given by the lift and drag of a two-dimensional airfoil whose angle of attack is specified by the flow velocities required to achieve flow tangency at the control point of the segment under consideration. As was discussed in the report, it follows that the applicable angle of attack of the two-dimensional segment is given by the kinematic properties of the blade and the downwash induced both by the free wake and the bound circulation in blades other than the blade in which the segment is located.

The downwash caused by elements of bound vorticity located in blades other than the blade being considered was neglected in the calculations performed in TBL-I. A subsequent introduction of these elements of downwash into the computational procedure demonstrated that these elements are a negligible contribution at low advance ratios. Even though these contributions may remain small at high advance ratios, these effects have been retained in the TBL-II model, in view of the requirement for computing the velocities caused by the elements of bound vorticity located in the blade containing the control point at which the boundary condition is being satisfied. This latter requirement stems, of course, from the

100

elimination of the Prandtl simplification (to be discussed below), since this simplification is permissible only when calculating loadings on large-aspect-ratio surfaces.

As was outlined in the body of the report, the objective of the TBL-II study requires the computation of loadings on lifting surfaces exposed to flows of varying obliquity. The helicopter rotor blade at a high advance ratio encounters flow obliquities which cause it to change continuously from a high-aspect-ratio surface to a low-aspect-ratio surface as it changes in azimuth through 90 degrees. However, it was recognized that the development of an aerodynamic-loading theory for a surface exposed to the flow alignments encountered by a slowly rotating rotary wing is a research task of considerable magnitude. Accordingly, a limited objective was selected, namely, to develop a loading calculation procedure utilizing as simple a vortex model as possible, where the validity of this model would be judged by its ability to yield correct loadings at the two extremes of low and infinite advance ratio. As discussed, in part, in the report, the achievement of this objective called for the following modifications to the aerodynamic model described in Reference [12]:

1. Move the spanwise-oriented bound vortex from the one-quarter chord to the leading edge in order to obtain a suitable vortex geometry for flows that are highly radial with respect to the blade.

2. Place the control point at the center (50-percent chord) of the blade segment.

3. Introduce tests to determine whether root or tip of blade is a leading or trailing edge.

4. Introduce logic that will trail vorticity from the rounded "leading" edge of the blade in the reversed flow region.

101

5. Add effects of spanwise and chordwise bound vorticity (from all blades) to the matrix of induced-velocity coefficients.

6. Redefine equations yielding the unknown bound circulations in terms of the flow-tangency requirement at the selected control point.

7. Develop methods for (a) adding viscous forces to the circulatory forces, (b) approximating the effects of Mach number, and (c) estimating the tangential location of the center of pressure.

Modifications (1) through (4) are straightforward in concept and execution. They involve changes in kinematic definitions having an influence on wake geometry and the motion of the control point. Accordingly, these changes are not documented in this appendix.

Modifications (5) and (6) are key items which convert the load-prediction scheme for high-aspect-ratio surfaces to one that will predict loadings also for low-aspect-ratio surfaces, as per the example case discussed in the body of the report. The method employed in TBL-II to introduce the effects of bound vorticity into the downwash computation is given below.

If an induced-velocity coefficient is defined to represent the combined influence of a horseshoe-vortex element fixed in the blade and the adjacent elements of free wake (assumed to have the same strength as the bound vortex), the resulting composite velocity coefficient can be written as

$$\sigma_{b,l}^{i,j} = \sigma_{ib,2,l}^{m,i,j} - \sigma_{ib,2,l+1}^{n,i,j} + \bar{\sigma}_{ib,l}^{m,i,j} + \bar{\sigma}_{ib,l}^{m,i,j} - \bar{\sigma}_{ib,l+1}^{m,i,j}$$

102

where

$\sigma_{ib,2,l}^{m,i,j} - \sigma_{ib,2,l+1}^{m,i,j}$ are the induced-velocity coefficients of the adjacent free wake.

$\bar{\sigma}_{ib,l}^{m,i,j}$ is the induced-velocity coefficient of a spanwise-oriented element of bound vorticity.

$\bar{\bar{\sigma}}_{ib,l}^{m,i,j} - \bar{\bar{\sigma}}_{ib,l+1}^{m,i,j}$ are the induced velocity coefficients of the chordwise-oriented elements of bound vorticity.

In the "strip" analysis applicable to low advance ratios, the Prandtl simplification is implemented by (a) neglecting all contributions from the barred coefficients when $ib = i$, and (b) assuming that $\widetilde{\omega}_{b_i,j} = \frac{\Gamma_{ib}}{2\pi b_j}$. In this manner, it becomes possible to compute section angles of attack and, thus, to use experimental lift and drag data. In a three-dimensional analysis, the velocity induced at a control point by the $ib = i$ components of bound vorticity approaches that induced by a constant strength, doubly infinite lifting line as the flow becomes primarily tangential at low advance ratios. Thus, at low advance ratios, a loading result roughly equivalent to that yielded by the "strip" analysis would be expected. (In effect, the retention of the $ib = i$ components of bound vorticity accounts for the influence of finite wing length.)

Notwithstanding this qualitative agreement between the "strip" and the more exact analysis at low advance ratios, significant differences would be obtained in actual calculations since one method uses the lift-curve slope of an actual airfoil immersed in a fluid of finite viscosity and the second method uses the theoretical lift-curve slope of a flat plate. There would also be differences in calculated loadings as a result of variations in experimental lift-curve slope with Mach number.

103

The calculation procedure developed for low-aspect-ratio surfaces was arbitrarily modified such that, at low advance ratios, calculated loadings approximate those yielded by the "strip" analysis. This modification consists of altering the strength of the induced-velocity coefficient of the $ib = i$ bound vortex, as a means of representing the circulation existing on a real airfoil, in contrast to the circulation that represents the bound-vortex equivalent of the circulation distributed across the surface of a flat plate. The appropriate correction to induced-velocity coefficients associated with radially or tangentially oriented components of bound vorticity is, for example, given by

$$\bar{\sigma}_{ib=i,l}^{m,i,j} = \frac{2\pi}{\frac{dC_l}{d\alpha}\bigg)_{m,ib=i,\,l=j}} \, \bar{\sigma}_{ib=i,l}^{m,i,j} \ .$$

Note that $\frac{dC_l}{d\alpha}\big)_{m,ib=i,\,l=j}$ can be obtained from experiment as a function of Mach number, a value of which can be computed for every i,j control point.

The appendix in Reference [12] shows that the unknown bound circulations required to satisfy the boundary condition (as expressed in the "strip" analysis) satisfy the following equation set:

$$\left[\sigma_{ib,l}^{i,j}\right]\left\{\Gamma_{m,i,j}\right\} = \left\{\Gamma_{m,i,j}^{g}\right\} \ .$$

The column matrix $\left\{\Gamma_{m,i,j}\right\}$ represents the unknown circulation strengths, and the column matrix $\left\{\Gamma_{m,i,j}^{g}\right\}$ represents that portion of the circulation at each spanwise segment as determined by all geometric and downwash contributions to the local angle of attack other than the downwash created by the adjacent elements of free wake and the elements of bound vorticity in all blades other than blade $ib=i$. The square matrix, $\left[\sigma_{ib,l}^{i,j}\right]$, represents

104

the composite influence of the induced-velocity coefficients of the free-wake elements adjacent to all blades and the bound vorticity in all blades other than the blade containing the i, j control point. Each term in the square matrix is given by

$$\sigma_{ib,l}^{i,j} = -b_j \left.\frac{dC_L}{d\alpha}\right)_{m,i,j} \left[\sigma_{ib,2,l}^{m,i,j} - \sigma_{ib,2,l+1}^{m,i,j} + \bar{\sigma}_{ib,l}^{m,i,j} + \bar{\bar{\sigma}}_{ib,l}^{m,i,j} - \bar{\bar{\sigma}}_{ib,l+1}^{m,i,j} \right] \qquad (11)$$

except for the terms on the diagonal which are given by

$$\sigma_{ib=i,l=j}^{i,j} = 1 - b_j \left.\frac{dC_L}{d\alpha}\right)_{m,i,j} \left[\sigma_{ib=i,2,l=j}^{m,i,j} - \sigma_{ib=i,2,l+1=j+1}^{m,i,j} \right].$$

The implementation of item (6) (see above) requires that the equation set as derived for the "strip" analysis be reformulated in terms of a three-dimensional boundary condition. Note that the condition of flow tangency at a control point may be expressed as

$$U_{\zeta_{m,i,j}}^{g} + \cos \tilde{\theta}_{m,i,j} \; \tilde{\tilde{w}}_{m,i,j} = 0 \qquad (12)$$

where $U_{\zeta_{m,i,j}}^{g}$ is the velocity of air normal to an i, j point on the blade as derives from geometric and kinematic considerations only, and $\tilde{\tilde{w}}_{m,i,j}$ is the total χ-component of downwash created at point i, j by all fixed and free components of circulation in the rotor-wake system. Since the total downwash, $\tilde{\tilde{w}}_{m,i,j}$, consists of the sum of the downwash created by (a) all elements of the wake except for the adjacent wake, $\tilde{w}_{r_{m,i,j}}$, and (b) the adjacent wake plus all bound vorticity in the blades, $\tilde{\tilde{w}}_{A_{m,i,j}}$, Equation (12) can be expressed as

$$\tilde{\tilde{w}}_{A_{m,i,j}} = \frac{U_{\zeta_{m,i,j}}^{g}}{\cos \tilde{\theta}_{m,i,j}} - \tilde{w}_{r_{m,i,j}}. \qquad (13)$$

105

The downwash component, $\widetilde{w}_{A_{m,i,j}}$, may be further subdivided into (a) downwash caused by the adjacent wake elements and the bound vorticity on blades other than that containing the i,j control point, and (b) downwash caused by bound vorticity on the blade containing the i,j control point. Accordingly, we find that the quantity $\widetilde{\widetilde{w}}_{A_{m,i,j}}$ may be expressed as

$$\widetilde{\widetilde{w}}_{A_{m,i,j}} = \sum_{ib=1}^{NB} \sum_{\ell=1}^{LCN} \Gamma_{m,ib,\ell} \left[\sigma_{D_{ib,\ell}}^{i,j} \right] + \sum_{\ell=1}^{LCN} \Gamma_{m,ib=i,\ell} \left[\bar{\sigma}_{D_{ib=i,\ell}}^{i,j} \right] .$$

The $\left[\sigma_{D_{ib,\ell}}^{i,j} \right]$ matrix in the above expression is identical to the quantity found within the brackets in Equation (11). The $\left[\bar{\sigma}_{D_{ib=i,\ell}}^{i,j} \right]$ matrix contains that portion of the original definition of $\sigma_{D_{ib,\ell}}^{i,j}$ which is omitted in the formulation of the "strip" analysis. Thus, the three-dimensional boundary condition may be expressed as

$$\left[\sigma_{D_{ib,\ell}}^{i,j} + \bar{\sigma}_{D_{ib=i,\ell}}^{i,j} \right] \left\{ \Gamma_{m,i,j} \right\} = \left\{ \widetilde{w}_{m,i,j}^{g} \right\} \tag{14}$$

where

$$\widetilde{w}_{m,i,j}^{g} = - \frac{U_{C_{m,i,j}}^{g}}{\cos \theta_{m,i,j}} - \widetilde{w}_{T_{m,i,j}} .$$

This form of the boundary condition shows that it is only necessary to evaluate some additional σ coefficients in order to modify the "strip" analysis, as per the objective stated in Item (6).

As was indicated in the body of the report, a "two-dimensional" stall limit is imposed on the values of circulation that are obtained from a solution of Equation (14). This limiting procedure restricts the strength of the tip vortex in the wake to values compatible with the maximum circulation that can be produced by a stalled blade. Thus, the boundary condition is not satisfied at all control points if and when a portion of the blade is considered to be stalled at low advance ratios.

106

Application of the Kutta-Joukowski law to obtain aerodynamic loadings from the computed bound circulations yields forces on the blade that derive only from potential flow considerations. Item (7) was thus implemented by arbitrarily introducing a tangential viscous force based on the two-dimensional angle of attack that is approached at low advance ratios. When the flow, relative to the blade, is primarily tangential in direction, the normal force on the blade is given by

$$LS_{m,i,j} = \rho U_{\eta_{m,i,j}} \Gamma_{m,i,j} \, ,$$

and the tangential force (chordwise) is given by a circulatory component,

$$DS_{m,i,j} = -\rho U_{\zeta_{m,i,j}} \Gamma_{m,i,j} \, ,$$

and a viscous component,

$$DV_{m,i,j} = \rho \left(U_{\eta_{m,i,j}} \right)^2 b_i \, C_{D_{\eta_{m,i,j}}} \, ,$$

where the drag coefficient, C_{D_η}, is determined as a function of $\alpha_{m,i,j}^{zo}$ as defined in the body of the report. Radial components of flow, $U_{\zeta_{m,i,j}}$, also produce a normal force on the blade which, because of the lumping process used, are lumped forces at the radial locations of tangentially directed elements of bound vorticity. These concentrated loads are given by

$$CL_{m,i,j} = 2\rho b_i U_{\zeta_{m,i,j}} \left[\Gamma_{m,i,j+1} - \Gamma_{m,i,j-1 \cdot 1} \right]$$

which loads are then "smeared" to yield a radial distribution of loading.

Pitching moments about the feathering and elastic axes are assumed to derive from quasi-static lift acting at the quarter chord and from the quasi-static moment about the quarter chord resulting from angular velocities in pitch and twist. The center of pressure of the quasi-static lift caused by pure effective plunging is also assumed to shift rearward as a function of the local two-dimensional angle of attack and the local Mach number. Curve fitting of experimental data obtained with NACA 0012 and 0015 airfoil sections yielded the following expressions for the

107

shift in the center of pressure of the lift caused by pure plunging:

$$\left(\frac{c.p.}{c} - 0.25\right)_{m,i,j} = min\begin{bmatrix} 0.092 + 0.0019\left|\alpha^{20}_{m,i,j}\right| \\ max\begin{bmatrix} -0.825(A_{m,i,j} - 0.645) + 0.018\left|\alpha^{20}_{m,i,j}\right| \\ 0 \end{bmatrix} \end{bmatrix}$$

for

$$0\ deg \le \left|\alpha^{20}_{m,i,j}\right| \le 140\ deg$$

$$\left(\frac{c.p.}{c} - 0.25\right)_{m,i,j} = 0.358 + 0.036\left\{\left|\alpha^{20}_{m,i,j}\right| - 140\right\}$$

for

$$140\ deg < \left|\alpha^{20}_{m,i,j}\right| \le 180\ deg$$

where

$$A_{m,i,j} = \sqrt{1 - M^2_{m,i,j}}\ .$$

The quasi-static moment about the quarter chord caused by pitching velocity is given by thin airfoil theory as (see Reference [23]):

$$M_{1/4}\ (due\ to\ \dot\alpha) = -\frac{b}{2}(2\pi\rho\, U b^2 \dot\alpha)$$

On defining $\dot\alpha$ as $(\dot\phi + \dot\theta)$, we have that

$$M_{1/4})_{m,i,j}\ (due\ to\ \dot\alpha) = -\frac{b_j}{2}\left[2\pi\rho\, U_{m,i,j}\, b_j^2(\dot\phi_{m,i,j} + \dot\theta_{m,i})\right]\ .$$

The total pitching moment about the one-quarter chord is thus defined as

$$M_{1/4})_{m,i,j} = -\bar{\bar{L}}_{m,i,j}\left[2b_j\left(\frac{c.p.}{c} - 0.25\right)_{m,i,j}\right]$$

$$-\frac{b_j}{2}\left[2\pi\rho\, U_{m,i,j}\, b_j^2(\dot\phi_{m,i,j} + \dot\theta_{m,i})\right].$$

108

APPENDIX III

THE DERIVATION OF THE EQUATIONS OF
MOTION NEEDED IN THE TBL-II STUDY

A Lagrangian approach was used to derive the equations of motion
for a rotor with articulated, flexible blades. As was discussed in the body
of the report, the introduction of the appropriate kinematic constraints
and the selection of the proper antisymmetric and/or symmetric bending
modes convert equations applicable to an articulated rotor to equations
applicable to a teetering rotor or the so-called "rigid" rotor.

As a result of specifying (1) the existence of offsets (as defined
in Figure 8) and (2) the blade to flap, lead-lag, and feather in the order
given, the following expressions are obtained for the x-y-$\textit{z}$ components
(see Figure 9) of the total absolute velocity of a mass point, P, located
in a blade by the ξ, η coordinates defined in Figure 9. (It should be noted
that the blade cross section is assumed to be thin and symmetrical.)

$$V_x = \dot{x} + U + q\textit{z} - ry$$

$$V_y = \dot{y} + V + rx - p\textit{z}$$

$$V_\textit{z} = \dot{\textit{z}} + W + py - qx$$

where

$$\dot{x} = -\dot{\delta}$$

$$\dot{y} = \dot{v}\cos\theta_\xi - \dot{w}\sin\theta_\xi - \dot{\phi}\eta\sin(\theta_\xi + \phi)$$

$$\dot{\textit{z}} = \dot{w}\cos\theta_\xi + \dot{v}\sin\theta_\xi + \dot{\phi}\eta\cos(\theta_\xi + \phi)$$

$$x = \xi - \delta$$

$$y = e_0 + v\cos\theta_\xi - w$$

$$\textit{z} = w\cos\theta_\xi + v\sin\theta_\xi + \eta\sin(\theta_\xi + \phi)$$

$$U = -\dot{\psi}\left\{(e_F - \tilde{c}_p\sin\beta)\sin\zeta + (\tilde{e}_D\cos\zeta + e_D\sin\zeta - \tilde{e}_p)\cos\beta\right\} - \dot{\beta}\tilde{c}_p\cos\zeta - \dot{\zeta}\tilde{e}_p$$

$$V = \dot{\psi}\left\{\left[e_F\cos\zeta + (e_D\cos\zeta - \tilde{e}_D\sin\zeta + e_p)\cos\beta - \tilde{c}_p\sin\beta\cos\zeta\right]\cos\theta \right.$$
$$\left. + \left[\tilde{e}_D - \tilde{e}_p\cos\zeta - e_p\sin\zeta\right]\sin\beta\sin\theta\right\} - \dot{\zeta}e_p\cos\theta$$
$$-\dot{\beta}\left\{\tilde{c}_p\sin\zeta\cos\theta - (e_D + e_p\cos\zeta - \tilde{e}_p\sin\zeta)\sin\theta\right\}$$

$$W = \dot{\psi}\left\{\left[\tilde{e}_D - (\tilde{e}_p \cos\zeta + e_p \sin\zeta)\right] \sin\beta \cos\theta \right.$$
$$- \left[e_R \cos\zeta + (e_D \cos\zeta - \tilde{e}_p \sin\zeta + e_p)\cos\beta - \tilde{c}_p \sin\beta \cos\zeta\right]\sin\theta\right\}$$
$$\left. + \dot{\beta}\left\{(e_D + e_p \cos\zeta - \tilde{e}_p \sin\zeta)\cos\theta + \tilde{c}_p \sin\zeta \sin\theta\right\} + \dot{\zeta} e_p \sin\theta\right.$$

$$p = \dot{\psi}\sin\beta\cos\zeta + \dot{\beta}\sin\zeta + \dot{\theta}$$

$$q = \dot{\psi}\left\{\sin\beta\sin\zeta\cos\theta + \cos\beta\sin\theta\right\} - \dot{\beta}\cos\zeta\cos\theta - \dot{\zeta}\sin\theta$$

$$r = \dot{\psi}\left\{\cos\beta\cos\theta - \sin\beta\sin\zeta\sin\theta\right\} + \dot{\beta}\cos\zeta\sin\theta - \dot{\zeta}\cos\theta$$

and δ is the shortening in the x-direction due to the blade being bent.

The shortening, δ, of the blade may be expressed as

$$\delta = \Delta + \frac{dw_1}{d\xi}\eta\sin(\theta_\xi + \phi) + \frac{dv_1}{d\xi}\eta\cos(\theta_\xi + \phi)$$

where

$$w_1 = w\cos\theta_\xi + v\sin\theta_\xi$$
$$v_1 = v\cos\theta_\xi - w\sin\theta_\xi$$

and Δ is the shortening of the elastic axis (in the x-direction) up to station ξ and is given, approximately, by

$$\Delta \cong \frac{1}{2}\int_0^\xi \left\{\left(\frac{dw_1}{d\xi}\right)^2 + \left(\frac{dv_1}{d\xi}\right)^2\right\}d\xi$$

$$\cong \frac{1}{2}\int_0^\xi \left\{\left(\frac{dw}{d\xi}\right)^2 + \left(\frac{dv}{d\xi}\right)^2 + 2\frac{d\theta_\xi}{d\xi}\left(\frac{dw}{d\xi}v - \frac{dv}{d\xi}w\right)\right.$$
$$\left. + \left(\frac{d\theta_\xi}{d\xi}\right)^2(w^2 + v^2)\right\}d\xi .$$

110

In order to express the kinetic and potential energy of a single blade, it is convenient to expand the blade displacements v, w, and ϕ in terms of the generalized coordinates, $w^{(P)}$ and $\phi^{(\Psi)}$, defined in Appendix I.

The kinetic energy of a single blade is given by

$$\mathcal{T} = \frac{1}{2} \int_{\substack{blade \\ mass}} (V_1^2 + V_y^2 + V_3^2) \, dm \ .$$

The potential energy can be expressed, following Reference [19], as a function of the incremental strain energy caused by elastic bending and torsional deformations of a thin twisted blade under initial tension. This initial tension is a function, primarily, of the shaft rotation velocity, $\dot{\psi}$. Thus, the incremental strain energy, $\mathcal{U}$, is given by

$$\mathcal{U} = \frac{1}{2} \int_0^R (EI_1 \zeta^2 + EI_2 \lambda^2) \, d\xi + \frac{1}{2} \int_0^R \left\{ \left[GJ + EB_1 \left(\frac{d\theta_\xi}{d\xi} \right)^2 \right] \left(\frac{d\phi}{d\xi} \right)^2 \right.$$

$$\left. - 2EB_2 \lambda \frac{d\theta_\xi}{d\xi} \frac{d\phi}{d\xi} + X k_A^2 \left[\left(\frac{d\phi}{d\xi} \right)^2 + 2 \frac{d\theta_\xi}{d\xi} \frac{d\phi}{d\xi} \right] \right\} d\xi$$

$$- \int_0^R X e_A \lambda \, d\xi$$

where

$\quad X \quad = \quad$ initial tension on blade section at station ξ and, on ignoring contributions due to lagging and flapping, may be expressed, approximately, as:

$$\dot{\psi} \int_0^R (e_H + \xi) m \, d\xi$$

$$\zeta \quad = \frac{d^2 w}{d\xi^2} + 2 \frac{d\theta_\xi}{d\xi} \frac{dv}{d\xi} + \frac{d^2\theta_\xi}{d\xi^2} v - \left(\frac{d\theta_\xi}{d\xi} \right)^2 w$$

$$\lambda \quad = \frac{d^2 v}{d\xi^2} - 2 \frac{d\theta_\xi}{d\xi} \frac{dw}{d\xi} - \frac{d^2\theta_\xi}{d\xi^2} w - \left(\frac{d\theta_\xi}{d\xi} \right)^2 v$$

$EI_1 = \quad$ flexural rigidity about major neutral axis

$EI_2 = \quad$ flexural rigidity about minor neutral axis

$GJ = \quad$ torsional rigidity

$$e_A = \frac{1}{A} \int_A \eta \, dA$$

111

$$k_A^2 = \frac{1}{A} \int_A \eta^2 \, dA$$

$$B_1 = \int_A \eta^2 (\eta^2 - k_A^2) \, dA$$

$$B_2 = \int_A \eta (\eta^2 - k_A^2) \, dA$$

and A is the blade cross-section area effective in taking tension, with η being the distance from the elastic axis to the element, dA (positive when dA is closer to the leading edge).

On applying Lagrange's equation to obtain the equations of motion for a rotor translating with a fixed velocity, with the generalized coordinates considered to be $\psi, \beta, \zeta, \theta, w^{(p)},$ and $\phi^{(q)}$, one finds that the required partial differentiation and the integration over the mass of the blade lead to a multiplicity of terms, many of which are of second and higher order. In this study, higher-order terms were dropped and small-angle assumptions were made, when permissible.

For example, we show below the equation that results for a blade-bending degree of freedom, namely, the rth mode of coupled flatwise and chordwise bending:

$$A_{\psi w}^{(r)} \ddot{\psi} + A_{\beta w}^{(r)} \ddot{\beta} + A_{\zeta w}^{(r)} \ddot{\zeta} + A_{\theta w}^{(r)} \ddot{\theta} + \sum_p \ddot{w}^{(p)} A_{ww}^{(p,r)} + \sum_q \ddot{\phi}^{(q)} A_{\phi w}^{(r,q)} + \dot{\psi}^2 \beta B_w^{(r)}$$

$$+ \dot{\psi}^2 \left[\sum_p w^{(p)} C_{w_1}^{(r,p)} + C_{w_2}^{(r)} + \sum_q \phi^{(q)} C_{w\phi}^{(r,q)} \right] + \frac{\partial u}{\partial w^{(r)}} = G.F.^{(r)} \ .$$

On defining the sectional properties of the blade as

m = mass per unit span, slugs/ft

e = chordwise distance of c.g. from the elastic axis, ft

μ = mass moment of inertia about the elastic axis per unit span, lb-sec^2

and on noting that the blade-bending mode shapes, as derived, are orthogonal (including flapping which can be considered to be a zero-order bending

112

mode), we find that the above coefficients are given by the following integrals:

$$A_{\psi w}^{(r)} = \int_0^R m(e_H + \xi)\left\{-f_w^{(r)}\sin(\theta_\xi + \theta) + k_\nu^{(r)}f_\nu^{(r)}\cos(\theta_\xi + \theta)\right\}d\xi$$

$$A_{\beta w}^{(r)} = 0$$

$$A_{\zeta w}^{(r)} = \int_0^R m(e_p + \xi)\left\{f_w^{(r)}\sin(\theta_\xi + \theta) - k_\nu^{(r)}f_\nu^{(r)}\cos(\theta_\xi + \theta)\right\}d\xi$$

$$A_{\theta w}^{(r)} = \int_0^R m\left\{e_o\sin\theta_\xi f_\nu^{(r)}k_\nu^{(r)} + (e_o\cos\theta_\xi + e)f_w^{(r)}\right\}d\xi$$

$$A_{ww}^{(p,r)} = 0, \quad r \neq p$$

$$A_{ww}^{(r,r)} = \int_0^R m\left\{\left[f_w^{(r)}\right]^2 + \left[k_\nu^{(r)}f_\nu^{(r)}\right]^2\right\}d\xi$$

$$A_{\phi w}^{(r,g)} = \int_0^R m e f_w^{(r)}f_\phi^{(g)}d\xi$$

$$B_w^{(r)} = 0$$

$$C_{w_1}^{(r,p)} = \int_0^R \left[\mu^{(r)}\mu^{(p)} + \nu^{(r)}\nu^{(p)}\right]A(\xi)d\xi$$
$$+ \int_0^R m\left[f_\nu^{(p)}k_\nu^{(p)}f_w^{(r)} + f_\nu^{(r)}k_\nu^{(r)}f_w^{(p)}\right]\sin(\theta_\xi + \theta)\cos(\theta_\xi + \theta)d\xi$$
$$- \int_0^R f_w^{(p)}f_w^{(r)}\sin^2(\theta_\xi + \theta)d\xi$$
$$- \int_0^R f_\nu^{(p)}k_\nu^{(p)}f_\nu^{(r)}k_\nu^{(r)}\cos^2(\theta_\xi + \theta)d\xi$$

where
$$A(\xi) = \int_\xi^R m(e_H + \xi)d\xi$$

and
$$\mu^{(r)} = \frac{df_w^{(r)}}{d\xi} + \frac{d\theta_\xi}{d\xi}k_\nu^{(r)}f_\nu^{(r)}$$
$$\nu^{(r)} = k_\nu^{(r)}\frac{df_\nu^{(r)}}{d\xi} + \frac{d\theta_\xi}{d\xi}f_w^{(r)}$$

$$C_{w_2}^{(r)} = \int_0^R m(e_H + \xi)e\nu^{(r)}d\xi + \int_0^R m e_o f_w^{(r)}\cos\theta\sin(\theta_\xi + \theta)d\xi$$

$$- \int_0^R m e_o f_\nu^{(r)}k_\nu^{(r)}\cos\theta\cos(\theta_\xi + \theta)d\xi - \int_0^R m e f_\nu^{(r)}k_\nu^{(r)}\cos^2(\theta_\xi + \theta)d\xi$$

$$+ \int_0^R m e_o f_w^{(r)}\sin(\theta_\xi + \theta)\cos(\theta_\xi + \theta)d\xi$$

113

$$C_{w\phi}^{(r,q)} = \int_0^R m(e_N + \xi)e\mu^{(r)}f_\phi^{(q)}\,d\xi$$

$$+\int_0^R me f_w^{(r)}f_\phi^{(q)}\sin^2(\theta_\xi + \theta)\,d\xi$$

$$+\int_0^R me f_w^{(r)}k_v^{(r)}f_\phi^{(q)}\sin(\theta_\xi + \theta)\cos(\theta_\xi + \theta)\,d\xi$$

$$\frac{\partial \mathcal{U}}{\partial w^{(r)}} = \sum_p w^{(p)} F_{ww}^{(r,p)} - \sum_q \phi^{(q)} G_{w\phi}^{(r,q)} - F_w^{(r)}$$

where
$$F_{ww}^{(r,p)} = \int_0^R \left[EI_1 f_\xi^{(r)}f_\xi^{(p)} + EI_2 f_\lambda^{(r)}f_\lambda^{(p)} \right]d\xi$$

$$G_{w\phi}^{(r,q)} = \int_0^R ED_2 \frac{d\theta_\xi}{d\xi} f_\lambda^{(r)} \frac{df_\phi^{(q)}}{d\xi}\,d\xi$$

$$F_w^{(r)} = \dot{\psi}^2 \int_0^R A(\xi)e_A f_\lambda^{(r)}d\xi - \dot{\psi}\dot{\zeta}\left[\int_0^R B(\xi)e_A f_\lambda^{(r)}d\xi + \int_0^R A(\xi)e_A f_\lambda^{(r)}d\xi\right].$$

(The integrals yielding the generalized force, $G F^{(r)}$, are discussed and defined in Appendix IV.)

In the above example, all terms have been retained except those inertial terms that become zero as a result of assuming orthogonal modes. Although the inertial coupling between bending and angular acceleration of the rotor shaft is small, these terms have been retained as a result of $\ddot{\psi}$ being very large whenever a braking torque is applied to the shaft of the rotor. A similar consideration applies to the retention of the inertial coupling between flapping and shaft acceleration.

In setting up the equations of motion in matrix form for machine solution, it is advantageous to expand further certain integrals to separate them into a time-independent and time-dependent part. Tables III and IV present, respectively, the equations of motion developed for this study and the coefficients required to repres .t the inertial, elastic, and centrifugal properties of a rotating, twisted blade experiencing large feathering displacements. It should be noted that Coriolis acceleration terms have been retained only in the equations for the shaft-rotation, flapping, and lead-lag degrees of freedom.

114

TABLE III
EQUATIONS OF MOTION FOR AN ARTICULATED
ROTOR WITH NB FLEXIBLE BLADES

Shaft-Rotation Degree of Freedom:

$$NB\ddot{\psi}A_{\psi\psi} + \sum_{i=1}^{NB}\ddot{\zeta_i}A_{\psi\zeta} + 2\dot{\psi}\left[\sum_{i=1}^{NB}\dot{\beta_i}\left(B_{\psi_i} + \beta_i B_{\psi 2}\right)\right]$$

$$+ 2\dot{\psi}\left[\sum_{i=1}^{NB}\dot{\zeta_i}\left(B_{\psi_3} + \zeta_i B_{\psi\psi}\right)\right] = \bar{Q}(t) + \sum_{i=1}^{NB}Q_{A_i}$$

Flapping Degree of Freedom:

$$\ddot{\psi}A_{\psi\beta_i} + \ddot{\beta_i}A_{\beta\beta} + \ddot{\theta_i}A_{\beta\theta_i} + \sum_q \ddot{\phi_i}^{(q)}A_{\beta\phi_i}^{(q)}$$

$$+ \dot{\psi}^2\left[B_{\beta_i} + \beta_i B_{\beta 2}\right] + 2\dot{\psi}\dot{\zeta_i}\left[C_{\beta_i} + \beta_i C_{\beta 2}\right] = G F^{(1)}$$

Lead-Lag Degree of Freedom:

$$\ddot{\psi}A_{\psi\zeta_i} + \ddot{\zeta_i}A_{\zeta\zeta} + \ddot{\theta_i}A_{\zeta\theta_i} + \sum_p \ddot{w_i}^{(p)}A_{\zeta w_i}^{(p)} + \sum_q \ddot{\phi_i}^{(q)}A_{\zeta\phi_i}^{(q)}$$

$$+ \dot{\psi}^2\left[B_{\zeta_i} + \zeta_i B_{\zeta 2}\right] + 2\dot{\beta_i}\dot{\psi}\left[C_{\zeta_i} + \beta_i C_{\zeta 2}\right] = G F^{(2)}$$

Feathering Degree of Freedom

$$\ddot{\psi}A_{\psi\theta_i} + \ddot{\beta_i}A_{\beta\theta_i} + \ddot{\zeta}A_{\zeta\theta_i} + \ddot{\theta_i}A_{\theta\theta} + \sum_p \ddot{w_i}^{(p)}A_{\theta w}^{(p)} + \sum_q \ddot{\phi_i}^{(q)}A_{\theta\phi}^{(q)}$$

$$+ \dot{\psi}^2\left\{B_{\theta_i} + B_{\theta\beta_i}\beta_i + \sum_p\left[C_{\theta w_i}^{(p)} + S_{\theta w_i}^{(p)}\right]w_i^{(p)} + \sum_p\bar{C}_{\theta w_i}^{(p)}\left[w_i^{(p)}\right]^2 + \sum_q C_{\theta\phi_i}^{(q)}\phi_i^{(q)}\right\} = G F^{(3)}$$

Coupled Flapwise and Chordwise Bending Degree of Freedom

$$\ddot{\psi}A_{\psi w_i}^{(r)} + \ddot{\zeta_i}A_{\zeta w_i}^{(r)} + \ddot{\theta_i}A_{\theta w_i}^{(r)} + \ddot{w_i}^{(r)}A_{ww}^{(r,r)} + \sum_q \ddot{\phi_i}^{(q)}A_{w\phi}^{(r,q)}$$

$$+ \dot{\psi}^2\left\{w_i^{(r)}C_{w_i}^{(r,r)} + C_{w 2}^{(r)} + \sum_q \phi_i^{(q)}C_{w\phi_i}^{(r,q)}\right\} + w_i^{(r)}F_w^{(r,r)} - F_{w_i}^{(r)} - \sum_q \phi_i^{(q)}G_{w\phi}^{(r,q)} = G F^{(r)}$$

Torsion Degree of Freedom

$$\ddot{\psi}A_{\psi\phi_i}^{(s)} + \ddot{\beta_i}A_{\beta\phi_i}^{(s)} + \ddot{\zeta_i}A_{\zeta\phi_i}^{(s)} + \ddot{\theta_i}A_{\theta\phi}^{(s)} + \sum_p \ddot{w_i}^{(p)}A_{w\phi}^{(p,s)} + \ddot{\phi_i}A_{\phi\phi}^{(s,s)}$$

$$+ \dot{\psi}^2\left\{\sum_p w_i^{(p)}C_{\phi w_i}^{(s,p)} + \sum_q \phi_i^{(q)}C_{\phi 1_i}^{(s,q)} + C_{\phi 2_i}^{(s)}\right\} - \sum_p w_i^{(p)}G_{w\phi}^{(p,s)} + \sum_q \phi_i^{(q)}F_{\phi_i}^{(s,q)} + F_{\phi_i}^{(s)} = G F^{(s)}$$

115

TABLE IV
DEFINITION OF COEFFICIENTS (INTEGRALS)
APPEARING IN TABLE III

$$A_{\psi\psi} = \int_0^R m(e_N + \xi)^2 d\xi$$

$$A_{\psi\zeta} = -\int_0^R m(e_N + \xi)(e_P + \xi) d\xi$$

$$B_{\psi 1_i} = -\left[\int_0^R m(e_N + \xi)\tilde{c}_p \, d\xi + \sin\theta_i \int_0^R m(e_N + \xi)(e_o + e) d\xi \right.$$
$$\left. + \cos\theta_i \int_0^R m(e_N + \xi) e\theta_\xi \, d\xi \right]$$

$$B_{\psi 2} = -\int_0^R m(e_N + \xi)(e_1 + \xi) d\xi$$

$$B_{\psi 3_i} = -\tilde{e}_D \int_0^R (e_P + \xi) m \, d\xi - \tilde{e}_p (e_F + e_D) \int_0^R m \, d\xi$$
$$+ \cos\theta_i (e_F + e_D) \int_0^R m(e_o + e) d\xi - \sin\theta_i (e_F + e_D) \int_0^R m e\theta_\xi \, d\xi$$

$$B_{\psi 4} = -(e_F + e_D) \int_0^R m(e_P + \xi) d\xi$$

$$A_{\psi 3_i} = \beta_i \left\{ (\tilde{e}_D - \tilde{e}_p) \int_0^R m(e_1 + \xi) d\xi + \cos\theta_i \int_0^R m(e_o + e)(e_1 + \xi) d\xi - \sin\theta_i \int_0^R m e\theta_3 (e_1 + \xi) d\xi \right\}$$
$$- \beta_i \zeta_i \int_0^R m(e_1 + \xi)(e_p + \xi) d\xi + \tilde{c}_p (\tilde{e}_D - \tilde{e}_p) \int_0^R m \, d\xi + \cos\theta_i \tilde{c}_p \int_0^R m(e_o + e) d\xi$$
$$+ \left[\cos\theta_i (\tilde{e}_D - \tilde{e}_p) - \sin\theta_i \tilde{c}_p \right] \int_0^R m e\theta_\xi \, d\xi + \sin\theta_i (\tilde{e}_D - \tilde{e}_p) \int_0^R m(e_o + e) d\xi$$
$$+ \cos 2\theta_i \int_0^R m e e_o \theta_\xi \, d\xi + \sin\theta_i \cos\theta_i \int_0^R m e_o (e_o + 2e) d\xi + \cos 2\theta_i \int_0^R \mu \theta_\xi \, d\xi$$
$$+ \cos\theta_i \sin\theta_i \int_0^R \mu \, d\xi - \cos\theta_i \sin\theta_i \int_0^R \mu \theta_\xi^2 \, d\xi - \zeta_i \left\{ \tilde{c}_p \int_0^R m(e_p + \xi) d\xi \right.$$
$$\left. + \sin\theta_i \int_0^R m e_o (e_p + \xi) d\xi + \cos\theta_i \int_0^R m e\theta_\xi (e_p + \xi) d\xi + \sin\theta_i \int_0^R m e(e_p + \xi) d\xi \right\}$$

TABLE IV - Continued

$$A_{\beta\beta} = \int_0^R m(e_1 + \xi)^2 d\xi$$

$$A_{\beta\theta_i} = \cos\theta_i \int_0^R m(\cap_i + \xi)(e_o + e)\, d\xi - \sin\theta_i \int_0^R m(e_1 + \xi)e\,\theta_\xi\, d\xi$$

$$A_{\beta\delta_i}^{(q)} = \cos\theta_i \int_0^R m(e_1 + \xi)e f_\phi^{(q)} d\xi - \sin\theta_i \int_0^R m(e_1 + \xi)e f_\phi^{(q)}\theta_\xi\, d\xi$$

$$B_{\beta1_i} = -B_{\psi1_i}$$

$$B_{\beta2} = -B_{\psi2}$$

$$C_{\beta1_i} = -\left[\mathcal{E}_p \int_0^R m(e_p + \xi)\,d\xi + \sin\theta_i \int_0^R m(e_p + \xi)(e_o + e)\,d\xi + \cos\theta_i \int_0^R m(e_p + \xi)e\,\theta_\xi\, d\xi \right]$$

$$C_{\beta2} = -\int_0^R m(e_p + \xi)(e_1 + \xi)\,d\xi$$

$$A_{\psi\zeta_i} = -\int_0^R m(e_N + \xi)(e_p + \xi)\,d\xi$$

$$A_{\zeta\zeta} = \int_0^R m(e_p + \xi)^2 d\xi$$

$$A_{\zeta\theta_i} = \cos\theta_i \int_0^R m(e_p + \xi)e\,\theta_\xi\, d\xi + \sin\theta_i \int_0^R m(e_p + \xi)(e_o + e)\,d\xi$$

$$A_{\zeta w_i}^{(P)} = \cos\theta_i \left[\int_0^R m(e_p + \xi) f_w^{(P)}\theta_\xi\, d\xi - \int_0^R m(e_p + \xi) k_v^{(P)} f_v^{(P)} d\xi \right]$$
$$\qquad + \sin\theta_i \left[\int_0^R m(e_p + \xi) f_w^{(P)} d\xi + \int_0^R m(e_p + \xi) k_v^{(P)} f_v^{(P)}\theta_\xi\, d\xi \right]$$

$$A_{\zeta\theta_i}^{(q)} = \cos\theta_i \int_0^R m(e_p + \xi)e f_\phi^{(q)}\theta_\xi\, d\xi + \sin\theta_i \int_0^R m(e_p + \xi)e f_\phi^{(q)} d\xi$$

TABLE **IV** - Continued

$$B_{\zeta 1_i} = \tilde{e}_p \int_0^R m(e_p + \xi)d\xi + \tilde{e}_p(e_r + e_p)\int_0^R md\xi - \cos\theta_i(e_r + e_p)\int_0^R m(e_o + e)d\xi$$

$$+ \sin\theta_i(e_r + e_p)\int_0^R me\theta_\xi d\xi$$

$$B_{\zeta 2} = (e_p + e_D)\int_0^R m(e_p + \xi)d\xi$$

$$C_{\zeta 1_i} = \tilde{c}_p \int_0^R m(e_p + \xi)d\xi + \cos\theta_i \int_0^R m(e_p + \xi)e\theta_\xi d\xi + \sin\theta_i \int_0^R m(e_p + \xi)(e_o + e)d\xi$$

$$C_{\zeta 2} = \int_0^R m(e_p + \xi)(e_r + \xi)d\xi$$

$$A_{\psi\theta_i} = -\sin\theta_i \int_0^R m(e_N + \xi)(e_o + e)d\xi - \cos\theta_i \int_0^R m(e_N + \xi)e\theta_\xi d\xi$$

$$A_{\theta\theta} = \int_0^R me_o(e_o + 2e)d\xi + \int_0^R \mu d\xi + \bar{m}(\bar{y}^2 + \bar{z}^2) + \int_0^R m\left\{\left[w(\xi)\right]^2 + \left[v(\xi)\right]^2\right\}d\xi$$

$$A_{\theta w}^{(P)} = \int_0^R m\left[e_o\theta_\xi f_v^{(P)}k_v^{(P)} + (e_o + e)f_w^{(P)}\right]d\xi$$

$$A_{\theta\phi}^{(q)} = \int_0^R mee_o f_\phi^{(q)}d\xi + \int_0^R \mu f_\phi^{(q)}d\xi$$

$$B_{\theta_i} = \sin\theta_i(\tilde{e}_D - \tilde{e}_p)\int_0^R (e_o + e)md\xi + \cos\theta_i(\tilde{e}_D - \tilde{e}_p)\int_0^R me\theta_s d\xi$$

$$+ \cos\theta_i \sin\theta_i \left[\int_0^R e_o^2 md\xi + 2\int_0^R me_o ed\xi + \bar{m}(\bar{y}^2 - \bar{z}^2)\right]$$

$$+ \cos 2\theta_i \left[\int_0^R mee_o\theta_\xi d\xi + \int_0^R \frac{\mu}{2}\sin 2\theta_\xi d\xi - \bar{m}\bar{y}\bar{z}\right]$$

$$+ \sin 2\theta_i \int_0^R \frac{\mu}{2}\cos 2\theta_\xi d\xi$$

TABLE IV - Continued

$$B_{\theta \rho_i} = \int_o^R m(e_N + \xi)(\bar{e}_o - \bar{e}_\rho)\,d\xi + \cos\theta_i \int_o^R m(e_N + \xi)(e_o + e)\,d\xi - \sin\theta_i \int_o^R m(e_N + \xi)e\,\theta_i\,d\xi$$

$$C_{\theta w_i}^{(P)} = \cos 2\theta_i \left\{ \int_o^R m e_o \left[f_w^{(P)} + k_v^{(P)} f_v^{(P)} \theta_\xi \right] d\xi + \int_o^R m e f_w^{(P)} d\xi + 2\int_o^R m e \theta_\xi k_v^{(P)} f_v^{(P)} d\xi \right\}$$

$$- 2\sin 2\theta_i \left\{ \int_o^R m e \theta_\xi f_w^{(P)} d\xi \right\} + \sin\theta_i \cos\theta_i \left\{ 2\int_o^R m e_o \left[k_v^{(P)} f_v^{(P)} - f_w^{(P)} \theta_\xi \right] d\xi \right.$$

$$\left. + 2\int_o^R m e f_v^{(P)} k_v^{(P)} d\xi \right\}$$

$$S_{\theta w_i}^{(P)} = \sum_r \left\{ \cos 2\theta_i \left[\int_o^R m f_w^{(P)} f_v^{(r)} k_v^{(r)} d\xi \right] - 2\sin 2\theta_i \left[\int_o^R m \theta_\xi f_w^{(P)} f_r^{(r)} k_v^{(r)} d\xi \right] \right\} w^{(r)}$$

$$\bar{C}_{\theta w_i}^{(P)} = \cos 2\theta_i \int_o^R m\theta_\xi \left[\left(k_v^{(P)} f_v^{(P)} \right)^2 - \left(f_w^{(P)} \right)^2 \right] d\xi$$

$$+ \sin\theta_i \cos\theta_i \int_o^R m \left[\left(k_v^{(P)} f_v^{(P)} \right)^2 - \left(f_w^{(P)} \right)^2 \right] d\xi$$

$$C_{\theta\theta_i}^{(q)} = \cos^2\theta_i \left[\int_o^R m e_o e f_\phi^{(q)} d\xi + \int_o^R \mu f_\phi^{(q)} d\xi \right]$$

$$- \sin\theta_i \cos\theta_i \left[\int_o^R m e e_o \theta_\xi f_\phi^{(q)} d\xi + 2\int_o^R \mu \theta_\xi f_\phi^{(q)} d\xi \right]$$

$$A_{\psi w_i}^{(r)} = \cos\theta_i \int_o^R m(e_N + \xi) \left[k_v^{(r)} f_v^{(r)} - f_w^{(r)} \theta_\xi \right] d\xi$$

$$- \sin\theta_i \int_o^R m(e_N + \xi) \left[f_w^{(r)} + k_v^{(r)} f_v^{(r)} \theta_\xi \right] d\xi$$

$$A_{\xi w_i}^{(r)} = \cos\theta_i \int_o^R m(e_\rho + \xi) \left[f_w^{(r)} \theta_\xi - k_v^{(r)} f_v^{(r)} \right] d\xi$$

$$+ \sin\theta_i \int_o^R m(e_\rho + \xi) \left[f_w^{(r)} + k_v^{(r)} f_v^{(r)} \theta_\xi \right] d\xi$$

$$A_{ww}^{(r,r)} = \int_o^R m \left[\left(f_w^{(r)} \right)^2 + \left(k_v^{(r)} f_v^{(r)} \right)^2 \right] d\xi$$

$$A_{w\phi}^{(r,q)} = \int_0^R m e f_w^{(r)} f_\phi^{(q)} d\xi$$

$$C_{w_1}^{(r,r)} = \int_0^R \left[\mu^{(r)} \mu^{(r)} + \nu^{(r)} \nu^{(r)} \right] A(\xi) d\xi \qquad \cdot$$

$$+ \cos^2\theta_{m,i} \left[2 \int_0^R m \theta_\xi f_w^{(r)} f_\nu^{(r)} k_\nu^{(r)} d\xi - \int_0^R m (k_\nu^{(r)} f_\nu^{(r)})^2 d\xi \right]$$

$$+ \cos\theta_i \sin\theta_i \left\{ 2 \int_0^R m f_w^{(r)} f_\nu^{(r)} k_\nu^{(r)} d\xi + 2 \int_0^R m \theta_\xi \left[(k_\nu^{(r)} f_\nu^{(r)})^2 - (f_w^{(r)})^2 \right] d\xi \right\}$$

$$- \sin^2\theta_i \left\{ 2 \int_0^R m \theta_\xi f_w^{(r)} f_\nu^{(r)} k_\nu^{(r)} d\xi + \int_0^R m (f_w^{(r)})^2 d\xi \right\}$$

$$C_{w_2}^{(r)} = \int_0^R m (e_N + \xi) e \nu^{(r)} d\xi$$

$$+ \cos^2\theta_i \left\{ \int_0^R m (e + e_0) \theta_\xi f_w^{(r)} d\xi - \int_0^R m (e + e_0) f_\nu^{(r)} k_\nu^{(r)} d\xi \right\}$$

$$+ \cos\theta_i \sin\theta_i \left\{ \int_0^R m (e + e_0) f_w^{(r)} d\xi + \int_0^R m (e_0 + 2e) \theta_\xi k_\nu^{(r)} f_\nu^{(r)} d\xi - \int_0^R m e \theta_\xi^2 f_w^{(r)} d\xi \right\}$$

$$- \sin^2\theta_i \int_0^R m e \theta_\xi f_w^{(r)} d\xi$$

$$C_{w\phi_i}^{(r,q)} = \int_0^R m (e_N + \xi) e \mu^{(r)} f_\phi^{(q)} d\xi$$

$$+ \cos^2\theta_i \left\{ \int_0^R m e \theta_\xi k_\nu^{(r)} f_\nu^{(r)} f_\phi^{(q)} d\xi - \int_0^R m e \theta_\xi^2 f_w^{(r)} f_\phi^{(q)} d\xi \right\}$$

$$+ \cos\theta_i \sin\theta_i \left\{ \int_0^R m e k_\nu^{(r)} f_\nu^{(r)} f_\phi^{(q)} d\xi - 2 \int_0^R m e \theta_\xi f_w^{(r)} f_\phi^{(q)} d\xi \right\}$$

$$- \sin^2\theta_i \left\{ \int_0^R m e \theta_\xi k_\nu^{(r)} f_\nu^{(r)} f_\phi^{(q)} d\xi + \int_0^R m e f_w^{(r)} f_\phi^{(q)} d\xi \right\}$$

$$F_w^{(r,r)} = \int_0^R \left\{ EI_1 \left[f_\xi^{(r)} \right]^2 + EI_2 \left[f_\lambda^{(r)} \right]^2 \right\} d\xi$$

TABLE IV - Continued

$$F_{\omega_i}^{(r)} = \dot{\psi}^2 \int_0^R A(\xi) e_A f_\lambda^{(r)} d\xi - \dot{\psi}\dot{\zeta}_i \left\{ \int_0^\xi \dot{B}(\xi) e_A f_\lambda^{(r)} d\xi + \int_0^R A(\xi) e_A f_\lambda^{(r)} d\xi \right\}$$

where

$$B(\xi) = \int_\xi^R (e_\rho + \xi) m d\xi$$

$$G_{\omega\phi}^{(r,s)} = \int_0^R E B_\varepsilon \frac{d\theta_\xi}{d\xi} f_\lambda^{(r)} \frac{d f_\phi^{(s)}}{d\xi} d\xi$$

$$A_{\psi\phi_i}^{(s)} = -\cos\theta_i \int_0^R m(e_H + \xi) e \theta_\xi f_\phi^{(s)} d\xi - \sin\theta_i \int_0^R m(e_H + \xi) e f_\phi^{(s)} d\xi$$

$$A_{\phi\phi}^{(s,s)} = \int_0^R \mu (f_\phi^{(s)})^2 d\xi$$

$$C_{\phi i}^{(s,q)} = \cos^2\theta_i \left\{ \int_0^R m e e_0 f_\phi^{(s)} f_\phi^{(q)} d\xi + \int_0^R \mu f_\phi^{(s)} f_\phi^{(q)} d\xi \right\}$$

$$+ \sin\theta_i \cos\theta_i \left\{ \int_0^R m e e_0 \theta_\xi f_\phi^{(s)} f_\phi^{(q)} d\xi + 4\int_0^R \mu \theta_\xi f_\phi^{(s)} f_\phi^{(q)} d\xi \right\} - \sin^2\theta_i \left\{ \int_0^R \mu f_\phi^{(s)} f_\phi^{(q)} d\xi \right\}$$

$$C_{\phi 2_i}^{(s)} = \cos^2\theta_i \left\{ \int_0^R m e e_0 \theta_\xi f_\phi^{(s)} d\xi + \int_0^R \mu \theta_\xi f_\phi^{(s)} d\xi \right\}$$

$$+ \cos\theta_i \sin\theta_i \left\{ \int_0^R m e e_0 f_\phi^{(s)} d\xi + \int_0^R \mu f_\phi^{(s)} d\xi \right\} - \sin^2\theta_i \int_0^R \mu \theta_\xi f_\phi^{(s)} d\xi$$

$$F_{\phi_i}^{(s,q)} = \int_0^R \left\{ GJ(\xi) + E B_1(\xi) \left(\frac{d\theta_\xi}{d\xi} \right)^2 \right\} \frac{d f_\phi^{(s)}}{d\xi} \frac{d f_\phi^{(q)}}{d\xi} d\xi + \dot{\psi}^2 \left\{ \int_0^R A(\xi) k_A^2 \frac{d f_\phi^{(s)}}{d\xi} \frac{d f_\phi^{(q)}}{d\xi} d\xi \right\}$$

$$- \dot{\psi}\dot{\zeta}_i \left\{ \int_0^R B(\xi) k_A^2 \frac{d f_\phi^{(s)}}{d\xi} \frac{d f_\phi^{(q)}}{d\xi} d\xi + \int_0^R A(\xi) k_A^2 \frac{d f_\phi^{(s)}}{d\xi} \frac{d f_\phi^{(q)}}{d\xi} d\xi \right\}$$

$$F_{\phi_i}^{(s)} = \psi^2 \left\{ \int_0^R A(\xi) k_A^2 \frac{d\theta_\xi}{d\xi} \frac{d f_\phi^{(s)}}{d\xi} d\xi \right\}$$

$$- \dot{\psi}\dot{\zeta}_i \left\{ \int_c^R B(\xi) k_A^2 \frac{d\theta_\xi}{d\xi} \frac{d f_\phi^{(s)}}{d\xi} d\xi + \int_0^R A(\xi) k_A^2 \frac{d\theta_\xi}{d\xi} \frac{d f_\phi^{(s)}}{d\xi} d\xi \right\}$$

APPENDIX IV

A DEFINITION OF THE GENERALIZED FORCES RESULTING FROM AERODYNAMIC LOADINGS AND OTHER RESTRAINTS

In a fully articulated rotor, the external forces on the blades arise from (1) aerodynamic loadings, (2) the drag link and damper, and (3) the pitch-control link. These external forces must be expressed as generalized forces or moments applied to the generalized degrees of freedom. It is the purpose of this appendix to define the aerodynamic transformations used in this study and to present the expressions used to compute the generalized forces designated by the symbol "GF".

If experimental lift, drag, and moment data are used to determine the aerodynamic forces on a spanwise segment of the rotor blade, the segment angle of attack and Mach number are evaluated as functions of the kinematics of the rotor and the velocity induced by the wake. Existing experimental data were curve-fitted by expressions similar to those developed by Blankenship and Harvey [Reference 1]. (The expression yielding the offset of the center of pressure from the one-quarter chord has already been given in Appendix II.) By specifying the angle of attack, $\bar{\alpha}_{i,j}$, to range between plus 180 degrees and minus 180 degrees, the lift and drag coefficients were evaluated from the following expressions:

$$\left| \bar{\alpha}_{i,j} \right| < 18°$$

$$C_{L_{i,j}} = \underset{\bar{\alpha}_{i,j}}{\text{sign of}} \times \min \begin{bmatrix} C_{L\alpha_{i,j}} \left| \bar{\alpha}_{i,j} \right| \\ CLX_{i,j} - (CLX_{i,j} - 0.677) \left\{ \dfrac{CLX_{i,j} - C_{L\alpha_{i,j}} \left| \bar{\alpha}_{i,j} \right|}{CLX_{i,j} - 18 C_{L\alpha_{i,j}}} \right\} \end{bmatrix}$$

$$C_{D_{i,j}} = \min \begin{bmatrix} \delta_0 + \delta_1 \left| \bar{\alpha}_{i,j} \right| + \delta_2 \bar{\alpha}_{i,j}^2 + \max \begin{bmatrix} M_{i,j} - 0.82 + 0.0332 \left| \alpha_{i,j} \right| \\ 0.0 \end{bmatrix} \\ 0.2 \end{bmatrix}$$

$|\bar{\alpha}_{i,j}| > 162°$

$$C_{L_{i,j}} = \begin{matrix} \text{sign of} \\ \bar{\alpha}_{i,j} \end{matrix} \times min \begin{bmatrix} C_{L_{\alpha_{i,j}}} |\bar{\alpha}_{i,j}| \\[2mm] CLB_{i,j} - (CLB_{i,j} - 0.677)\left\{ \dfrac{CLB_{i,j} - C_{L_{\alpha_{i,j}}}|\bar{\alpha}_{i,j}|}{CLB_{i,j} - 18 C_{L_{\alpha_{i,j}}}} \right\} \end{bmatrix}$$

$$C_{D_{i,j}} = min \begin{bmatrix} \delta_0 + \delta_1 |\bar{\alpha}_{i,j}| + \delta_2 \bar{\alpha}^2_{i,j} + max \begin{bmatrix} M_{i,j} - 0.82 + 0.0332 |\bar{\alpha}_{i,j}| \\ 0.0 \end{bmatrix} \\[2mm] 0.1986 \end{bmatrix}$$

where $\bar{\alpha}_{i,j} = \bar{\alpha}_{i,j} + 180$ when $\bar{\alpha}_{i,j} < -162°$

  $\bar{\alpha}_{i,j} = \bar{\alpha}_{i,j} - 180$ when $\bar{\alpha}_{i,j} > 162°$

$18° \leq |\bar{\alpha}_{i,j}| \leq 162°$

$$C_{L_{i,j}} = 1.15 \sin 2\bar{\alpha}_{i,j}$$

$$C_{D_{i,j}} = 2.08 \sin^2 \bar{\alpha}_{i,j}$$

where

$$CLX_{i,j} = C_{L_{max}} (M=0) - 0.767 M_{i,j} + 1.986 M^2_{i,j} - 3.21 M^3_{i,j}$$

$$CLB_{i,j} = 0.6 (CLX_{i,j})$$

$$A_{i,j} = \sqrt{1 - M^2_{i,j}} \qquad \text{for} \qquad 0 \leq M_{i,j} \leq 0.75$$

$$= 0.66144 + 4.5 (M_{i,j} - 0.75) \qquad M_{i,j} > 0.75$$

$$C_{L_{\alpha_{i,j}}} = \frac{C_{L_\alpha} (M=0)}{A_{i,j}}$$

and the airfoil section properties, $C_{L_\alpha}(M=0)$, $C_{L_{max}}(M=0)$, δ_0, δ_1, and δ_2 are experimental data applicable to the airfoil section employed in a given rotor.

Since lift and drag are defined as forces perpendicular and parallel, respectively, to the local total velocity vector, the normal and chordwise forces on the blade are given by

$$\bar{L}_{m,i,j} = L_{m,i,j} \cos \alpha_{m,i,j} + D_{m,i,j} \sin \alpha_{m,i,j}$$

$$\bar{D}_{m,i,j} = - L_{m,i,j} \sin \alpha_{m,i,j} + D_{m,i,j} \cos \alpha_{m,i,j}$$

123

where
$$L_{m,i,j} = \rho U_{m,i,j}^2 \, b_j \, C_{L_{m,i,j}}$$

$$D_{m,i,j} = \rho U_{m,i,j}^2 \, b_j \, C_{D_{m,i,j}} \; .$$

If, however, the aerodynamic loadings are determined by means of the aerodynamic model described in Appendix II, the normal-force loading, $\bar{L}_{m,i,j}$, and the chordwise-force loading, $\bar{D}_{m,i,j}$, are obtained directly from the analysis.

In order to obtain (1) the drag force on the blade parallel to the shaft plane and (2) the pitching moment about the feathering axis, it was convenient to resolve the normal and chordwise forces into other axis systems and to define the moment arms to the feathering axis in terms of coordinates based on an axis system whose y axis is located along the chord of the blade root. Figure 9 (see page 23) shows that "lift and drag" forces defined with respect to the y-z and y_d-z_d axes, respectively, are:

$$\hat{L}_{m,i,j} = \cos \hat{\theta}_{m,i,j} \, \bar{L}_{m,i,j} - \sin \hat{\theta}_{m,i,j} \, \bar{D}_{m,i,j}$$

$$\hat{D}_{m,i,j} = \sin \hat{\theta}_{m,i,j} \, \bar{L}_{m,i,j} + \cos \hat{\theta}_{m,i,j} \, \bar{D}_{m,i,j}$$

$$\bar{L}_{m,i,j} = \cos \tilde{\theta}_{m,i,j} \, \bar{L}_{m,i,j} - \sin \tilde{\theta}_{m,i,j} \, \bar{D}_{m,i,j}$$

$$\bar{D}_{m,i,j} = \sin \tilde{\theta}_{m,i,j} \, \bar{L}_{m,i,j} + \cos \tilde{\theta}_{m,i,j} \, \bar{\bar{D}}_{m,i,j}$$

where
$$\hat{\theta}_{m,i,j} = \theta_j + \phi_{m,i,j}$$

$$\tilde{\theta}_{m,i,j} = \theta_{m,i} + \theta_j + \phi_{m,i,j} \; .$$

By utilizing the kinematic derivation procedure outlined in Appendix I, the following expressions are obtained for the distance of the one-quarter chord point from the feathering axis

$$\hat{y}_{m,i,j} = e_o + v_{m,i,j} + \eta_{1/4j} - \theta_j \left[w_{m,i,j} + \phi_{m,i,j} \, \eta_{1/4j} \right]$$

$$\hat{z}_{m,i,j} = \theta_j \left[e_{o_j} + v_{m,i,j} + \eta_{1/4j} \right] + w_{m,i,j} + \phi_{m,i,j} \, \eta_{1/4j}$$

where we have assumed that $\cos \theta_j = 1$ and $\sin \theta_j = \theta_j$.

124

The generalized forces and moments presented below were derived by using a procedure similar to that outlined in Appendix V of Reference [8]. It should be noted that the concentrated load arising from the drag link was assumed (in this study) to act on that portion of the blade (inboard) which is taken to be infinitely stiff or rigid. Accordingly, the drag-damper force does not enter into the generalized forces applicable to the blade-bending degrees of freedom. The drag damper does, however, contribute to the generalized moment about the lead-lag hinge.

On neglecting the effects of blade bending, lead-lag displacement, and flapping displacement on the moment arm to the rotor shaft, we have that the aerodynamic torque, Q_A , produced by blade, i , is

$$Q_{A_{m,i}} = -\int_0^R (e_N + \xi)\, \bar{D}_{m,i}(\xi)\, d\xi \; .$$

The total external torque (or generalized force) about the rotor shaft is

$$\bar{Q}(t) + \sum_{i=1}^{NB} Q_{A_{m,i}}$$

where $\bar{Q}(t)$ is the mechanical torque produced by the helicopter power plant.

On neglecting the effects of blade bending and lead-lag displacement on the moment arm to the flap hinge, the generalized flapping moment can be expressed as

$$GF_{m,i}^{(1)} = \int_0^R (e_1 + \xi)\, \bar{L}_{m,i}(\xi)\, d\xi \; .$$

Similarly, the generalized lead-lag moment can be expressed as

$$GF_{m,i}^{(2)} = \int_0^R (e_p + \xi)\, \bar{D}_{m,i}(\xi)\, d\xi + N_{\dot{\zeta}}\, \dot{\zeta}_{m,i}$$

where

$N_{\dot{\zeta}}$ is the drag-damper moment per unit lead-lag velocity, $\dot{\zeta}$.

125

The generalized moment about the feathering axis can be expressed
as

$$GF_{m,i}^{(\theta)} = \int_0^R \left[\hat{L}_{m,i}(\xi)\hat{y}_{m,i}(\xi) + \hat{D}_{m,i}(\xi)\hat{z}_{m,i}(\xi) + M_{\theta_{m,i}}(\xi) \right] d\xi + M_\theta \left[\bar{\theta}_i(t) - \theta_{m,i} \right]$$

where $M_\theta \left[\bar{\theta}_i(t) - \theta_{m,i} \right]$ is the pitching moment caused by compression or
tension in the pitch link and $\bar{\theta}_i(t)$ is the effective swashplate angle for
blade i, as caused by the combined collective- and cyclic-pitch settings.
It should be noted that the pitching moment can be defined to include other
torques such as would be caused by hub properties that yield pitching
moments due to displacements about the flapping hinge.

The generalized force for the rth mode of coupled flatwise and
chordwise bending is

$$GF_{m,i}^{(r)} = \int_0^R \left[L_{m,i}(\xi) f_w^{(r)} - D_{m,i}(\xi) k_w^{(r)} f_w^{(r)} \right] d\xi$$

and the generalized torque for the sth torsion mode is

$$GF_{m,i}^{(s)} = \int_0^R \left[L_{m,i}(\xi)\eta_{1/4}(\xi) + M_{1/4}(\xi) \right] f_\phi^{(s)} d\xi$$

where $\eta_{1/4}$ is the distance between the elastic axis and the one-quarter chord
and $M_{1/4}$ is the aerodynamic pitching moment about the one-quarter chord.

126

DOCUMENT CONTROL DATA - R&D

(Security classification of title, body of abstract and indexing annotation must be entered when the overall report is classified)

1. ORIGINATING ACTIVITY (Corporate author)	2a. REPORT SECURITY CLASSIFICATION
Cornell Aeronautical Laboratory, Inc. Buffalo, New York	Unclassified
	2b. GROUP

3. REPORT TITLE

Rotor Air Loads, Blade Motion, and Stress Caused by Transient Inputs of Shaft Torque as Related to Stoppable Rotor Operation

4. DESCRIPTIVE NOTES (Type of report and inclusive dates)

5. AUTHOR(S) (Last name, first name, initial)

Segel, L.

6. REPORT DATE	7a. TOTAL NO. OF PAGES	7b. NO. OF REFS
May 1967	144	24

8a. CONTRACT OR GRANT NO.	9a. ORIGINATOR'S REPORT NUMBER(S)
DA 44-177-AMC-77(T)	
b. PROJECT NO.	USAAVLABS Technical Report 67-18
1F121401A142	
c.	9b. OTHER REPORT NO(S) (Any other numbers that may be assigned this report)
d.	

10. AVAILABILITY/LIMITATION NOTICES

Distribution of this document is unlimited.

11. SUPPLEMENTARY NOTES	12. SPONSORING MILITARY ACTIVITY
	US Army Aviation Materiel Laboratories Fort Eustis, Virginia

13. ABSTRACT

The transient-response calculation method reported in USAAVLABS Technical Report 65-65 is extented to yield aerodynamic loadings and elastic-blade motions in response to changes of shaft torque input.

Loadings, bending moments, and modal responses are obtained for a teetering rotor experiencing both a 100- and a 50-percent power loss. Similarly, responses are computed for a hingeless rotor experiencing a 100-percent power loss and for a hingeless rotor being braked from an initial operational condition corresponding to 100-percent rpm and a nominal value of zero lift. This hingeless rotor is also started up from a stopped position. Examination of the results obtained in these computations indicates that (1) reasonable aerodynamic loadings can be predicted irrespective of the radial to tangetial velocity ratio and (2) no loading or structural response phenomena result in the examined flight condition which would indicate that power loss, braking, and rotor stopping have serious consequences with respect to the creation of unusual blade-wake interaction phenomena.

14. KEY WORDS	LINK A		LINK B		LINK C	
	ROLE	WT	ROLE	WT	ROLE	WT
Stoppable Rotor						
Hingeless Rotor System						
Unsteady Aerodynamic Loading						
Loads Resulting from Sudden Power Loss						

INSTRUCTIONS

1. ORIGINATING ACTIVITY: Enter the name and address of the contractor, subcontractor, grantee, Department of Defense activity or other organization (corporate author) issuing the report.

2a. REPORT SECURITY CLASSIFICATION: Enter the overall security classification of the report. Indicate whether "Restricted Data" is included. Marking is to be in accordance with appropriate security regulations.

2b. GROUP: Automatic downgrading is specified in DoD Directive 5200.10 and Armed Forces Industrial Manual. Enter the group number. Also, when applicable, show that optional markings have been used for Group 3 and Group 4 as authorized.

3. REPORT TITLE: Enter the complete report title in all capital letters. Titles in all cases should be unclassified. If a meaningful title cannot be selected without classification, show title classification in all capitals in parenthesis immediately following the title.

4. DESCRIPTIVE NOTES: If appropriate, enter the type of report, e.g., interim, progress, summary, annual, or final. Give the inclusive dates when a specific reporting period is covered.

5. AUTHOR(S): Enter the name(s) of author(s) as shown on or in the report. Enter last name, first name, middle initial. If military, show rank and branch of service. The name of the principal author is an absolute minimum requirement.

6. REPORT DATE: Enter the date of the report as day, month, year; or month, year. If more than one date appears on the report, use date of publication.

7a. TOTAL NUMBER OF PAGES: The total page count should follow normal pagination procedures, i.e., enter the number of pages containing information.

7b. NUMBER OF REFERENCES: Enter the total number of references cited in the report.

8a. CONTRACT OR GRANT NUMBER: If appropriate, enter the applicable number of the contract or grant under which the report was written.

8b, 8c, & 8d. PROJECT NUMBER: Enter the appropriate military department identification, such as project number, subproject number, system numbers, task number, etc.

9a. ORIGINATOR'S REPORT NUMBER(S): Enter the official report number by which the document will be identified and controlled by the originating activity. This number must be unique to this report.

9b. OTHER REPORT NUMBER(S): If the report has been assigned any other report numbers (either by the originator or by the sponsor), also enter this number(s).

10. AVAILABILITY/LIMITATION NOTICES: Enter any limitations on further dissemination of the report, other than those imposed by security classification, using standard statements such as:

(1) "Qualified requesters may obtain copies of this report from DDC."

(2) "Foreign announcement and dissemination of this report by DDC is not authorized."

(3) "U. S. Government agencies may obtain copies of this report directly from DDC. Other qualified DDC users shall request through

_____ ."

(4) "U. S. military agencies may obtain copies of this report directly from DDC. Other qualified users shall request through

_____ ."

(5) "All distribution of this report is controlled. Qualified DDC users shall request through

_____ ."

If the report has been furnished to the Office of Technical Services, Department of Commerce, for sale to the public, indicate this fact and enter the price, if known.

11. SUPPLEMENTARY NOTES: Use for additional explanatory notes.

12. SPONSORING MILITARY ACTIVITY: Enter the name of the departmental project office or laboratory sponsoring (paying for) the research and development. Include address.

13. ABSTRACT: Enter an abstract giving a brief and factual summary of the document indicative of the report, even though it may also appear elsewhere in the body of the technical report. If additional space is required, a continuation sheet shall be attached.

It is highly desirable that the abstract of classified reports be unclassified. Each paragraph of the abstract shall end with an indication of the military security classification of the information in the paragraph, represented as (TS), (S), (C), or (U).

There is no limitation on the length of the abstract. However, the suggested length is from 150 to 225 words.

14. KEY WORDS: Key words are technically meaningful terms or short phrases that characterize a report and may be used as index entries for cataloging the report. Key words must be selected so that no security classification is required. Identifiers, such as equipment model designation, trade name, military project code name, geographic location, may be used as key words but will be followed by an indication of technical context. The assignment of links, rules, and weights is optional.